GEOMAR REPORT

GEOMAR

Helmholtz-Zentrum für Ozeanforschung Kiel

RV POSEIDON Fahrtbericht / Cruise Report POS509

ElectroPal 2: Geophysical investigations of sediment hosted massive sulfide deposits on the Palinuro Volcanic Complex in the Tyrrhenian Sea

Malaga (Spain) – Catania (Italy)
15.02.-03.03.2017

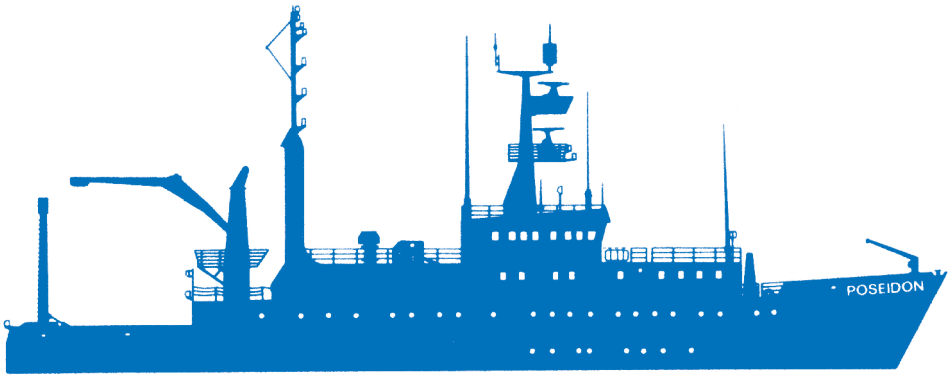

Berichte aus dem GEOMAR
Helmholtz-Zentrum für Ozeanforschung Kiel

Nr. 39 (N. Ser.)

December 2017

GEOMAR

Helmholtz-Zentrum für Ozeanforschung Kiel

RV POSEIDON Fahrtbericht / Cruise Report POS509

ElectroPal 2: Geophysical investigations of sediment hosted massive sulfide deposits on the Palinuro Volcanic Complex in the Tyrrhenian Sea

Malaga (Spain) – Catania (Italy)
15.02.-03.03.2017

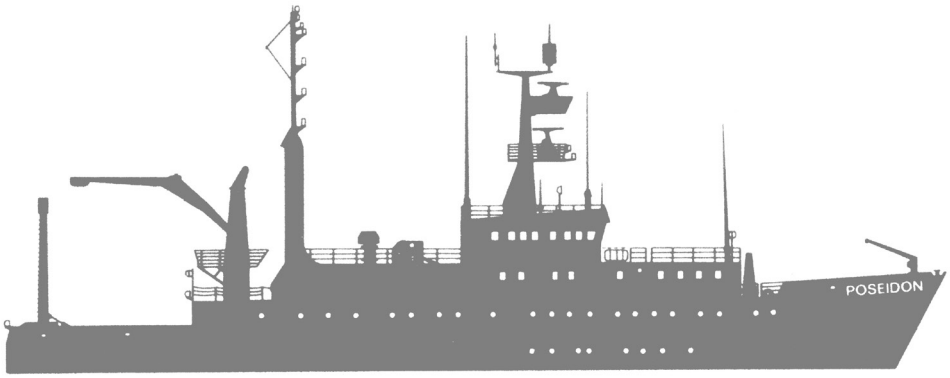

Berichte aus dem GEOMAR
Helmholtz-Zentrum für Ozeanforschung Kiel

Nr. 39 (N. Ser.)

December 2017

GEOMAR
Helmholtz-Zentrum für Ozeanforschung Kiel

Das GEOMAR Helmholtz-Zentrum für Ozeanforschung Kiel ist Mitglied der Helmholtz-Gemeinschaft Deutscher Forschungszentren e.V.

The GEOMAR Helmholtz Centre for Ocean Research Kiel is a member of the Helmholtz Association of German Research Centres

Herausgeber / Editor:
Sebastian Hölz

GEOMAR Report
ISSN Nr.. 2193-8113, DOI 10.3289/GEOMAR_REP_NS_39_2017

Helmholtz-Zentrum für Ozeanforschung Kiel / Helmholtz Centre for Ocean Research Kiel
GEOMAR
Dienstgebäude Westufer / West Shore Building
Düsternbrooker Weg 20
D-24105 Kiel
Germany

Helmholtz-Zentrum für Ozeanforschung Kiel / Helmholtz Centre for Ocean Research Kiel
GEOMAR
Dienstgebäude Ostufer / East Shore Building
Wischhofstr. 1-3
D-24148 Kiel
Germany

Tel.: +49 431 600-0
Fax: +49 431 600-2805
www.geomar.de

Poseidon Bericht

Cruise POS509

Palinuro Volcanic Complex, Tyrrhenian Sea

2017

Sebastian Hölz

ElectroPal 2

Geophysical investigations of sediment hosted massive sulfide deposits on the Palinuro Volcanic Complex in the Tyrrhenian Sea with novel electromagnetic instrumentation in combination with geophysical and geological investigations in preparation for future target-oriented drilling.

15.2. - 3.3.2017

Malaga (Spain) – Catania (Italy)

Table of Contents

1. Summary - Zusammenfassung

At present, investigations of submarine massive sulfides (SMS) are mostly limited to active systems due to the available methods and technologies, which rely on the detection of water column anomalies (temperature or chemical tracers) and the study of seafloor's morphology. They fail to detect sites where hydrothermal activity has ceased and former landmarks such as black smokers have been eroded or are covered by sediments. During RV Poseidon cruises POS483 (“ElectroPal”) and POS484 (”MARSITE”) we have successfully collected EM and airgun seismic data over an inactive and sediment covered SMS site at Palinuro, which had previously been found by chance in 1986 and was drilled to 5m depth during research cruise M73/2. EM measurements, carried out with the novel system MARTEMIS[1], not only showed high conductivities in the vicinity of the SMS deposit, but also revealed a second anomaly, possibly a zone of buried mineralization at greater depth.

During cruise POS509 previous measurements were continued and extended to get a full areal coverage of the structure to fully delineate and characterize the SMS sites. EM investigations were accompanied by measurements of the ambient electrical field (→ selfpotential (SP)) and additional geophysical (heat probe) and geological (gravity core) measurements for ground truthing and further structural insight. The combination of experiments proved to be convenient in terms of handling on the ship, as EM experiments on the one hand and measurements with heat probe and gravity coring on the other hand were performed in an alternating manner each other day. This alternating style of experiments gave each method time for adjustments and repairs as well as time to take a first look at results so that following investigations could be directly aimed at a specific target. As an example, an anomaly detected in the SP measurements in the NNW was used to guide the last gravity coring, which then found sulfide muds in an area where sulfides were previously not expected.

In summary, the following first results were derived directly during the cruise:

1. Strongly elevated temperature gradients (>3K/m) were observed in the vicinity of the area of previous drilling. There seems to be a good correlation between the extent of this area with the area, in which investigations with the MARTEMIS system in 2015 had recovered high conductivities at shallow depths. Additionally, a second area with elevated temperature gradients (~2K/m) was found to the NE of the crater. This area could coincide with the second area of elevated conductivities at greater depth, also found in MARTEMIS measurements in 2015.
2. Measurements of the ambient electrical field revealed anomalies coinciding with the anomalous temperature gradients, but also a second anomaly in the NNW.
3. Gravity cores not only showed sulfide muds in areas with high temperature gradients, where they had previously been found and could be expected, but also in areas indicated by SP measurements (see above) and previous TEM measurements.

Upcoming work will aim to further integrate results of all methods into a joint interpretation and may lead the road to target-oriented deeper drilling in the future.

1 Marine transient electromagnetic induction system

Die Erkundung submariner Massivsulfide (SMS) beschränkt sich derzeit auf die Untersuchung aktiver Systeme, da die eingesetzten Technologien auf das Aufspüren von Anomalien in der Wassersäule (Temperatur, chemische Tracer) und das Kartieren der Meeresbodenmorphologie stützen. Sie sind somit nicht zur Detektierung von inaktiven Systemen geeignet, die durch Erosion und Sedimentation bereits überprägt sind. Im Rahmen der Poseidon-Ausfahrten POS483 ("ElectroPal") und POS484 ("MARSITE") wurden erfolgreich EM und seismische Airgun Messungen an einer 1986 zufällig entdeckten Fundstelle am Palinuro Seamount durchgeführt, die im Rahmen der Ausfahrt M73/2 bis in 5m Tiefe erbohrt worden war. EM Messungen mit dem neuartigen System MARTEMIS[1] zeigten nicht nur eine Leitfähigkeitsanomalie im Bereich der bekannten SMS Vererzung, sondern auch eine zweite Anomalie, die wir aktuell als bisher unbekannte SMS Mineralisation unter einer Sedimentschicht interpretieren.

Im Rahmen der Ausfahrt POS509 wurden Messungen fortgeführt und auf die gesamte Fläche des Vulkankegels ausgedehnt um die Ausdehnung der SMS Vorkommen vollständig zu kartieren. Messungen mit EM Systemen wurden ergänzt durch Messungen des natürlichen E-Feldes (→ Eigenpotential (SP)) und durch weitere geophysikalische (Wärmelanze) und geologische (Schwerelot) Messungen, zum einen zur Bestätigung der EM Messungen und weiterhin um zusätzliche Einblicke in die Struktur zu erhalten. Die Kombination der Experimente erwies sich im Einsatz auf dem Schiff als sehr gut abgestimmt, da durch den täglichen Wechsel der Methoden – EM Experimente an einem Tag, Wärmelanze und Schwerelot am nächsten Tag – den einzelnen Arbeitsgruppen jeweils genug Zeit blieb um Arbeiten an den Systemen durchzuführen und außerdem erste Ergebnisse zu produzieren, die dann wiederum zu einer zielgerichteten Einsatzplanung verwendet werden konnten. Als Beispiel sei hier aufgeführt, daß die Entdeckung einer SP Anomalie im NNW zu einer Anpassung der Lokation für eine Schwerelotstation verwendet wurde. In dieser wurden dann auch Sulfidschlämme in gefunden und das in einem Gebiet, in dem dieses vorher nicht vermutet worden war.

Zusammenfassend wurden die folgenden ersten Erkenntnisse während der Fahrt gewonnen:

1. Stark erhöhte Temperaturgradienten (>3K/m) wurden in der Umgebung der vorherigen Bohrungen gemessen. Der Bereich mit erhöhten Gradienten scheint gut mit dem Bereich in Übereinstimmung zu stehen, in dem mit dem MARTEMIS System 2015 eine flache Leitfähigkeitsanomalie detektiert wurde. Weiterhin wurden erhöhte Temperaturgradienten (~2K/m) im NNO des Kraters gemessen, wo 2015 eine Leitfähigkeitsanomalie in größeren Tiefen detektiert worden war.
2. SP Messungen zeigen eine ausgeprägte Anomalie in dem Bereich, der auch erhöhte Gradienten in der Temperatur aufweist. Weiterhin sind anomale Werte im NNW auffällig.
3. Mit dem Schwerelot gewonnene Kerne zeigen Sulfidschlämme nicht nur in dem Bereich mit erhöhten Temperaturgradienten, wo sie auch schon in vergangenen Ausfahrten gefunden worden waren, sondern auch in der Gegend, die anhand der SP Messungen ausgewählt wurde (s. Oben) und auch in der Gegend, die in vorherigen TEM Messungen mit dem MARTEMIS System in größeren Tiefen auffällig war.

Weiterführende Arbeiten werden sich auf die Integration der gewonnenen Datensätze in eine gemeinsame Interpretation konzentrieren, um somit zukünftige zielgerichtet tiefere Bohrungen zu ermöglichen.

2. Participants

	Name	Position (Affiliation)	Function on board
1	Sebastian Hölz	Senior Scientist (Blue Mining, Geomar)	Chief scientist, Marine EM
2	Sven Petersen	Senior Scientist (Geomar)	Co-Chief scientist, Gravitycore, Heatflow
3	Gesa Franz	Master student (CAU)	Marine EM
4	Roxana Safipour	PhD-student (Colorado School of Mines)	Marine EM
5	Katerina Ivanova	Scientist (Geomar)	Marine EM
6	Sofia Martins	Senior Scientist (University of Lisbon)	Gravitycore
7	Martin Wollatz-Vogt	Technician (Geomar)	Marine EM
8	Gero Wetzel	Technician (Geomar)	Gravitycore, Heatflow
9	Benedikt Broda	Observer (Industry)	Marine EM

3. Research Program

3.1. General

Seafloor massive sulfide deposits (SMS) are formed through hydrothermal circulation of seawater, a process by which metal bearing ores are leached out of the host rock by hot fluids. The mineral rich fluid rises to the seafloor where they cool and the precipitation of metals may form SMS deposits. Venting may occur either through high-temperature fluids at chimney structures such as black smokers or at lower temperatures in more diffuse vents. Hydrothermal circulation is driven by heat and occurs mainly at marine plate boundaries such as mid ocean ridges, volcanic arcs and at back arc basin where heat is supplied by increased magmatic activity. Along oceanic plate boundaries, which stretch to a length of about 89.000 km (Bird, 2003), approximately 330 sites – most of them with present hydrothermal activity – have been observed at the seafloor. Of these sites 237 contain massive sulfide mineralization (Beaulieau et al., 2015; Monecke et al., 2016). A statistical extrapolation of the occurrence of known vent fields and deposits suggest that on globally about 500 to 5000 vent fields and associated sulfide deposits with a total accumulated volume of 600 million tons containing 30 million tons of copper and zinc are present in the immediate vicinity of the oceanic plate boundaries (Hannington et al., 2011). Due to the fact that SMS are compact (i.e. localized) structures close to the seafloor with potentially high ore grades, the possibility of mining such massive sulfide deposits has gained much attention on a national and international level (Boschen et al., 2013). While much knowledge has been gained by studying SMS formed at active vent fields close to plate boundaries, there has been a shift in focus lately to also take a closer view at extinct SMS sites (eSMS), which are no longer connected to any high-temperature hydrothermal activity: these sites have reached there maximum size and, thus, are believed to host 10 times more metals than the active systems and are not associated with endemic chemoautotrophic macrofaunal communities (Hannington et al., 2011).

At present, the detection of SMS is strongly limited by the available technology and methods to the detection of actively forming sites. This is due to the fact that the detection of SMS mainly relies on seafloor morphological observations as well as the detection of temperature anomalies or chemical tracers of the plume in the water column, which is connected to the active hydrothermal venting. While these methods have proven to be valuable tools for the detection of actively forming SMS, they do not allow the detection of deposits which are no longer hydrothermally active and which have undergone erosional processes and are possibly covered by sediments or lava. Also, these methods can only give very limited information about the lateral or vertical extent of an SMS deposit. Only a very few blind or sedimented deposits are currently known and have been found more or less coincidental, e.g. through heat flow data (Middle Valley Bent Hill deposit; Davis et al., 1987) or by chance sampling (Palinuro volcanic complex; Minniti and Bonavia, 1984). Therefore, to broaden the scope of investigations it is necessary to develop new technologies to allow for the detection of eSMS deposits which have finished their active phase.

Although investigations for seafloor massive sulfides have started to also look at systems in island arc settings in the past decade – e.g. at the Palinuro volcanic complex – there are still large gaps in our knowledge with respect to the formation of deposits in this tectonic environment. Again, the available exploration technology has led to a focus on active hydrothermal fields (de Ronde et al., 2007) and very little is known about mature SMS systems from island arc volcanoes. Thus, it is currently impossible to compare the size of SMS systems in an island arc setting to those forming at mid-ocean ridges.

In summary, general open questions are:

1. Where are extinct SMS sites and how do they compare to actively forming SMS sites?
2. What is the resource potential of eSMS sites and can this be determined cost efficiently without primarily relying on drilling?
3. What is the resource potential of hydrothermal systems at island arcs? Do large sulfide deposits actually form in island arc volcanoes or do frequent volcanic eruptions prohibit formation of large deposits?

Within the scope of the previous project *ElectroPal* (cruise POS483, 2015) it was demonstrated that the developed marine transient electromagnetic system MARTEMIS is capable of detecting SMS. Within the current project *ElectroPal 2* and associated cruise POS509 (2017), which is summarized in this cruise report, we aim to show that within a limited amount of time the system can be used to delineate a deposit in terms of its horizontal and vertical extent. The interpretation results of EM surveys – in combination with heatflow measurements and investigations on gravity cores – are aimed to serve as the basis for later target-oriented deep drilling, a prerequisite for a reliable resource estimate.

The work proposed here is technologically new and of interest to both academia and industry:

The academic interest lies in the fact that these new EM exploration tools will allow to get a more complete understanding on the distribution of SMS systems in various tectonic settings, since it will help to shift the focus of investigations from the search of systems which are currently connected to hydrothermal activity to those, where buried eSMS are hidden geological markers of past hydrothermal activity.

The industrial relevance of the research is well documented through the industrial financing of the EM modeling study and equipment design through industry as well as industrial partners in the Blue Mining consortium. These new EM exploration tools can be used to identify buried massive sulfide deposits and derive information on their tonnage allowing a better assessment of the size of sulfide deposits and therefore also providing a better estimate of the resource potential of this type of marine mineral resource.

Geological Target & Recent Investigations

The Palinuro Volcanic Complex is part of the Aeolian Volcanic arc in the Tyrrhenian Sea (Fig. 1), a semi-closed basin in the Western Mediterranean Sea, which has opened due to the roll-back of the Ionian slab (Kastens and Mascle, 1990, Carminati et al., 1998). The volcanic arc itself surrounds the Marsili back arc basin that rests on an up to 15 – 20 km thick continental basin (Morelli et al., 1975). The volcanism at Palinuro seems to be very recent, with analysis of basalt to basaltic andesites sample showing an age of 0.8 to 0.3 my (Savelli, 2002).

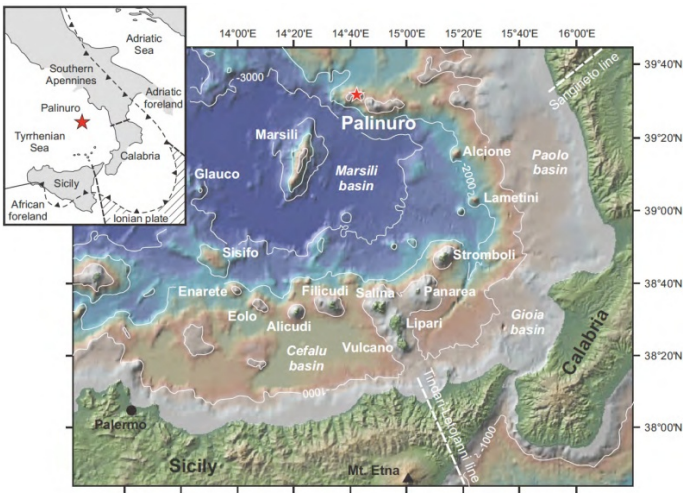

Fig. 1: Location of the Palinuro Volcanic Complex in the Tyrrhenian Sea (from Petersen, 2014).

The western sector of the Palinuro volcanic complex is host to two known sites of hydrothermal mineralization: Fe-oxyhydroxides in the west and polymetallic sediment-hosted sulfide mineralization in the east (Minniti and Bonavia, 1984; Petersen et al., 2014).

The latter site can be considered the best geological and geochemical investigated site at any back-arc complex, since it has been re-visited by several cruises in the past years. The sulfide mineralization was the target of a number of research cruises including a drilling cruise in 2007 (Meteor M73/2), during which the barite and sulfide occurrences of the Palinuro complex, which are largely concealed by sediments, were drilled and verified in the western part of the central crater using BGS Rockdrill 1 (Petersen et al., 2014). The thickness of the overlying sediment varies from a few cm in the center of the deposit to several meters of unconsolidated hemipelagic mud and volcanoclastic deposits in the surrounding. The true lateral extent of the mineralization could not be assessed since the vibro-corer/drill used could not penetrate more than 5m into the sediments and some of the stations show indication for sulfides at the base of these sections. The sulfides are thought to be more widespread and to occur under a thickening sediment cover away from the center of the deposit.

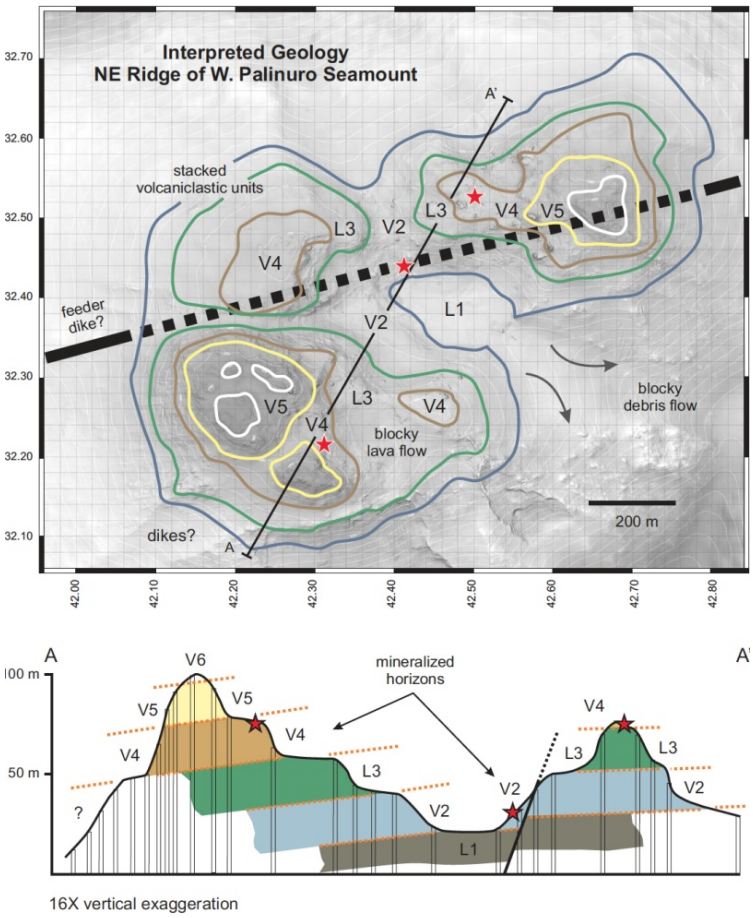

Fig. 2: Interpreted geology (from Jegen, 2015) of the NE Ridge of West Palinuro Seamount. The map view shows the outlines of the lower contacts of volcanic units in the summit area. The present volcanic geomorphology is erosional, dominated by 3 erosional remnants of a much larger volcanic cone. The inferred locations of a feeder dike – likely source of the volcanoclastics – and of the known mineralization are indicated (bold dashed line and stars, respectively). Section AA' shows the interpreted stratigraphy, which comprises S-dipping volcaniclastic units on the S side of the complex and flat-lying or N-dipping units in the N.

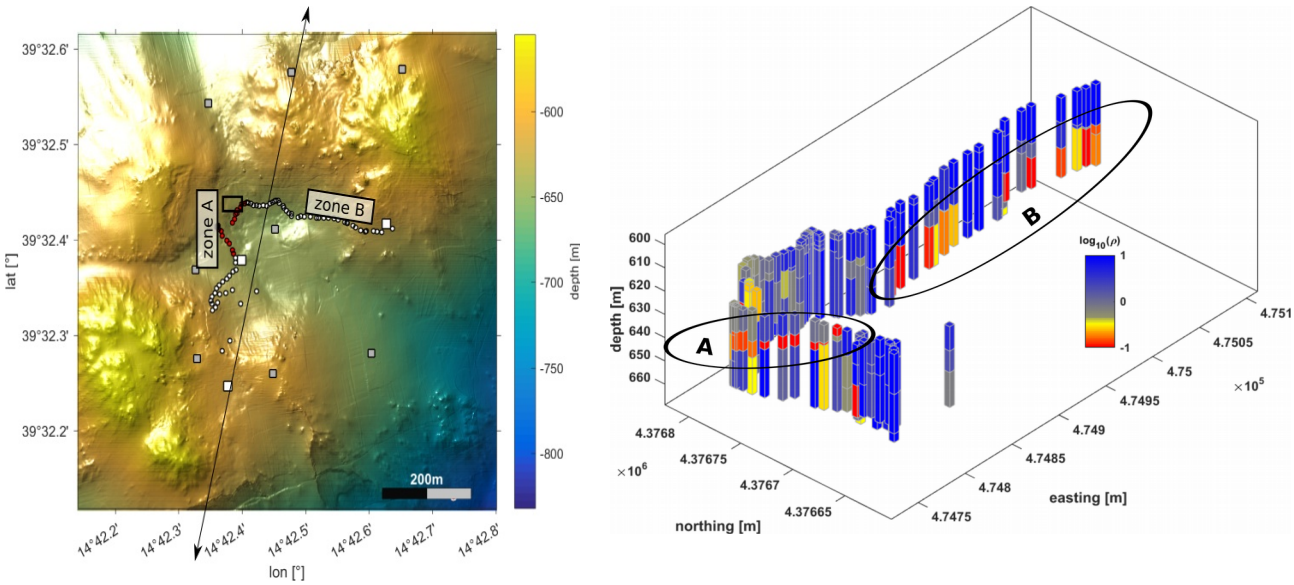

Fig. 3: Bathymetric map (left) of the Palinuro seamount with MARTEMIS measurements taken during cruise POS483 (circles) and the drilling area where massive sulfides were found (rectangle). High amplitudes (red circles) show up as conductive layers in the interpretation of TEM measurements in terms of 1D models (right, view direction towards NE). Zone "A" coincides with the drill area, zone "B" marks a so far unknown conductive feature which is possibly related to massive mineralizations at greater depths.

Previous gravity coring during cruises Meteor M73/2, Poseidon P412 (2011), and Meteor M86/4 (2011) characterized the sediment in the immediate vicinity of the sulfide mineralization and showed that the hydrothermally influenced area extends beyond the drilled area. Additional coring, performed over two profile lines during recent cruises with RV Poseidon, was used to delineate the sub-seafloor extent of hydrothermal alteration and to document the nature of the hydrothermal fluids circulating within the sediment pile (Volz, 2012; Kraeft, 2013).

No black smoker activity was observed (Petersen et al., 2008; Monecke et al., 2009; Thiel et al., 2012) but the widespread staining of the fine-grained sediments, shimmering water and the presence of tube-worm bushes showed the presence of low-temperature hydrothermal activity with diffuse venting. Sediment sampling and the measurements of the temperatures within the sediment showed very heterogeneous thermal characteristics. Maximum temperatures reached up to 58°C at 3m depth. However, adjacent cores showed almost background temperatures (ca. 13°C) suggesting advective fluid flow associated with fault structures, e.g. the inner fault hosting the central depression. Seismic investigations were limited to a single profile acquired across the eastern segment during RV URANIA cruise TIR10 in 2010 (Ligi et al., 2014). Additional seismic investigations were carried out during cruise POS484 (2015).

During cruise POS442 (2012) additional chimney- and mound-like structures were identified by AUV surveys using high-resolution bathymetry and sidescan sonar investigations to the E and to the N of the crater (Petersen, 2014). Initially, they were interpreted as inactive sulfide chimneys and, thus, as indicators for former hydrothermal activity and possibly massive sulfidization in this area.

However, visual inspections during cruise POS483 (2015) revealed that at least the chimney-like structures to the E were not of hydrothermal origin as originally interpreted, but instead turned out to be composed mainly of blocky coherent volcanic material, possibly eroded remnants of the smaller dikes, which are now

partly covered by coral formations (Jegen, 2015). This came as a surprise, since chimney structures are attributed to be one of the most reliable indicators of hydrothermal circulation. It clearly demonstrates that new tools are indeed needed for the investigation of eSMS systems. The current interpretation of the geology of the Palinuro Seamount based on the results of cruise POS483 are shown in Fig. 2.

A first experiment with the MARTEMIS system during cruise POS483 (2015) served as proof of principle for the method (Fig. 3, left). Elevated amplitudes in TEM measurements were measured in the vicinity of he previous drill sites, where SMS had been recovered. The interpretation in terms of 1D models (Fig. 3, right) demonstrates that the TEM coil measurements are indeed sensitive to the known mineralization: it shows up as conductive layer (red) under a more resistive cover (blue) in zone "A". From the interpretation it seems evident that the that the area of mineralization is larger than previously outlined by drilling. Furthermore, the inversion results demonstrate the usefulness for a first order resource estimation since the thickness of the conductive layer is resolved within the inversion. In addition to the known mineralization, the inversion of the data also revealed a second zone "B" of high conductivities at a depth of ~20m below the seafloor, which was previously unknown and shows that it might be possible to deduce information about SMS occurrences, which are invisible to other geophysical methods and also hard to reach with drilling. Results of this experiment were presented by Hölz et al. (2015b).

During the experiment with the MARTEMIS system the transmitted coil signals were also picked up by OBEM receivers (see Fig. 8), which actually had been deployed for a dipole-dipole experiment similar to the one sketched in Fig. 3. This very uncommon experimental configuration with a coil source and dipole receivers yielded good data quality for transmitter-receiver offsets of up to 250m (Fig. 4). Similar to a regular dipole-dipole CSEM configuration, changes in amplitude and phase of these curves can be interpreted in terms of the distribution of resistivities in the subsurface. A first evaluation of this "bonus" data set – which is still work in progress – indicates that conductive features evident in the coil data were indeed also picked up with this configuration. This is relevant since this mixed data set ideally extends the pure coil data set: due to the offset between transmitter (coil) and receiver (dipole) it only offers a lower lateral resolution but extend the depth of investigation from the roughly 25m for the coil system to an estimated 100m for this mixed configuration. First considerations of this new type of experiment have recently been published in Safipour et al. (2017).

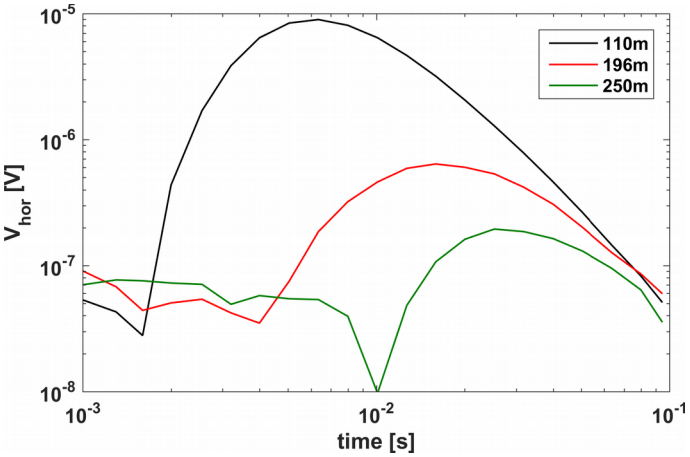

Fig. 4: Signals measured with OBEM receiver during TEM coil experiment (cruise POS483) at various transmitter-receiver offsets.

4. Narrative of Cruise

14.2. - 20.2.2017

After a seamless mobilization on the 14th we left the harbor of Malaga (Spain) on schedule the next morning. For the first 48h strong head wind and high waves prevented *RV Poseidon* to go faster than 5kn, which lead to a considerable delay of about 24h in the transfer to the working area at Palinuro, which we reached in the morning of the 20th of February. Since wind and waves had somewhat died down during the second half of the transit, we arrived well prepared in the working area to start of the scientific program right away.

20.2.2017

To prepare experiments we first performed a pressure test of the releases and at the same time acquired a CTD-profile, which yielded data necessary for the calibration of the Posidonia USBL-system (sound-velocity profile) as well as for the later interpretation of the EM data (conductivity profile). The following installation of the USBL-system at first proved to be somewhat problematic, since a stable communication between the USBL-PC and the USBL processing unit could not be established. After some tries and telephone calls to colleagues at Geomar the problems could be resolved. To avoid problems during future installations of the system we have left a Guide on the USBL-PC[1], which we hope to be helpful for future users. After establishing the communication the calibration of the USBL system was carried out and confirmed to yield acceptable precision in the order of 5 – 8m. Later this afternoon we deployed the first OBEM receiver.

21.2.2017

Most of the day was used to deploy eight additional OBEM receivers, which were lowered via the winch cable down to about 30m above the seafloor and then released and deployed to the predetermined positions

- around the previous drill site (NW of the central depression),
- around the the area where an anomaly had been detected in the EM data measured during cruise POS483 (NNE of the central depression),
- in an area considered to be background (S of the central depression),
- to the NE of the central depression, where some weak indications for hydrothermal activity had been found in previous cruises.

The deployment of stations was finished ahead of schedule, which left enough time for a first deployment of the heat probe at two stations. With temperatures of 15.9°C (@80cm) and 17.0°C (@210cm) measurements at both stations indicated temperatures well above the ambient temperature level of seawater of about 14.2°C. Since both stations were at some distance (~ 200m) to the previous drilling sites, these elevated temperatures were a first hint towards horizontal fluid migration pathways.

22.2.2017

Measurements with the heat probe were continued (3 stations, 5 additional tries) until the early afternoon, again showing slightly elevated temperature levels in the sediments. In the afternoon the first two gravity cores with core recoveries of 45cm and 272cm were taken. In the second core layers of sulfide sand

1 File located at *C:\Programme (x86)\IXSEA\Posidonia_Installation_Guide.doc*.

(@210cm) and massive sulfide layers (1cm thick @ 244cm) were recovered, thus, giving direct proof to the previously made assumption of horizontal fluid migration pathways, which lead to a wider deposition of massive sulfides as previously expected.

During measurements with the heat probe and gravity coring the MARTEMIS coil system was assembled and dry tested on deck.

23.2.2017

The morning hours were used for a first test deployment of the MARTEMIS system and after some adjustments to the rigging and the deployment procedure a first test measurement of about 2h was started after lunch. After recovery of the system in the early afternoon we had to find out that the two receivers (primary and backup), which were connected to the receiving coil of the MARTEMIS system, had been damaged during the test. In a first assessment we were able to find out that the protection circuits, which were actually designed to protect the receivers from high voltages, had failed and damaged the receivers. Since it was not possible to repair the receivers or prepare an alternative backup on short notice, it was decided to start the EM experiment in the early evening (~18h) without these receivers attached to the MARTEMIS system. This still left us with three EM experiments, namely

1. the controlled source electromagnetic (CSEM) experiment with the coil source (→ MARTEMIS) and the nine stationary receiver nodes, which we had deployed to the seafloor,
2. the selfpotential (SP) experiment, for which we used a third receiver with two additional pairs of electrodes, which all had been mounted to the coil of the MARTEMIS system,
3. and an additional experiment with the same configuration as mentioned in (2.).

After lowering the system to the seafloor the coil was operated until about noon of the following day along seven N-S striking lines covering the central depression of the seamount with a combined profile length of about 7.5km.

24.2.2017

After recovery of the MARTEMIS system we continued sampling with the gravity corer (1 station, 57cm, volcanoclastics) and measurements with the heat probe (4 stations) in the afternoon. Measurements with the heat probe in the vicinity of the previous drilling sites showed - as expected - significantly elevated temperatures of up to 26.4°C (@170cm).

Attempts to repair the damaged receivers of the MARTEMIS system proved to be futile with the equipment available on board

25.2.2017

To allow for measurements with the receiving coil of the MARTEMIS system in the upcoming days, we prepare an alternative receiver system, which required some mechanical work on of the OBEM receivers (usually used for the stationary receiver nodes) as well as preparation of new cables.

On the scientific side the day was used to take measurements with the heat probe (9 stations, highest value of 49.4°C @210cm measured within previous drilling area) and to get one gravity core (290cm) at a location, where previous EM measurements during cruise POS483 had indicated an electromagnetic anomaly at greater depth. A first inspection of the core showed oxidized Fe-stained sediment overlying mottled clay

with sulfide patches (100 – 190cm). This finding can be considered to be one a highlight of this cruise, since the location for sediment coring with finding of sulfides was chosen according to results from previous EM interpretations in an area, which showed no surface expression indicating such finding.

26.2.2017

With the replaced receiver, measurements with the MARTEMIS system were started in the morning. After a smooth deployment of the system in just 7min (!) and lowering to the seafloor, the system was operated for the next 22h along eleven E-W striking lines covering the whole seamount with a combined profile length of about 10km.

27.2.2017

After recovery of the MARTEMIS system the day was used for the final measurements with the heat probe at eleven locations of which four did not penetrate more than 20cm. Successful measurements confirmed the trend already observed during the first days with high temperatures in the vicinity of the previous drill site (30.9°C @ 210cm) and elevated temperatures at more distal sites (~17°C @210cm).

In the afternoon two gravity cores were taken:

- The first core only recovered 77cm with some indication for hydrothermal activity,
- the second core was taken at a location at which SP measurements of the previous night had indicated an anomaly. The core contained oxidized clay over reduced clay and thick layer of massive sulfide mud (> 1m) below 180cm. This again was remarkable, since the location determined by SP measurements did not have any surface indications for the occurrence of massive sulfides.

28.2.2017

The morning and early afternoon of the day was used to recover the first eight OBEM receivers. Measurements with the MARTEMIS system were started in the afternoon in the vicinity of the remaining ninth OBEM receiver, which had been deployed to the NE of the seamount. After about 1km of profile measurements had to be halted due to communication problems with the transmitter electronics. By the time the system had been fixed, wind had picked up considerably and with a forecast of storm and high waves for the night it was decided to abandon the experiment.

1.3.2017

After recovery of the last OBEM receiver, experiments at the Palinuro Seamount were officially finished and we transferred to Stromboli volcano, where crew and scientists enjoyed dinner with a magnificent view.

2.3.2017

As requested by Morelia Urlaub, we recovered 3 tiltmeters and 6 OBS stations, which had been deployed off the coast of Sicily in the early summer of 2015. Recovery of systems went flawless and in the early afternoon we entered our final destination the port of Catania, Sicily.

5. Applied Methods & Preliminary Results

5.1. Electric and Electromagnetic Instruments & Experiments

5.1.1. General

In land-based exploration it has been common practice for several decades to use electromagnetic methods to detect and characterize massive sulfide deposits (i.e. Palacky, 1987). Investigations on marine samples indicate that conductive anomalies may also be expected in the marine environment (e.g. Iturrino et al., 2000). Consequently, it seems promising to use both passive and active EM methods for the investigation of SMS and the associated hydrothermal systems:

1. active experiments rely on the fact that the generated electromagnetic field couples to the conductive ore body and is distorted by the coupled current systems, which are channeled into the ore body,
2. passive self-potential (SP) measurements detects naturally occurring anomalies in electrical potential which can arise from buried conductive bodies (e.g., massive sulfides, graphite shear zones) or from streaming potentials caused by fluid flow (e.g., groundwater).

However, only a few electric and electromagnetic experiments have ever been conducted on marine SMS targets:

- The SP method has been shown to work in marine environments, where both graphite and massive sulfide bodies have been detected by marine SP systems (Brewitt-Taylor, 1975; Corwin, 1976; Von Herzen et al., 1996; Heinson et al., 1999, 2005; Beltenev et al., 2007, 2009; Cherkashov et al., 2010; Shilov et al., 2012; Cherkashev et al., 2013). However, prior to our study, the SP method had not been tested over a hydrothermally inactive SMS site which is buried under sediment.
- Cairns et al. (1997) report about an electromagnetic pilot study to image the TAG hydrothermal field (26°N, Mid-Atlantic Ridge) SMS deposit. However, at that time marine electromagnetic instrumentation was in its infancy and 3D modeling capabilities were just in development such that a 3D image of the sulfide deposit could not be derived
- Kowalczyk (2008) reports on a shallow penetration ROV based EM, which was used to map anomalies of the electrical conductivity at the Solwara site offshore Papa New Guinea. Later drilling confirmed that anomalous electrical conductivity anomalies were indeed associated with occurrences of SMS at or directly beneath the seafloor.

5.1.2. Overview of Experiments and Instruments

Electric and electromagnetic measurements were carried out during four deployments of the MARTEMIS system (Fig. 5). The first deployment of the system was exclusively dedicated to familiarize the crew with the deployment of the system, to test the system at shallow water depths (~100m) and to acquire some first background data. During the second and third deployment measurements were taken on a total of 20km of profile lines crossing the central part of the Palinuro Seamount along N-S and E-W profiles, respectively. The fourth deployment started well outside the crater towards the NE but had to be abandoned after the first profile of about 300m length due to upcoming weather conditions and problems with the electronics of the TX data logger.

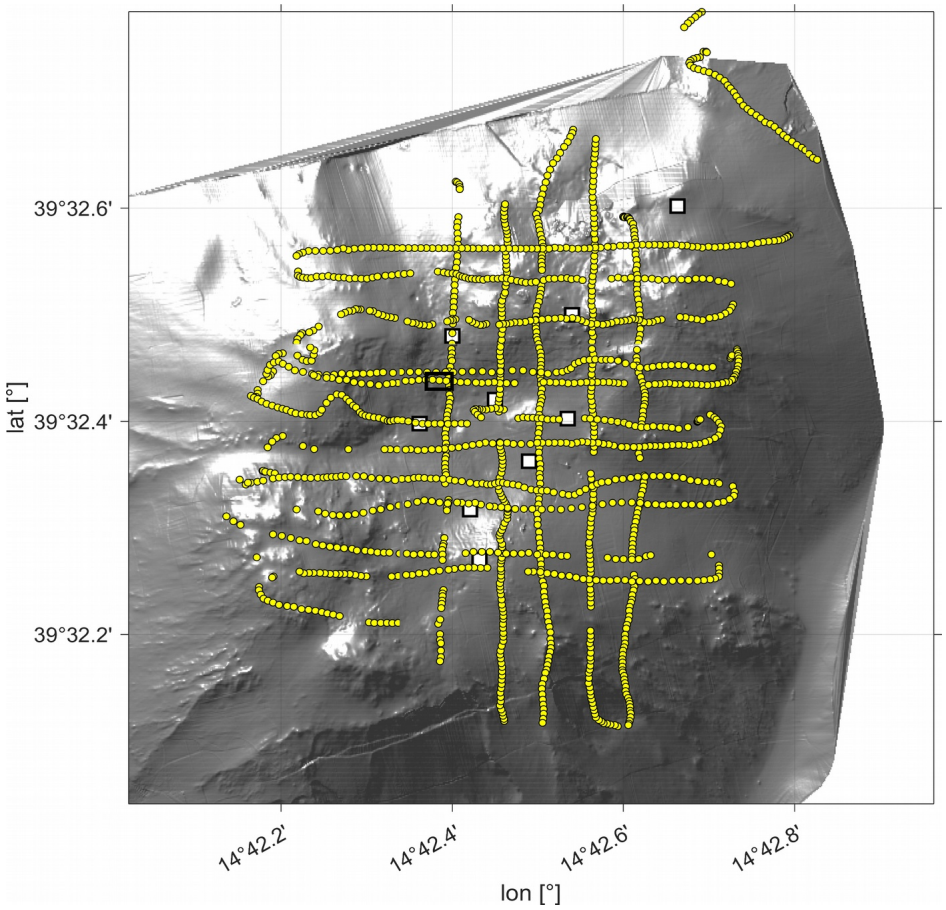

Fig. 5: Bathymetric map with EM experiments carried out during cruise POS509: locations of OBEM receivers (white squares), MARTEMIS coil system (yellow circles) and area of the previous drill sites (black rectangle).

During deployments of the system to the seafloor the transmitter system to the seafloor the transmitter was activated at a total of 1465 stations (for summary see table below) along profile lines with a total length of about 18km (see Fig. 5). Instruments will be described in the following paragraphs, a description of the experiments can be found in the next sub-chapters starting at page 18.

Deployment (Stations)	Date	TEM	Coil2Dipole	SP	Comment
Test	23.2.	3 meas.	no	yes	Test measurement at 100m depths, both Hydra logger damaged.
1 (S0001 - S0569)	23. - 24.2.	no	yes	yes	N ↔ S profiles
2 (S0570 - S1420)	26. - 27.2.	yes	yes	yes	E ↔ W profiles
3 (S1421 - S1465)	28.2.	yes	yes	yes	Short profile NE of crater

MARTEMIS Coil System

Similar to measurements during cruise POS483 (2015), we used the coincident loop TEM system MARTEMIS (marine transient electromagnetic induction system), which was developed by our workgroup at GEOMAR in the scope of the EU project *Blue Mining* (EU-FP7 project, Grant No. 604500, "Break-through Solutions for the Sustainable Exploration and Extraction of Deep Sea Mineral Resources").

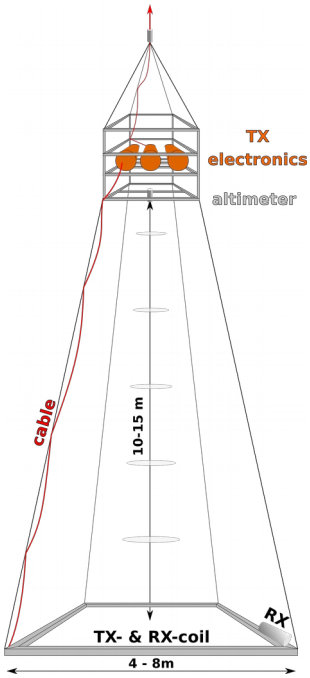

Fig. 6: MARTEMIS system.

Fig. 6 shows a sketch of the system, which consists of a square frame holding the cables of the coincident transmitter (TX) and the receiver (RX) coils. The frame is constructed from glass fiber reinforced tubes (GFK tubes) with corner connectors made of stainless steel. The robust connector system allows for flexible loop sizes by simply using GFK tubes with different lengths, which of course also requires matching cables within the frame. Thus, the system may be adjusted to the available space on different ships by up- or downsizing. As an example, in last year's project in the vicinity of the TAG hydrothermal field with the *R/V James Cook* we used a 6.3 x 6.3m^2 coil to get a deeper depth of penetration, whereas the smaller A-frame of the *R/V Poseidon* limited the maximum coil sized to 4.3 x 4.3m^2 during this project and cruise POS483 (2015). Additionally, weights, two attitude sensors and two pressure tubes with the RX electronics are also mounted to the coil frame. The receiver units have one input channel with 24bit resolution, which are sampled at a frequency of 10kHz and have a storage capacity to acquire about 24h of continuous data. In experiments we use more than one receiver to facilitate simultaneous measurements with different gain settings and to also be redundant and fail-save in the acquisition of data. Currently, we do not have the capability to monitor the received signal in real-time. Therefore, it is important to have more than one acquisition system in place to ensure a successful measurement. For future experiments we plan to have online communication to the logger from the ship which would allow for real-time evaluation of incoming data and direct detection of conductivity anomalies which would offer the possibility to adapt the survey plan in the course of an experiment.

To minimize external noise and unwanted distortions of the measured secondary signal on the RX loop, all additional electronic components and associated metal pressure housings are housed by a second frame, which is mounted at a distance of 10 -15m above the coil frame (11.6m at TAG, ~14m this experiment). This second frame holds the TX- and communication-electronics, attitude sensors, a downward looking altimeter and an acoustic ranging system (see chapter 5.1.4) which is used to measure the distance to remote OBEM receivers on the seafloor, which are described in the next sub-chapter. The two frames are connected via four ropes at the corners. Additionally, cables connect the TX- and general electronics to the TX-coil and attitude sensors on the coil frame, respectively.

We use the same transmitter, which was previously developed for the Sputnik CSEM system. The transmitter generates a bipolar square waveform with a 50% duty cycle. Repetition frequencies may be switched to 0.25Hz (for CSEM measurements) or 2.5Hz (for TEM measurements) and signal amplitudes can be selected to be 19A, 38A or 57A. The transmitter current is supplied and regulated through DC/DC converters, buffer batteries and a microprocessor controller unit. These units are housed in titanium cylinders, which are mounted to the upper frame.

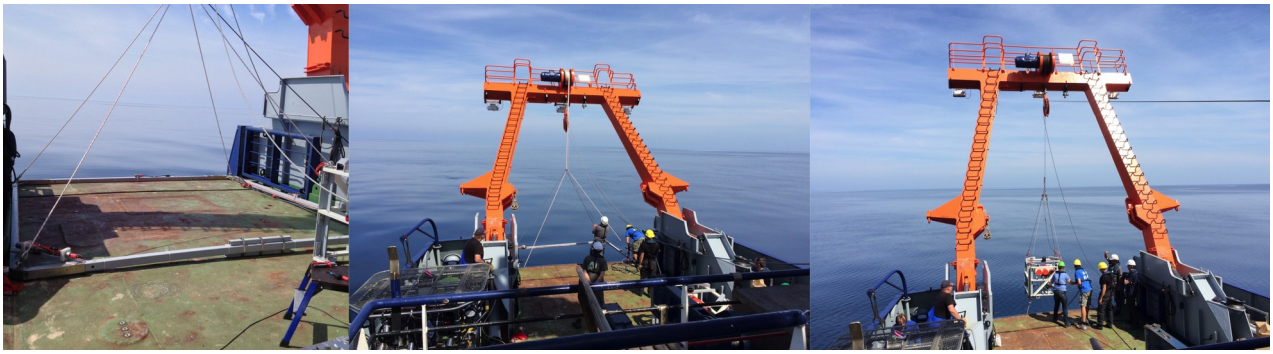

Fig. 7: Deployment of the MARTEMIS system on R/V Poseidon (pictures taken during cruise POS483).

Generally, for experiments the MARTEMIS system is assembled on the aft of the ship (Fig. 7, left). After assemblage, the coil frame is lowered into the water (Fig. 7, middle) and attached at a vertical distance of 14m beneath the second frame (Fig. 7, right), which holds the TX- and communication electronics. It is worthwhile to note that the during this cruise the duration of the deployment was optimized from about 75min (1st deployment) to just above 7min last deployment. After deployment the whole system is lowered towards the seafloor using the ship's winch cable and "flown" across the seamount by moving the ship at a slow speed, approximately 0.3kn during the experiments at the Palinuro Seamount. By using an altimeter the position of the loop is kept at a close distance between above the seafloor by constantly adjusting the length of the winch cable. During experiments at Palinuro we tried to keep the 4.3 x 4.3m^2 coil at a distance of 3-5m above the seafloor (for comparison: during cruise JC138 at TAG, where we measured with a larger coil (6.3 x 6.3m^2) at greater water depth (~3600m) and with greater speeds of up to 0.7kn).

Additional Sensors & Receivers

With the configuration described in the previous sub-chapter, the MARTEMIS system was used for TEM measurements, which we will describe in the following chapter 5.1.3. However, with some modifications / additions the system was used as platform for additional experiments:

- Measurements of the self-potential (SP), which actually measure the ambient electrical field (see chapter 5.1.5) were carried out by attaching two pairs of Ag/AgCl-electrodes to the coil frame: the four electrodes were placed at the centers of the coil edges. This allowed for measurements of two perpendicular components of the horizontal electrical field, from which the horizontal component of the ambient electrical field was constructed. As logger we used a modified OBEM logger equipped with an internal battery which allowed for approximately 24h of SP measurements,
- the deployment of stationary OBEM (ocean bottom electromagnetic) receiver nodes (Fig. 8) allowed for an additional EM experiment with an increased depth of investigations (see chapter 5.1.4). Each OBEM receiver is equipped with a three component

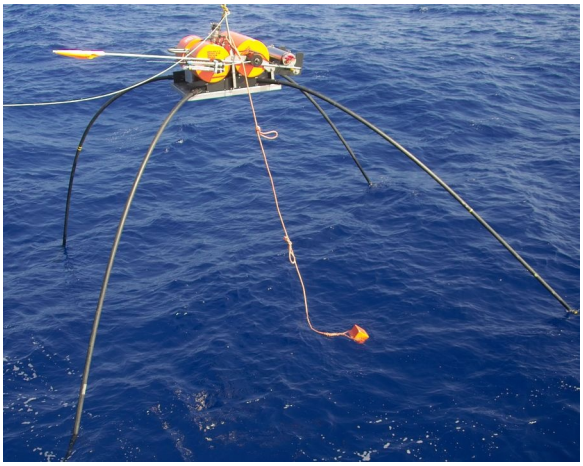

Fig. 8: OBEM receiver during deployment.

fluxgate magnetometer, and can measure two components of the horizontal electric field. The components of the electric field are measured using Ag/AgCl-electrodes, which are attached at the end of four flexible arms. The total length of each receiver dipole is 11.2m. Additional sensors allow measurements of the attitude (pitch, roll) and the temperature. The receivers can either be used in an MT-mode, in which all sensors are logged at sampling rates of up to 10Hz, or switched into a CSEM-mode, in which only two components of the E-field are recorded at a high sampling rate of 10kHz. This high frequency is necessary to acquire transient data at short offsets on the order of 100m and was used in this experiment. Generally, the switch from one mode to the other can be performed by using a preset timetable or alternatively by an external acoustic signal.

Online Planing Tool

Safe operation of the system requires an appropriate planing tool, since the system has only a downward looking altimeter, which can be used to keep the coil at a safe distance but is not suitable to avoid the collision with obstacles within the pathway of the system. To facilitate safe operations we have developed a suitable software, which is depicted in Fig. 9. Development of the tool was started during the TAG cruise (JC138) – the displayed screenshot of the planing tool was taken during that cruise – and was continued during this cruise. The left panel shows the bathymetric map with the real-time position of MARTEMIS taken from the ship's USBL system (red dot). It is connected to the planned profile (white line with white marker), which may be manipulated online. The right plots shows the elevation along the chosen profile line (black line) along with elevations along parallel profile lines within a predefined corridor around the main profile line (gray lines). Furthermore, the plot allows for estimation of distances and times to the next obstacle and can be used to measure rates for hauling or veering the winch cable at the given speed. All components of the planing tool operate in real-time with data supplied by the ship (i.e. USBL-positions, speed) and the online interactions of the user.

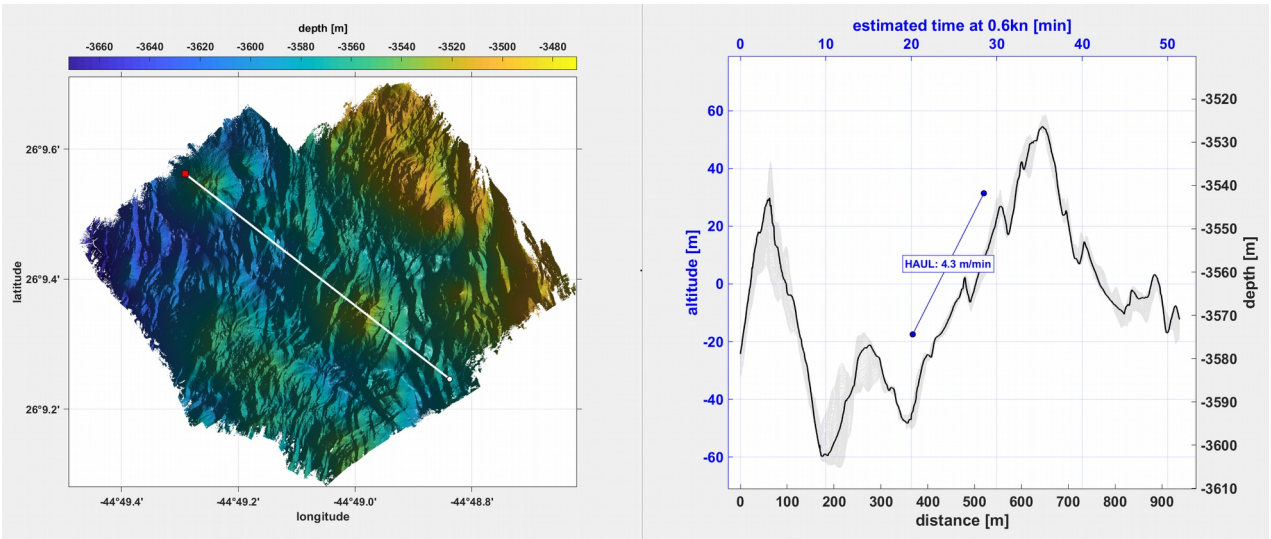

Fig. 9: Planing tool for online navigation of the MARTEMIS system (screenshot taken during experiment at the TAG hydrothermal field). Left panel: bathymetric map with the real-time position of MARTEMIS (red dot) and planned profile line (white line with white marker). Right panel: elevation along profile line (black line) and elevation along parallel profile lines within a predefined corridor (gray lines). Distances, estimated travel times and haul-rates for the winch can be manipulated online and are all updated in real-time.

5.1.3. Transient Electromagnetics

Generally, the TEM method is used to investigate the distribution of the electrical conductivity of the subsurface. Since the method measures the secondary fields of actively induced current systems, it is inherently sensitive to good conductors like massive sulfides.

TEM systems usually use a bipolar waveform to generate a current in a transmitter loop (Fig. 10, black symbols), which excites a quasi-static primary magnetic field while being turned on. Based on Faraday's law of induction, the current switch-off in the transmitter and the breakdown of the associated primary magnetic field induces eddy-currents in conductive materials in the vicinity of the coil (Fig. 10, dotted line). The strength and geometry of these eddy-currents depends on the spatial distribution of the conductivity around the coil. Thus, the secondary magnetic field associated with the decaying eddy-currents carries information about the conductivity distribution and is the measured quantity (Fig. 10, gray symbols). The decay of the secondary field is measured with a receiver loop, which may coincide with the transmitter loop, in which case the configuration is called coincident loop configuration.

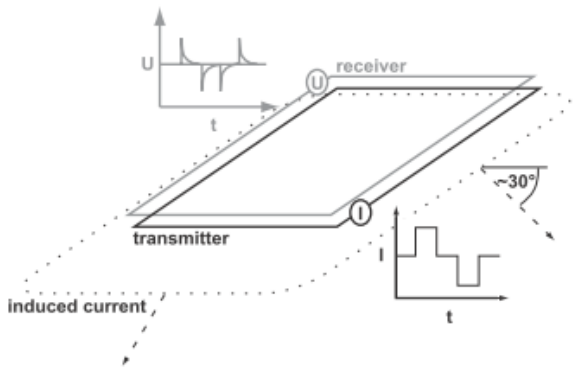

Fig. 10: Basic sketch of coincident loop TEM system with transmitter (black), receiver coil (gray), associated waveforms and the induced current system.

TEM measurements at Palinuro were carried out during the first test deployment, during the third deployment along E-W profiles across the central part of the structure and during the last deployment in the NE section of the Seamount (see Fig. 5).

During the first test deployment both Hydra III receivers were damaged by induced high voltages of transmitter coil. A new over-voltage diode protection, which had been integrated into the receivers after consultations with the manufacturer prior to the cruise, had failed and basically left the electronics of the loggers unprotected. Attempts to repair the loggers with the equipment and spare parts available on-board proved futile. Consequently, it was not possible to perform TEM measurements during the second deployment on the 23rd. For the next deployment of the MARTEMIS system we prepared one of the spare OBEM loggers for the TEM measurements, which required considerable mechanical work inside the pressure tube in order to make room for a battery pack, which had enough capacity to power the logger for about 24h (note: usually these loggers are powered with an external power pack contained in a separate pressure tube). For this logger we used the old diode protection, which was molded into the connection cable between receiver coil and the OBEM receiver. This spare logger then worked without problems during the 3rd and 4th deployment.

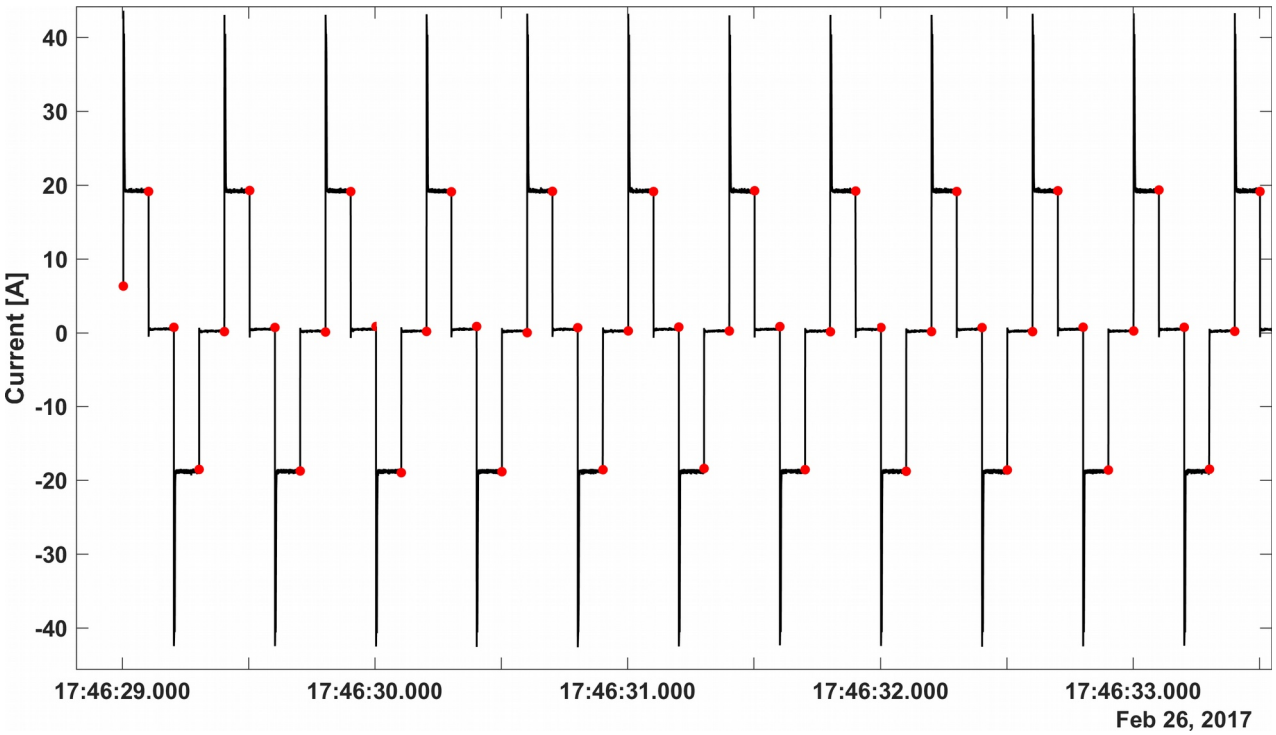

Fig. 11: Example of transmitter waveform measured at station S1000 during the 3rd deployment. The red dots mark picked times when the transmitter was either turned on or off.

General procedure for all measurements with the MARTEMIS system was to keep the coil at a distance of about 4-6m from the seafloor while drifting along profile lines at a speed of about 0.3kn. With the loop close to the seafloor, a regular cycle of measurements was performed as follows:

- ranging measurement,
- TX activation for 10s (50% duty-cycle, I = 19A, repetition frequency 2.5Hz), 10s pause
- TX activation for 10s (50% duty-cycle, I = 38A, repetition frequency 2.5Hz), 10s pause

This measurement cycle was used at a total of 1465 stations along profiles with a total length of about 18km (see Fig. 5 and table on same page). Fig. 11 shows an example data set of TX data, which was transmitted at station S1000 during the 3rd deployment. For the processing of data measured at the receivers (both TEM and OBEM receivers) it is necessary to know the exact times of the TX turn-on and turn-off. As first step it is therefore necessary to determine these time points (red dots in Fig. 11), which is done by an automated picking routine, which still requires visual inspection of all picks and – where necessary – manual correction of possible mistakes. This process of generating "ShotTables" (a more appropriate name would be SwitchTables …) was finished a few weeks after the cruise. The second step for processing is then to assure the correct time-synchronization between the transmitter and receiver clock(s). For the TEM data this was also finished directly after the generation and correction of the ShotTables. With these two steps finished it is possible to perform a batch processing of the TEM data, which simply comprises the import of the RX data for the correct time-interval, stacking of successive transients and log-gating of the stacked transient (see Hölz et al., 2015 for details).

A first appraisal of processed transients shows that there is a shift or incorrect amplification, which leads to an unexpected behavior of all transients. A similar shift is was also observed in TAG data sets, but was not evident in measurements performed during cruise POS483 in 2015. We are currently performing test mea-

surements on land and will perform a test in the Kieler Förde in October 2017 to determine the cause for this distortion. Recent work on TAG data set shows that a correction of this distortion is possible, if an extended processing scheme is applied. For the data set acquired during POS509, application of this extended processing scheme will be the next step in the evaluation of data.

5.1.4. Coil2Dipole

For the Coil2Dipole experiment we used 9 OBEMs (Fig. 12) which were synchronized to GPS time prior and after the experiment. The receivers were lowered via the winch cable towards the seafloor being hooked onto a release with USBL beacon. At an altitude of approximately 30m above the seafloor the OBEMs where then released. Three OBEMs were placed around the previous drill site (NW of center), two OBEMs in the area, where the interpretation of TEM measurements of the previous cruise had indicated a deeper conductor (NE of center), one OBEM was placed in the center of the crater and two OBEMs to the S of the center, where we expected to measure background values. The last OBEM was placed further to the NW (see Fig. 5), where previous investigations had given some indications for hydrothermal activity.

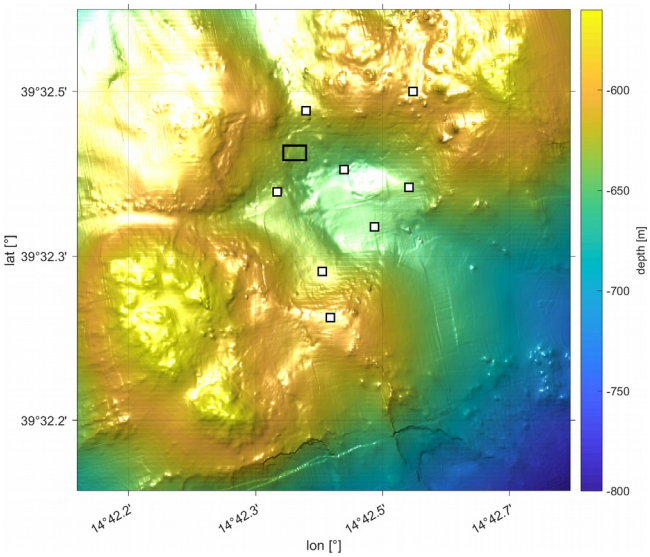

Fig. 12: Station map of OBEM receivers (white squares) for Coil2Dipole experiment. Note that one receiver towards the NW of the crater is outside the map. The area of previous drilling is marked by a black rectangle.

For experiments like the Coil2Dipole experiment it is important to know the exact distance between the transmitter antenna and the remote receivers. While the USBL positioning system can provide locations with an accuracy of about ±5m at the given water depth of about 600m (value taken from the calibration measurements), higher accuracies are needed especially for short transmitter receiver offsets. Such improved distance measurements can be achieved with the on-board ranging system, which is mounted to the upper frame of the MARTEMIS system. It consists of a transducer, which sends an acoustic interrogation pulse at 11kHz and receives reply pulses, which are send out by transducers mounted to the remote

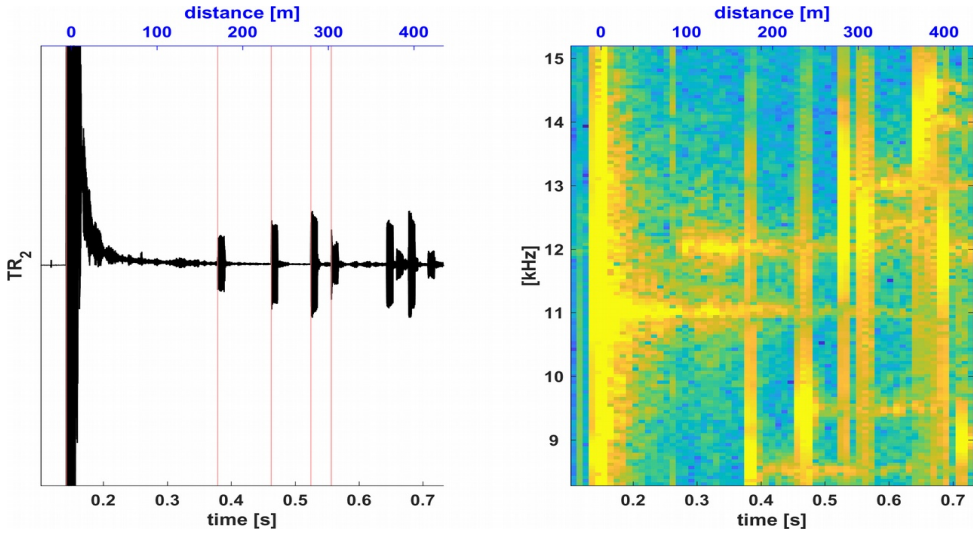

Fig. 13: Example of measurement with MARTEMIS ranging system with the accoustic waveform (left) and the associated spectrogramm (right). The initial interrogation pulse (11kHz) with high amplitudes (@0m) is followed by several replies of transducers mounted to the remote receivers.

OBEM receivers. Fig. 13 shows an example, in which the initial interrogation pulse is followed by eight replies at various time offsets. Past experiments, where the ranging system was mounted to the Sputnik system, have shown that measurements with the ranging system are repeatable with ranges varying by at maximum a few centimeters, even for large offsets, which of course assumes that the TX-RX distance does not vary between measurements. Thus, the accuracy of the ranging system is mainly determined by the knowledge of the sound velocity at the seafloor and we expect it to be better than 1m for the ranges relevant in this experiment (<300m), possibly even better than 10cm.

For the experiment at Palinuro we have used individual reply frequencies for each OBEM, which allows for a simple and unique identification of OBEMs by the frequencies of received signal in the spectrogramm. In the given example the four first replies, which cover a distance range between ~ 150 – 300m were hand-picked. Similarly, the pings of all 1465 ranging measurements were already picked and the derived distances will be used in the upcoming evaluation of the Coil2Dipole data.

Turning to the data acquired with the OBEM receivers we found that during this experiment all loggers had worked properly and that there were no dead E-field channels. Thus at first sight, the data set seems to be complete. This comes as great relief given the fact that during the last experiment at Palinuro (POS483, 2015), 8 out of 9 loggers had stopped logging after 24h of operation. The reason for this past failures – an issue within the data logger caused by the wear level management of the used µSD cards – had been tracked down and resolved in cooperation with the manufacturer in late 2015. After a new firmware update uploaded in early 2016 the loggers have not skipped out anymore and, thus, this issue can be considered to be resolved. Also, the mystery of dead E-field channels, which had been showing up every now and then over the past years, finally seems to be resolved. In past experiments it occasionally happened that E-field channels did only showed constant measurements. Back in the laboratory we were never able to reproduce theses failures, which made tracking down of these errors quite difficult. For this experiment we have replaced all connector cables for the connection between the data logger and the electrodes with a new set of cables. Also, in the preparation of loggers during the cruise we found some loose metal parts within the loggers (metal casing of the SeaScan clocks), which might have short-circuited the E-field channels on the electronic boards. In summary, the combination of new cables and fixed metal parts within the loggers has remedied the problem with dead E-field channels.

Since the Coil2Dipole experiment uses the MARTEMIS coil signal as source the primary processing step – namely the creation of the transmitter's ShotTables has already been accomplished as part of the processing of TEM data (see previous chapter). The time synchronization between the MARTEMIS system and the OBEM receivers was checked by looking for TX stations with a short offset – i.e. in the order of 30m or less – to each OBEM station. At such short offsets the diffusion time is very short, usually in the order of 0.2 – 0.5s. This can be used to check and, where necessary, correct the clocks. For the given data set all OBEM clocks were found to be within 0.1 – 0.2ms of the TX clock and only station RX03 (logger DEV51) required larger corrections due to a substantial drift of the clock and for station RX05 (logger DEV39) the correct time synchronization needed to be established because the clock was not synchronized after the recovery of the instrument.

Thus, the data set is now ready for processing. We are currently working on an imaging algorithm, which will allow for a quick evaluation of the data and will start the interpretation in terms of 1D inversions and 3D modeling in the near future.

5.1.5. Selfpotential

SP data were collected over two days: on the first day the frame was towed along seven N-S profiles and on the second day along twelve E-W profiles over the study area. The system was towed at a very low speed of 0.4 knots (0.2 m/s) while the cable length was adjusted to keep the frame between 5–10 m above the seafloor as determined by the on-board altimeter. At the beginning and end of each profile, the system was

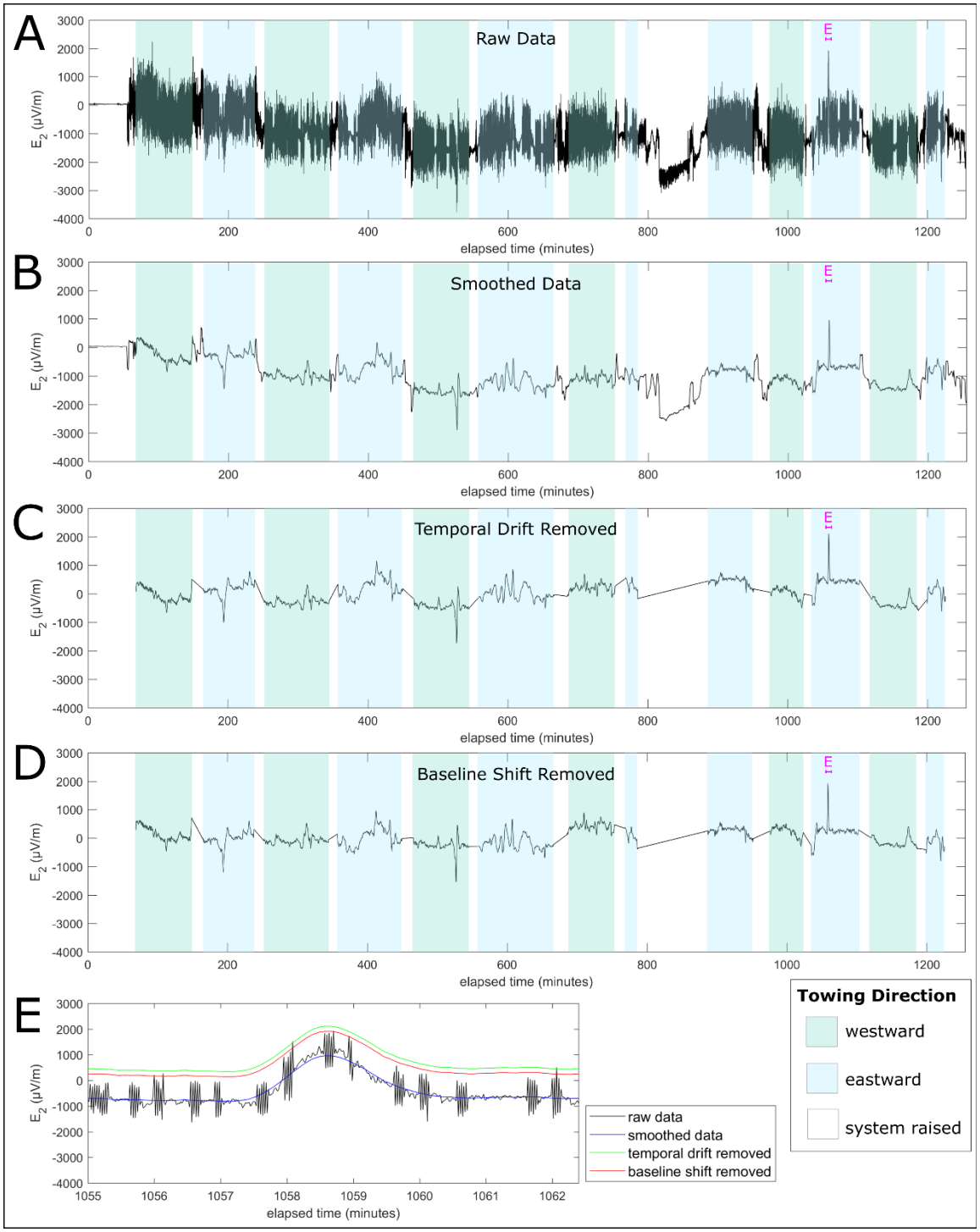

Fig. 14: SP raw data (A), after downsampling (B), drift correction (C) and removing of baseline shift (D). Subplot (E) shows a zoom into a short time segment with time series after the various processing steps.

raised to a height of 100 m above the seafloor and kept at this height for 5 minutes to measure the background noise without any geologic signal from the seafloor. These periods were used as control points to correct for temporal electrode drift.

Voltages were recorded by the two pairs of electrodes every 1 second. The voltages measured by the electrode pairs were converted to electric fields, E1 and E2, by dividing by the separation distance of the electrodes (4.3 m). Tilt sensors attached to the frame show that pitch and roll were on average 1.2° (± 4.0°@ 2σ) and 2.4° (± 4.4°@ 2σ) respectively; since the tilt angles were small at all times, E1 and E2 are effectively horizontal.

The data were smoothed using a moving average with a window size of 60 seconds to remove oscillations in the data caused by the transmitter from the EM experiment which was being carried out simultaneously. A temporal electrode drift curve was calculated by fitting a 2nd order polynomial through the control points when the system was high in the water column and removed from the data. When the ship winch was moving the system up or down in the water column, the vertical movement produced electrical noise; thus the data during vertical instrument movement were trimmed. For the E-W profiles, an overall shift was apparent in the data from the eastward-towed lines versus the westward-towed lines, with the eastward-towed lines showing fields on average 222 mV/m higher than the westward-towed lines for E1 and 397 mV/m higher for E2. We are currently unsure of the exact cause of this shift. To remove this effect, the data from the east-towed and west-towed lines were leveled to each other by subtracting half the average difference from the east-towed lines and adding half the average difference to the west-towed lines for each electrode pair. The data processing steps are summarized in Fig. 14.

Since the system is free to rotate horizontally about the winch cable, E1 and E2 represent arbitrary orthogonal directions at any given time. We calculated the magnitude of the total horizontal field, Eh, which is

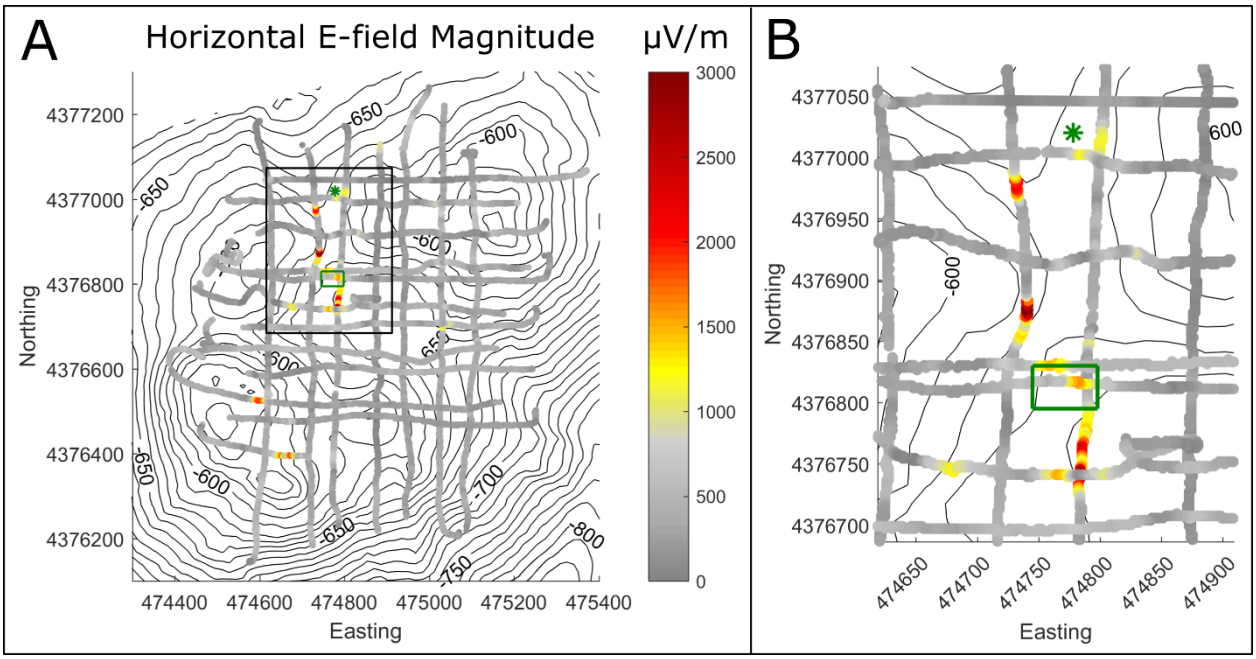

Fig. 15: Magnitude of the horizontal electric field, Eh. The area containing previously drilled massive sulfide samples is indicated by the green rectangle. A gravity core sediment sample containing a thick layer of massive sulfides is indicated by the green asterisk. Bathymetry is indicated by the black contours. A) Full survey area. B) A close-up of the zone around the massive sulfide samples, indicated by the black square in part A.

independent of the orientation of the system. In addition, heading data from an on-board compass were used to calculate the northward and eastward components of the horizontal electric field, referred to as Ex and Ey, respectively.

Several areas at Palinuro were found to have elevated Eh values on the order of 1–3 mV/m, which is an order of magnitude greater than the background Eh values of a few hundred mV/m (Fig. 15). Most of the areas of high Eh values can be spatially correlated with massive sulfide samples collected at Palinuro. Previous shallow drilling has recovered 11 core samples containing massive sulfides in the northwestern part of the crater (Petersen et al., 2014). The location of these drill core samples, indicated by the green bounding box in Figure 3, corresponds spatially with high Eh values on both the N-S and E-W profiles.

On the N-S profiles, high Eh values are seen to occur both to the NW and SE of the drilling site, which is consistent with our working hypothesis that a possible NW-SE trending fault structure can be interpreted from the bathymetry at the drilling site. In addition, high Eh values are observed ~200 m to the north of the drilling site on both the N-S and E-W profiles, located outside of the crater hosting the drilled mineralization. After observing these anomalies in the SP data, a gravity coring device was used to collect samples of seafloor sediment in the area of the anomalies. A gravity corer sample indicated by the green asterisk on Figure 3, located between high Eh values on the N-W profiles and proximal to elevated Eh values on an E-W profile, contained a thick layer (>1 m) of sediments bearing massive sulfides starting at 180 cm below the seafloor. Two additional zones of high Eh values in the SW part of the field area observed on the E-W profiles correspond with areas which were not sampled during this cruise.

5.2. Heatflow

Gero Wetzel & Sven Petersen

Heat-flow measurements were performed using GEOMARs short violin-bow type heat-flow probe (Hyndman et al., 1979, Lister, 1979) which allows multiple, closely spaced penetrations and in-situ thermal conductivity measurements(Fig. 16). The probe used is 3 m long and contains 22 thermistors in the sensor string with a temperature resolution of 1 mK. *In-situ* thermal conductivity is measured with the heat pulse method (Lister, 1979) where the sensor string is heated up for typically 20 to 30 s and the thermal conductivity is derived from the 10 minute long temper. During P509 the data was stored internally in the logger. Transmission of the data in real-time to the vessel was not possible. Due to the known high-sediment temperatures at Palinuro (up to 58°C), the probe was run using the calibration file Mem21260.prb that can be used in the temperature range the -2°C to 60 °C. The complete data reduction scheme for obtaining undisturbed sediment temperatures and in situ thermal conductivities as well as heat-flow values is described in Villinger and Davis (1987).

The probe was deployed from the main deck over the port-side of the ship and was then lowered towards the seafloor using winch W3 with speeds of 1.0 – 1.3m/s. The position of the probe was monitored with a USBL beacon, which was attached to the winch cable at a position 30m above the probe. After reaching predetermined positions the probe was “dropped” for the last 100m to the seafloor “free falling” with winch speeds of 1.2. - 1.4m/s.

After penetration of the probe into the seafloor, a preset measurement cycle was initiated at each station:

1. Measurement of temperatures for about 400s,

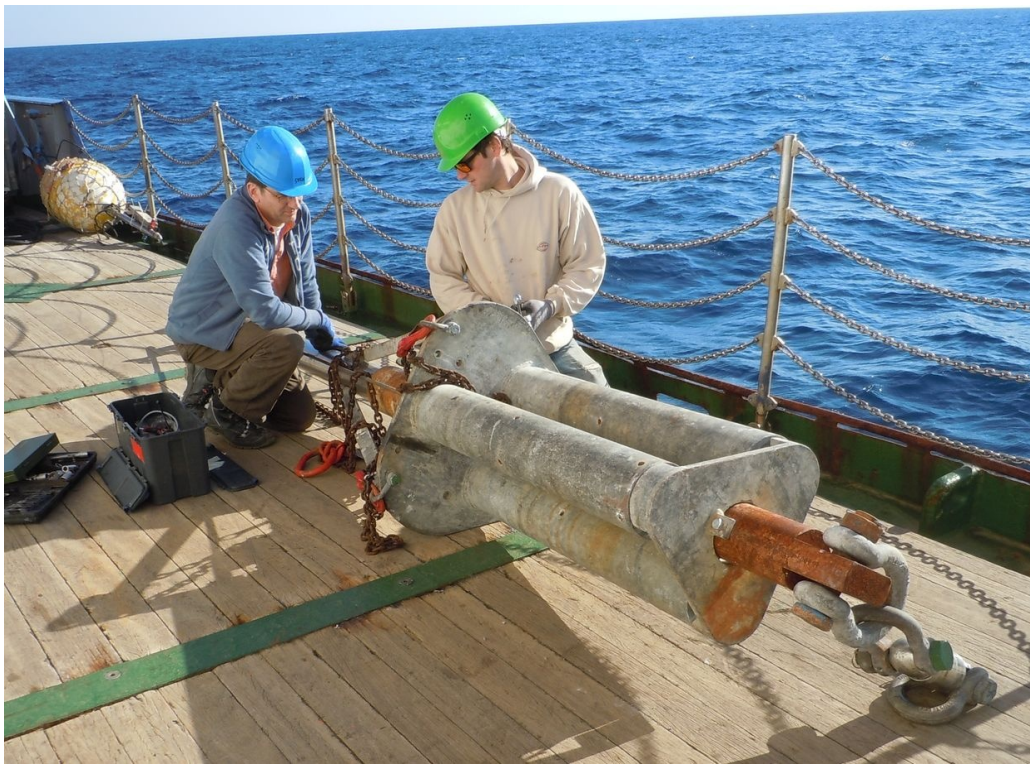

Fig. 16: Preparation of heatflow probe for deployment.

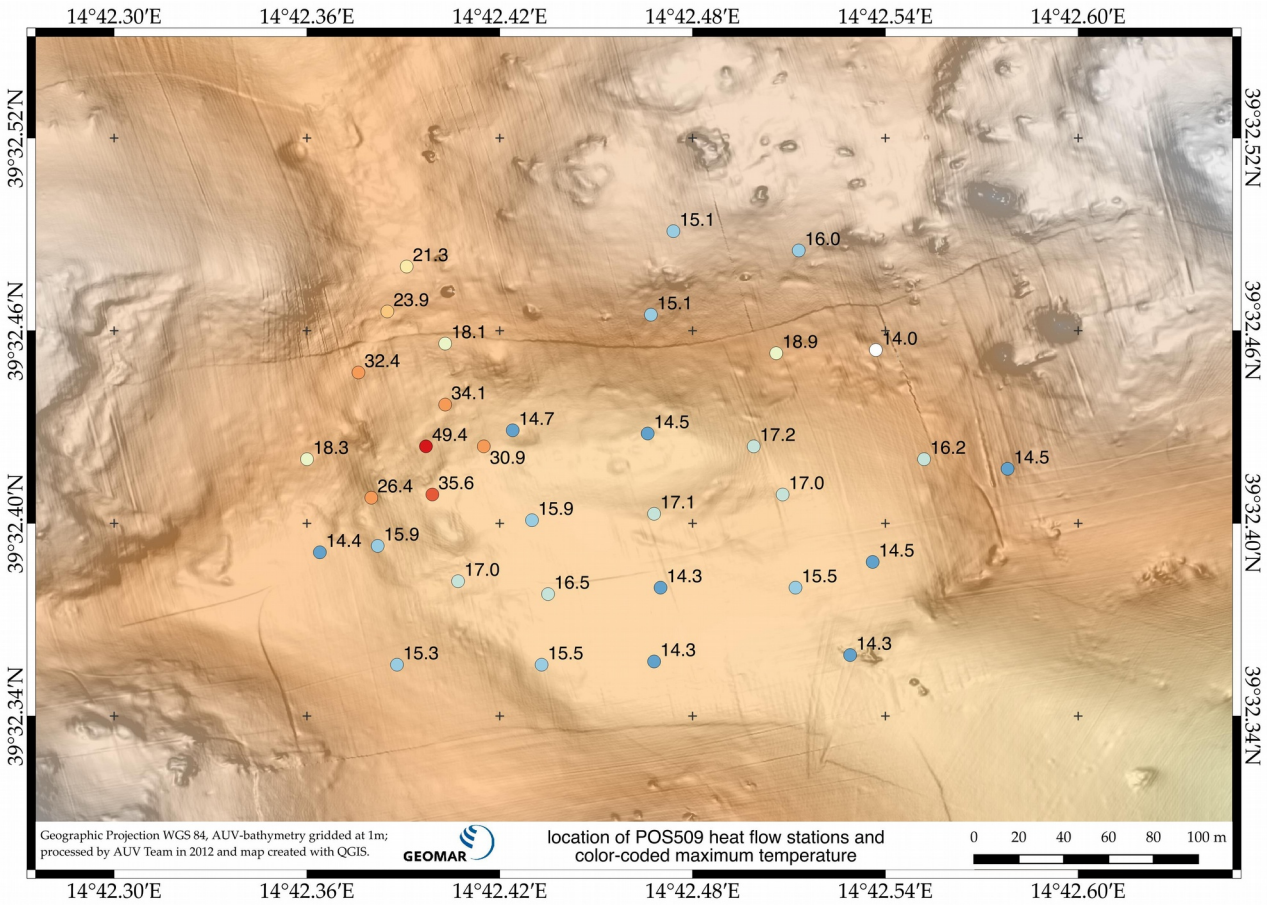

Fig. 17: Station map of measurements with heatflow probe. Colors and numbers at stations indicate the maximum temperature reached at the deepest sensor. Please note that these temperatures are not related to the same depths below seafloor, since the penetration depth at different stations varied between 10cm to at maximum 220cm.

2. generation of heat-pulse with a duration of 30s,
3. measurement of decaying heat-pulse for about 550s.

Thus, a full measurement cycle at each station took about 17min to complete.

Fig. 17 shows the station map together with the maximum temperatures at each station. Measurements with the heat probe were carried out during three deployments at a total of 34 stations, of which 33 acquired temperature measurements and 23 stations acquired thermal conductivity data. One station (HF28) did not penetrate at all. A summary of measurements can be found in the appendix (chap. 9.2, pp. 47). Since the penetration depths varied significantly at different stations, these maximum temperatures do not relate to the same depths below seafloor and, thus, they may not be compared directly. However, from the map it is clearly evident that the highest temperatures of up to 49°C were recorded towards the NW in the vicinity around the drilling sites, where massive sulfides had been found during cruise M73/2 (Petersen et al., 2014). This is close to the known vent fluid exit temperature (Petersen et al., 2008). Additionally, towards the NNE temperatures along the inner rim of the crater also show significantly elevated values of up to 18.9°C. This area coincides with the conductivity anomaly at greater depth, which was found in TEM measurements during the previous cruise POS483 (Hölz et al., 2015). Measurements towards the S and SW show temperatures, which are only slightly elevated (<15.5°C) above the ambient temperature of seawater of ~14.05°C. Still,

this elevation above the temperature of ambient seawater several hundreds of meters away from the mineralized area indicates that hot pore fluids underlie large areas of the depression. This is consistent with the observation of sulfides in some sediment cores, e.g. stations 15GC and 20GC. The distribution of elevated temperatures and heat flow values suggests that the faults rimming the central depression act as fluid pathways. It should be noted, however, that all heat flow values are well above background values. No heat flow stations were performed near gravity corer 23GC (1m of sulfide mud at a depth of 2m) outside the depression due to high seas prohibiting station work on the last working day.

Again, it should be noted that at some of these stations the penetration of the probe only reached a few decimeter.

As an example, we show two data sets of stations with deep penetration, which can be considered to be end-members of the full data set:

shows the data acquired at Station HF11, which is located towards the SW of the crater's center. The maximum temperature at 210cm depth reached 15.3°C, which is about 1.25°C above the ambient temperature of bottom seawater, thus resulting in a temperature gradient of about 0.45K/m. Even though this is well above the average global geothermal gradient (0.3K / 100m), it reflects only minor activity in terms of hydrothermal activity. Thermal conductivites are mainly around 1W/m/K.

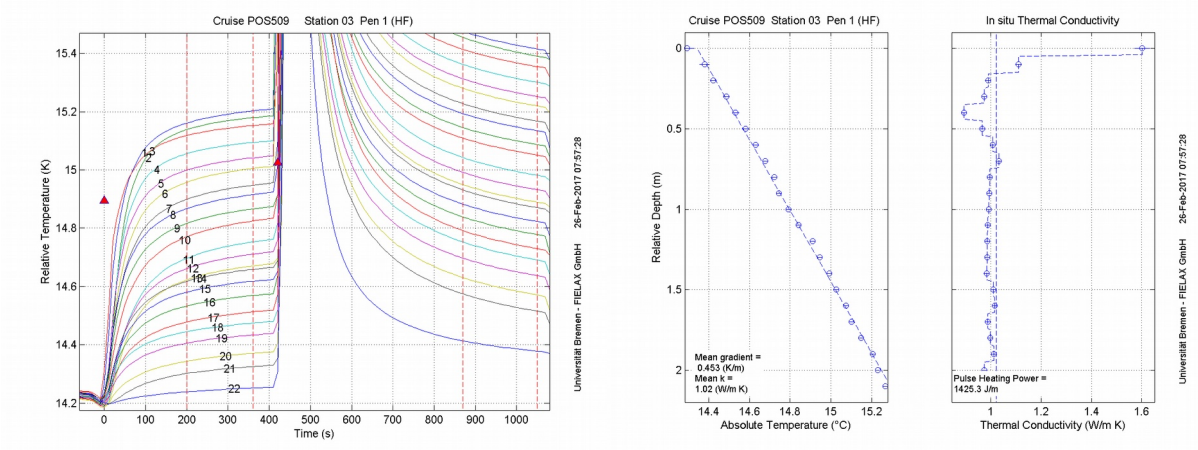

Fig. 18: Measurements at station HF11 with time-series of temperatures measured with the 22 sensors, which penetrated the seafloor (left), profile of equilibrium temperatures measured after ~360s (middle) and the derived thermal conductivity (right).

In comparison, Fig. 19 shows data acquired at Station HF19 which is located just NW of the crater's center in the area where SMS were found in previous drilling. The maximum temperature at 180cm depth reached 47°C, resulting in a temperature gradient of about 15.5K/m and, thus, reflecting the maximum observed activity so far. Looking at temperatures after the heat-pulse (left plot, 600 – 900s) show that temperatures are slightly increasing again, which can only be the case if there is a significant upward migration of fluids. Thermal conductivites are mostly below 1W/m/K.

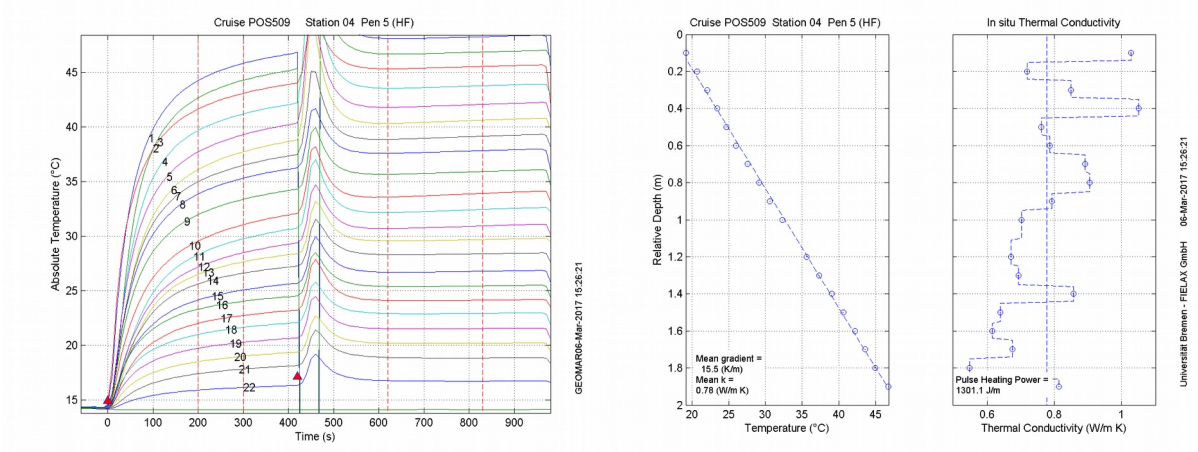

Fig. 19: Measurements at station HF19 with time-series of temperatures (left), profile of equilibrium temperatures measured after ~420s (middle) and the derived thermal conductivity (right).

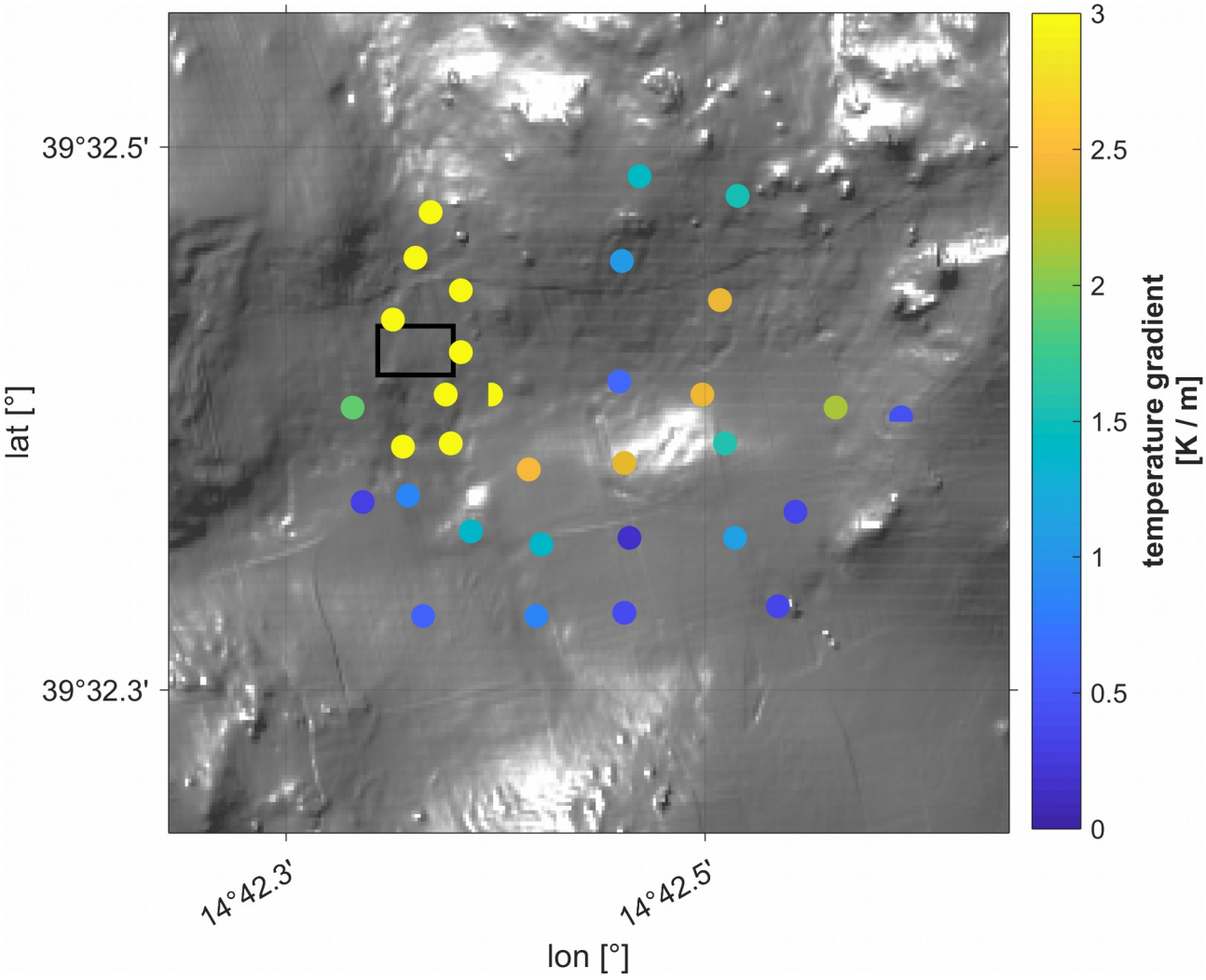

Fig. 20: Map of the thermal gradient with the area of the previous drill sites indicated by a black rectangle. Please note that the colorscale was chosen in a way which allows to distinguish high gradients (>3.0K/m, yellow), intermediate gradients (~2.5K/m, green - orange) and low gradients (<1.5K, blue). Values in the active area are indeed much higher than 3K/m (s. appendix).

Fig. 20 summarizes the present status of the evaluation of heat probe data with a map of the thermal gradient, which highlights the currently active area (yellow) in the vicinity of the previous drilling sites (black square) and a band of stations with elevated gradients (orange) from the center of the crater towards the NNE.

Fig. 21 summarizes measurments of the thermal conductivity. Extreme values are shown at some stations. A first view a the data from these stations indicates that these values are due to the advection of fluids along the probe sensor. Thus, they have to be considered artifacts.

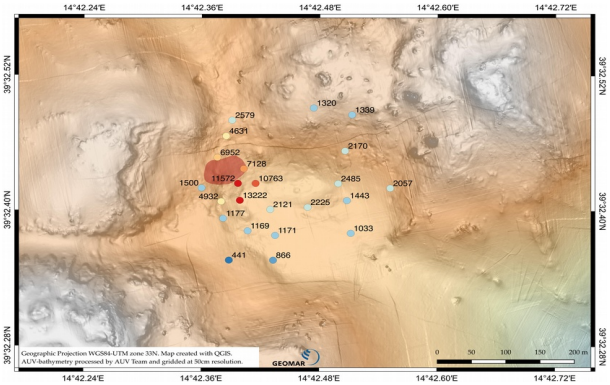

Fig. 21: Thermal conductivity (mW/m2)

5.3. Gravity Coring

Sven Petersen & Sofia Martins

The objective of the sediment sampling of cruise POS509 was to extend the sampling into the central depression and to the east in order to identify compositional and geochemical gradients away from the mineralization by using a 3m gravity corer. Overall 7 gravity core stations (3 m length, 125 mm diameter, 900kg weight on top) were completed during cruise P509 recovering 11.6 m of sediment. One station (23GC) was taken outside the central depression, based on a small self-potential anomaly observed at one of the EM-stations during this cruise.

Core handling

Upon recovery, the first operation was removal of the core catcher and measurement of several parameters (pH, Eh and temperature) with a portable multi-parameter probe (Lange SenSion) in the sediment. The liners containing the sediment were cut into 1 m long sections and the multi-parameter measurements were repeated for the bottom of each core section. The ends of the liner sections were sealed with caps and the sections were transferred to the "wetlab" for further processing. The core sections were split longitudinally using a hand-held, power disc-saw (Fein-Multimaster), opened in two halves, photographed, described and subsampled for pore waters and bulk geochemistry (see below). After subsampling both halves were stored

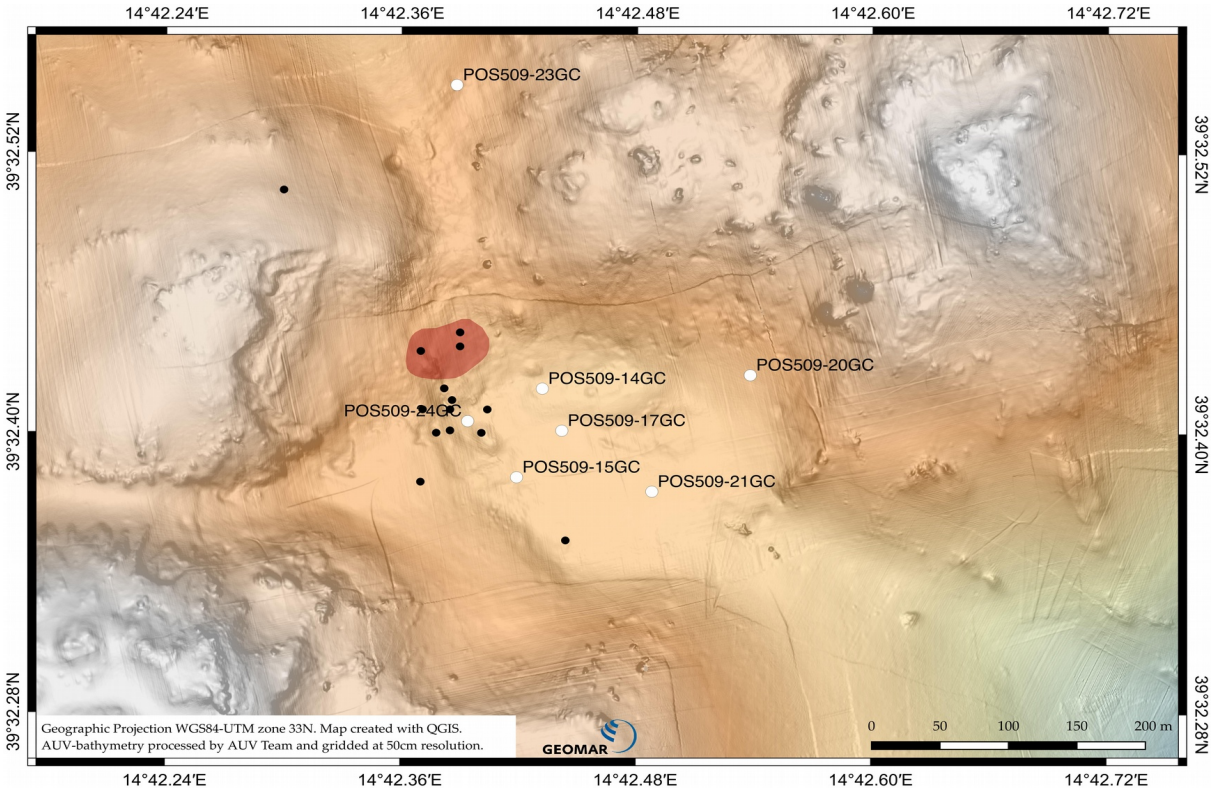

Abbildung 1: Location of sediment cores obtained during P509 (white dots). The mineralized area defined in 2007 during drilling operations is indicated by the red patch. Black dots denote gravity corer stations taken during previous cruises in the area. The underlying AUV-based high-resolution bathymetry was obtained during POS442 (2012) and is gridded at 50cm resolution.

in plastic sleeves and heat-sealed. Working half and archive half will be stored at the core repository of GEOMAR.

Table 1: Summary of gravity corer stations of POS509.

Station	Latitude / Longitude	Water depth	Recovery	Description
POS509/14GC	39°32.419'N / 014°42.432'E	640 m	45 cm	Oxidized sediment overlying coarse-grained volcaniclastics with minor sulfide mud and fine aggregates. T_{max} = 15°C.
POS509/15GC	39°32.381'N / 014°42.419'E	637 m	272 cm	Oxidized sediment overlying coarse-grained volcaniclastics with abundant Mn-oxide mud and fine aggregates; Layers of sulfide sand and massive sulfide mud layers at depth. T_{max} = 17°C.
POS509/17GC	39°32.401'N / 014°42.442'E	636 m	57 cm	Oxidized Fe-stained pelagic sediment overlying reduced clay layer on top of Fe-oxyhydroxide crusts. T_{max} = 15°C.
POS509/20GC	39°32.425'N / 014°42.538'E	628 m	290 cm	Oxdized Fe-stained sediment overlying mottled clay with abundant, diffuse sulfide patches; volcaniclastic material at bottom (below 264cm). T_{max} = 17°C.
POS509/21GC	39°32.375'N / 014°42.488'E	637 m	77 cm	Pelagic sediment with brown staining related to hydrothermal activity; increasingly darker with depth; two discrete dark brown Fe-Mn-rich layers; layered Fe-oxides below 68 cm and in core catcher. T_{max} = 14°C
POS509/23GC	39°32.549'N / 014°42.388'E	620 m	290 cm	Oxidized clay overlying reduced mottled clay overlying thick layer of massive sulfide mud below 180 cm. T_{max} = 15°C.
POS509/24GC	39°32.405'N / 014°42.394'E	635 m	130 cm	Oxidized clay overlying reduced mottled clay overlying sulfide-rich mud with some native sulfur present. T_{max} = 25°C.

Pore fluid extraction

Pore fluids were extracted from the open core using Rhizon Soil Moisture samplers. These samplers consist of a small microporous polymer tube (0.2 µm pore size) that is supported by a stabilizing glass fibre wire and connected to a PVC tube (Seeberg-Elverfeldt *et al*., 2005). The pore water was recovered using negative pressure produced by the attached 20 mL syringes (Luer-Lock connection). Small dead volume (< 0.5 mL) allows sampling of very small volumes of pore water. The applied method permitted extraction of the pore water with minimal disturbance of the sediment. Before usage all Rhizon soil moisture samplers had been thoroughly cleaned and stored in artificial seawater of approximately Mediterranean salinity (36 g salt in 1 L Milli-Q water). Pore fluids sampled with Rhizon samplers are *in-situ* filtrated by principle through the micro-porous membrane. The pore fluids were transferred from the syringe into acid-cleaned 20ml HDPE mini vials. From this pore fluid one aliquot (3 ml) was transferred into an acid-cleaned 3ml HDPE mini vial and acidified with 30 µl concentrated subb. HNO_3. The remaining pore fluid was kept as original

sample without further treatment. A total of 80 pore fluid samples (including method blanks) has been sampled for subsequent analysis on shore.

Analytical methods - sediments

Sediment samples for geochemical analyses have been taken at the same depths as pore fluid samples whenever possible. Sampling was done using 20ml syringes or by using a spatula for hard layers or crusts. Samples were transferred to plastic zip bags. For the determination of bulk chemical composition all sediment samples will be homogenized, dried, milled and dissolved following a multi-step mixed acid protocol. Subsamples will also be analyzed by Neutron Activation in a commercial certified lab (ACTLABS, Canada) for selected trace elements. A total of 93 sediment samples have been stored for subsequent analysis.

In order to better characterize the sample intervals a hand-held colorimeter (Spectrophotometry - CM - Konica Minolta 700d) was used to record the color and visible reflection parameters including the Munsell sediment parameters. The archive half cores were covered with spectrophotometrically tested film (Glad®) to enable contact of the colorimeter sensor. The spots chosen for for subsampling (porefluids and sediments) were also analyzed for pH and Eh using a multi-sensor probe (Lange senSION + portable meter and 50 45 Probe).

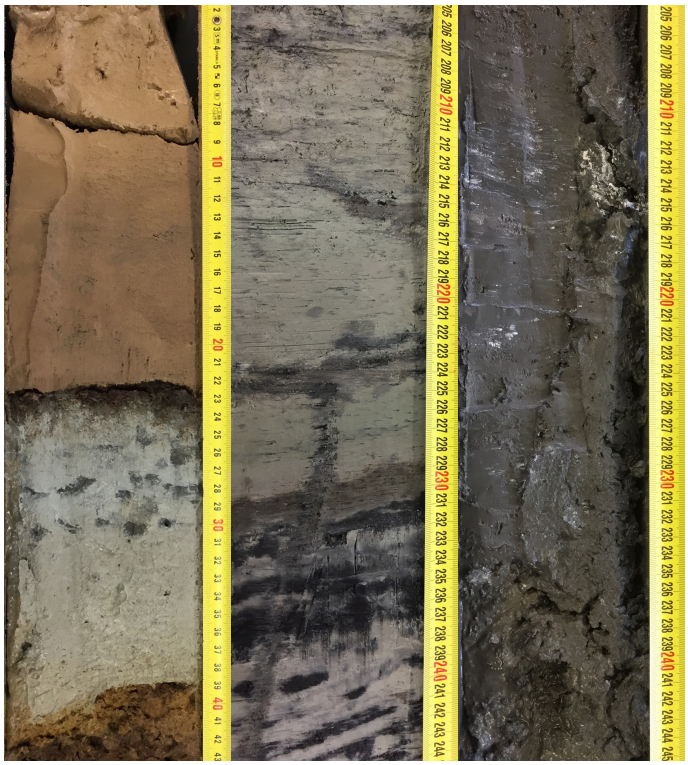

Fig. 22: Examples of sediment cores from the Palinuro Seamount: Left (P509-17GC): oxidzed pelagic sediment overlying reduced clay followed by Fe-oxyhydroxides. Center (P509-20GC): Greenish clay showing diffuse patches of black sulfide mud and a crosscutting soft-sediment vein that stops within the sediment package. Right (P509-23GC): Part of the 1m long black sulfide mud section recovered outside central depression below a clay-rich sediment cover.

Sediment description

The sediments show a large variety in composition and texture (Fig. x2). Cores 17GC and 21GC from the central part of the crater are fully oxidized, whereas the deeper parts of the other cores along the crater wall (14GC, 15GC, and 20GC) are dominated by reduced grey to greenish-grey clay. These cores show intense hydrothermal fluid flow with disseminated patches of sulfide-rich clay, mineralization in stratigraphic layers or along fluid pathways in the soft sediment that cut stratigraphy. Core 24GC was taken close to the area of active fluid venting (ca. 60°C in 2006 and 2007; Petersen et al., 2008) and contains sulfide sand as well as discrete sulfide crusts that were broken during impact and distorted many parts of the core preventing the recovery of intact stratigraphy. Core 23GC, taken outside the depression along a proposed N-S-trending fault, consists of similar grey clay underlain by a thick layer of black, sulfidic material.

5.4. CTD

CTD measurements were carried out using an autonomous microcat CTD sensor from Seabird. Measurements were carried out during the initial release test on the 20th of February and during the 4th and last deployment of the MARTEMIS system on the 28th of February (see Fig. 23).

The initial measurements of the velocity profile (black curve in Fig. 23) were used for the initial calibration of the Posidonia USBL system. A comparison with the profiles obtained during the last deployment of the MARTEMIS system (red curves) shows that there are some differences of velocities in the upper 150m of the profiles, which however should only have a minor effect on the positional accuracy of the system. Variations in the temperature and conductivity in the upper 150m are more pronounced and demonstrate that mixing of water masses is a dynamic process on short time scales in the work area. For the evaluation of EM data the conductivities at greater depth, i.e. close to the transmitter and receivers, is more important and a comparison of the two measurements in Fig. 23 shows that conductivities at greater depth remain essentially constant within the time frame covered during cruise POS509. It is worthwhile to mention that the measured conductivities of ~4.67S/m at greater depth are significantly higher than the ones observed in regular ocean seawater, which is typically in the order of 3S/m. The increase is mainly due to the higher salinity and to a much lesser degree to the relatively warm temperature of seawater in the working area.

Measurements acquired during cruise POS483 in 2015 (Fig. 5.2.1 in Jegen, 2015) show very similar profiles for temperature, conductivity and velocity for greater depth (>200m) as compared to the ones measured during POS509. Thus, it seems evident that for the Palinuro working area these profiles are at least representative for the seawater conditions in spring time, possibly for the whole year.

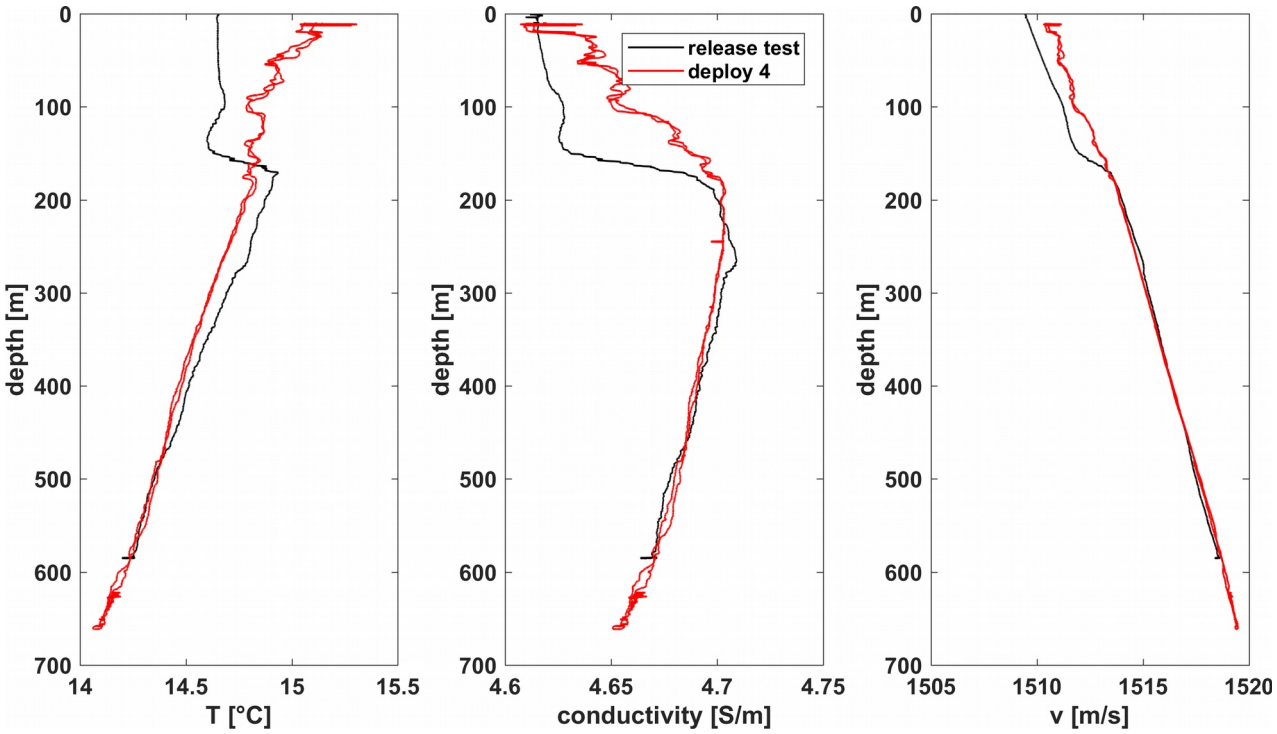

Fig. 23: Temparature, conductivity and velocity profiles acquired during experiments at the Palinuro Seamount (see text for details).

6. Data and Sample Storage and Availability

In Kiel a joint data management team of GEOMAR and Kiel University organizes and supervises data storage and publication by marine science projects in a web-based multi-user system. The geophysical data that has been acquired will be for use of GEOMAR scientists and collaborators only for the first phase and can be made available to other researcher by request to Dr. Sebastian Hölz (shoelz@geomar.de) or Dr. S. Petersen (spetersen@geomar.de). All metadata are immediately available publicly via the GEOMAR portal (https://portal.geomar.de/metadata/leg/show/341041).

In addition the portal provides a single downloadable KML formatted file (portal.geomar.de/metadata/leg/kmlexport/341041) which retrieves and combines up-to-date cruise related information, links to restricted data and to published data for visualization e.g. in Google Earth.

7. Acknowledgments

We would like to thank the crew of *R/V Poseidon* for their excellent support during cruise POS509, especially Captain M. Günther and the bridge for patient help in all organizational matters and excellent ship handling, Bosun Achim Mischker and his deck crew for helping us to optimize the deployment procedure of the MARTEMIS system and handling of our gear, and finally the crew down in the engine for the support in fixing our instruments. We would also like thank the directorate of GEOMAR, who granted substantial financial support for the cruise. Additional financial support was provided through the EU-FP7 project Project: "Breakthrough Solutions for the Sustainable Exploration and Extraction of Deep Sea Mineral Resources", grant number: No. 604500

8. References

Beaulieu, S.E., Baker, E.T., German, C.R., 2015: Where are the undiscovered hydrothermal vents on oceanic spreading ridges? Deep Sea Research Part II,121, 202–212.

Beltenev, V., V. Ivanov, I. Rozhdestvenskaya, G. Cherkashov, T. Stepanova, V. Shilov, A. Pertsev, M. Davydov, I. Egorov, I. Melekestseva, E. Narkevsky, and V. Ignatov, 2007, A new hydrothermal field at 13_30'N on the Mid-Atlantic Ridge: InterRidge News, 16, 9–10.

Bialas, J. (2015). POS484/2, RV POSEIDON - MARSITE: Seismic investigations at the Palinuro volcanic complex, Cruise Report.

Bird, P., 2003: An updated digital model of plate boundaries. Geochem., Geophysics, Geosystems, 4, 1027.

Boschen, R.E., Rowden, A.A., Clark, M.R. & Gardner, J.P.A., 2013: Mining of deep-sea seafloor massive sulfides: A review of the deposits, their benthic communities, impacts from mining, regulatory frameworks and management strategies. Ocean and Coastal Management, 84, 54–67.

Brewitt-Taylor, C., 1975, Self-potential prospecting in the deep oceans: Geology, 3, 541–543.

Cairns, G.W., Evans, R.L. & Edwards, R.N., 1996: A time domain electromagnetic survey of the TAG hydrothermal mound. Geophysical Research Letters, 23, 3455-3458.

Carminati, E., Wortel, M.J.R., Spakman, W. & Sabadini, R., 1998: The role of slab detachment processes in the opening of the western-central Mediterranean basins: Some geological and geophysical evidence. Earth and Planetary Science Letters, 160, 651–665.

Chen, J., Heincke, B., Jegen, M. & Moorkamp, M., 2012: Using empirical mode decomposition to process marine MT data. Geophysical Journal International, 190, 293-309.

Cherkashev, G., V. Ivanov, V. Beltenev, L. Lazareva, I. Rozhdestvenskaya, M. Samovarov, I. Poroshina, M. Sergeev, T. Stepanova, I. Dobretsova, and V. Kuznetsov, 2013, Massive sulfide ores of the northern equatorial Mid-Atlantic Ridge: Oceanology, 53, 607–619.

Cherkashov, G., I. Poroshina, T. Stepanova, V. Ivanov, V. Beltenev, L. Lazareva, I. Rozhdestvenskaya, M. Samovarov, V. Shilov, G. Glasby, Y. Fouquet, and V. Kuznetsov, 2010, Seafloor massive sulfides from the northern equatorial Mid-Atlantic Ridge: New discoveries and perspectives: Marine Georesources & Geotechnology, 28, 222–239.

Corwin, R., 1976, Offshore use of the self-potential method: Geophysical Prospecting, 24, 79–90.

Davis, E.E., Goodfellow, W.D., Bornhold, B.D., Adshead, J., Blaise, B., Villinger, H., Le Cheminant, G.M., 1987: Massive sulfides in a sedimented rift valley, northern Juan de Fuca Ridge. Earth and Planetary Science Letters, 82, 49–61.

de Ronde, C.E.J., Baker, E.T., Massoth, G.J., Lupton, J.E., Wright, I.C., Sparks, R.J., Bannister, S.C., Reyners, M.E., Walker, S.L., Greene, R.R., Ishibashi, J., Faure, K., Resing, J.A. & Lebon, G.T., 2007: Submarine hydrothermal activity along the mid-Kermadec Arc, New Zealand: Large-scale effects on venting. Geochemistry, Geophysics, Geosystems, 8, Q07007.

Evans, R., Webb, S., Jegen, M. & Sananikone K., 1998: Hydrothermal Circulation at the Cleft-Vance Overlapping Spreading Center: Results of a Magnetometric Resistivity Survey. Journal of Geophysical Research, B6, 12, 321-12 338.

German, C.R., Petersen, S. & Hannington, M.D., 2016: Hydrothermal exploration of mid-ocean ridges: Where might the largest sulfide deposits be forming? Chemical Geology, 420, 114–126.

Haase, K.M., Koschinsky, A., Petersen, S., Devey, C.W., German, C., Lackschewitz, K.S., Melchert, B., Seifert, R., Stecher, J., Giere, O., Paulick, H. & the M64/1, M68/1 and M78/2 Scientific Parties, 2009. Diking, young volcanism and diffuse hydrothermal activity on the southern Mid-Atlantic Ridge: the Lilliput field at 9°33'S. Marine Geology, 266, 52-64.

Hannington, M.D., Jamieson, J., Monecke, T. & Petersen, S., 2010: Modern Sea-Floor Massive Sulfides and Base Metal Resources: Toward an Estimate of Global Sea-Floor Massive Sulfide Potential. Economic Geology Special Publication, 15, 317–338.

Hannington M., Jamieson, J., Monecke, T., Petersen, S. & Beaulieu, S., 2011: The abundance of seafloor massive sulfide deposits. Geology, 39, 1155-1158.

Heinson, G., A. White, S. Constable, and K. Key, 1999, Marine self potential exploration: Exploration Geophysics, 30, 1–4.

Heinson, G., A. White, D. Robinson, and N. Fathianpour, 2005, Marine self-potential gradient exploration of the continental margin: Geophysics, 70, G109–G118.

Hölz, S., Swidinsky, A. & Jegen, M., 2013: Investigations on Small Scale Targets with Sputnik, A Two Polarization Transmitter System. Talk with extended abstract during CSEM Workshop (WS09), EAGE, Amsterdam, 16.-19.6.2014.

Hölz, S., Swidinsky, A., Jegen, M. & Bialas, J., 2015a: The use of rotational invariants for the interpretation of marine CSEM data with a case study from the North Alex mud volcano, West Nile Delta. Geophysical Journal International, 1, 224-245.

Hölz, S., Jegen, M., Petersen, S. & Hannington M., 2015b: How to Find Buried and Inactive Seafloor Massive Sulfides using Transient Electromagnetics - A Case Study from the Palinuro Seamount in the Tyrrhenian Sea. Extended abstract for presentation at the Underwater Mining Conference, Tampa Bay, USA, 1.-6.11.2015.

Hyndman, R.D., Davis, E.E., and Wright, J.A., 1979. The measurement of marine geothermal heat flow by a multipenetration probe with digital acoustic telemetry and in situ thermal conductivity, Marine Geophysical Res., 4, 181–205.

Iturrino, G.J., Davis, E., Johnson, J., Groeschel-Becker, H., Lewis, T., Chapman, D. & Cermak, V., 2000: Permeability, electrical and thermal properties of sulfide, sedimentary and basaltic units from the Bent Hill area of Middle Valley, Juan de Fuca ridge. Proceedings of the ODP, Scientific Res., Vol. 169.

Jegen, M. & Edwards, R.N, 1998: The Electrical Properties of a 2D Conductive Zone underneath the Juan de Fuca Ridge, Geophysical Research Letters, 25, 3647.

Jegen-Kulcsar, M., Hobbs, R.W., Tarits, P. & Chave, A., 2009. Joint inversion of marine magnetotelluric and gravity data incorporating seismic constraints: preliminary results of sub-basalt imaging of the Faroe Shelf. Earth and Planetary Science Letters, 282, 47-55.

Jegen, M., Hölz, S., Swidinsky, A. & Brückmann, W., 2011: Quantification of marine sulfide deposits using marine electromagnetic methods. Extended abstract, OCEANS '11 MTS/IEEE Kona, 19.09.-22.09.2011, Kona, Hawaii, USA.

Jegen, M., 2015: EMPAL: Electromagnetic investigation of sedimented Massive Sulphide deposits on the Palinuro Volcanic Complex in the Tyrrhenian Sea. Cruise report for cruise POS483 (RV Poseidon) to the Palinuro Volcanic Complex, Tyrrhenian Sea, 55pp.

Kastens, K., & Mascle, J., 1990: The geological evolution of the Tyrrhenian Sea: An introduction to the scientific results of ODP Leg 107, in Kastens, K.A., and Mascle, J., eds., Proceedings of the Ocean Drilling Program, Scientific Results 107. College Station TX, 3–26.

Kowalczyk, P., 2008. Geophysical prelude to first exploitation of submarine massive sulphides, First Break, 26.

Kraeft, R., 2012: Hydrothermalismus im Tyrrhenischen Meer: Porenwasser-Studien bei Palinuro und Panarea. Unpubl. Diploma thesis, CAU Kiel. 39 pp.

Ligi, M., Cocchi, L., Bortoluzzi, G., D'Oriano, F., Muccini, F., Carartori Tontini, F., de Ronde, C.E.J. & Carmisciano, C., 2014: Mapping of Seafloor Hydrothermally Altered Rocks Using Geophysical Methods: Marsili and Palinuro Seamounts, Southern Tyrrhenian Sea. Economic Geology, 109, 2103-2117.

Lister, C.R.B., 1979. The pulse-probe method of conductivity measurement. Geophys. J. R. Astr. Soc., 57, 451–461.

Minniti, M. & Bonavia, F., 1984: Copper-ore grade hydrothermal mineralization discovered a seamount in the Tyrrhenian Sea (Mediterranean): Is the mineralization related to porphyry-coppers or to base metal lodes?. Marine Geology, 59, 271–282.

Monecke, T., Petersen, S., Lackschewitz, K., Hügler, M., Hannington, M.D. & Gemmell, J.B., 2009: Shallow submarine hydrothermal systems in the Aeolian volcanic arc, Italy. Eos Trans. AGU, 90, 110–111.

Monecke, T., Petersen, S., Hannington, M.D., Samson, I. & Grant, H., 2016: Critical element inventory of seafloor massive sulfide deposits. Reviews in Economic Geology. In press.

Moorkamp, M., Roberts, A. W., Jegen, M. D., Heincke, B. & Hobbs, R. W., 2013: Verification of velocity-resistivity relationship derived from structural joint inversion with borehole data. Geophysical Research Letters, 40, 3596-3601.

Morelli, C., Giese, P., Cassinis, R., Colombi, B., Guerra, I., Luongo, G., Scarascia, S. & Schütte K.G., 1975: Crustal structure of southern Italy: A seismic refraction profile between Puglia–Calabria-Sicily. Bolletino di Geofisica teorica ed applicata, 17, 183–210.

Palacky, G.V., 1987: Resistivity characteristics of geologic targets, in Electromagnetic Methods in Applied Geophysics, Vol. 1, Theory, pp 1351, SEG.

Pertsev, M. Davydov, I. Egorov, I. Melekestseva, E. Narkevsky, and V. Ignatov, 2007, A new hydrothermal field at 13_30'N on the Mid-Atlantic Ridge: InterRidge News, 16, 9–10.

Peters, M., Strauss, H., Petersen, S., Kummer, N.-A. &Thomazo, C., 2011: Hydrothermalism in the Tyrrhenian Sea: Inorganic and microbial sulfur cycling as revealed by geochemical and multiple sulfur isotope data. Chemical Geology, 280, 217–231.

Petersen, S., Herzig, P.M., Kuhn, T., Franz, L., Hannington, M.D., Monecke, T. & Gemmell, J.B., 2005: Shallow Drilling of Seafloor Hydrothermal Systems Using the BGS Rockdrill: Conical Seamount (New Ireland Fore-Arc) and PACMANUS (Eastern Manus Basin), Papua New Guinea. Marine Georesources and Geotechnology, 23, 175–193.

Petersen, S., Monecke, T., Augustin, N., De Benedetti, A. A., Esposito, A., Gärtner, A., et al. (2008). Drilling submarine hydrothermal systems in the Tyrrhenian Sea, Italy. Interridge News 17, 21-23.

Petersen, S., Kuhn, K., Kuhn, T., Augustin, N., Hékinian, R., Franz, L. & Borowski, C., 2009: The geological setting of the ultramafic-hosted Logatchev hydrothermal field (14°45′N, Mid-Atlantic Ridge) and its influence on massive sulfide formation. Lithos, 112, 40–56.

Petersen, S. (ed.), 2014: RV Poseidon Cruise Report POS 442, "AUVinTYS": High-resolution geological investigations of hydrothermal sites in the Tyrrhenian Sea using the AUV "Abyss". GEOMAR, 30 pp.

Petersen, S., Devey, C.W., Walter, M., Jamieson, J.W., Yeo, I., Nakamura, K., Rothenbeck, M., Steinführer, A., & Triebe, L. 2013: AUV-based long-range exploration for hydrothermal activity between 13°-33°S along the Southern Mid-Atlantic Ridge. Proceedings of the Underwater Mining Institute 2013, Rio de Janeiro.

Petersen, S., Monecke, T., Westhues, A., Hannington, M.D., Gemmell, J.B., Sharpe, R., Peters, M., Strauss, H., Lackschewitz, K., Augustin, N., Gibson, H. & Kleeberg, R., 2014: Drilling Shallow-water Massive Sulfides at the Palinuro Volcanic Complex, Aeolian Island Arc, Italy. Economic Geology, 109, 2129-2157.

Savelli, C., 2002: Time-space distribution of magmatic activity in the western Mediterranean and peripheral orogens during the past 30 Ma. Journal of Geodynamics, 34, 99–126.

Seeberg-Elverfeldt, J., Schlüter, M., Feseker, T., & Kölling, M., 2005. Rhizon sampling of pore waters near the sediment/water interface of aquatic systems. Limnology and oceanography: Methods, 3(8), 361-37.

Shilov, V., V. Beltenev, V. Ivanov, G. Cherkashev, I. Rozhdestvenskaya, I. Gablina, I. Dobretsova, E. Narkevskii, A. Gustaitis, and V. Kuznetsov, 2012, New hydrothermal ore fields in the Mid-Atlantic Ridge: Zenith-Victoria (20°08'N) and Petersburg (19°52'N): Doklady Earth Sciences, 442, 63–69.

Sommer, M., Hölz, S., Moorkamp, M., Swidinsky, A., Heincke, B., Scholl, C. & Jegen, M., 2013: GPU parallelization of a three dimensional marine CSEM code. Computers & Geosciences, 58, 91-99.

Swidinsky, A., Hölz, S. & Jegen, M.: On mapping seafloor mineral deposits with central loop transient electromagnetics. Geophysics, 2012, 77, E171-E184.

Swidinsky, A., Hölz, S. & Jegen, M., 2015: Rapid resistivity imaging for marine CSEM surveys with two transmitter polarizations: An application to the North Alex mud volcano. Geophysics, 80, E97-E110.

Thiel, V., Hügler, M., Blümel, M., Baumann, H.I., Gärtner, A., Schmaljohann, R., Strauss, H., Garbe-Schönberg, D., Petersen, S., Cowart, D.A., Fisher, C.R., & Imhoff, J.F., 2012: Widespread occurrence of two carbon fixation pathways in tubeworm endosymbionts: lessons from hydrothermal vent associated tubeworms from the Mediterranean Sea. Frontiers in Microbiology, 3, 423.

Villinger, H., and Davis, E.E., 1987. A new reduction algorithm for marine heat-flow measurements. Journal of Geophysical Research, 92(B12), 12846-12856.

Volz, J., 2013: Hydrothermal imprint on the geochemistry of pore fluids from Palinuro volcanic complex, Tyrrhenian Sea. Unpubl. Bachelor thesis. CAU Kiel. 34 pp.

Von Herzen, R., J. Kirklin, and K. Becker, 1996, Geoelectrical measurements at the TAG hydrothermal mound: Geophysical Research Letters, 23, 3451–3454.

Worzewski, T., Jegen, M., Kopp, H., Brasse, H. & Taylor, W. T. , 2011: Magnetotelluric image of the fluid cycle in the Costa Rican subduction zone, Nature Geoscience, 4, 108-111.

9. Station List POS509

9.1. Station Log

Event	Time [UTC]	Latitude	Longitude	Depth [mbsl]	Gear	Title	Notes
1-1	20.02.17 07:19	39,542200	14,705600	601,4	CTD	in the water	For SVP including releaser test
1-1	20.02.17 07:29	39,542450	14,705417	627,4	CTD	max depth/on ground	
1-1	20.02.17 08:39	39,542867	14,706300	606,9	CTD	on deck	
2-1	20.02.17 09:01	39,540583	14,704217	579,9	POSIDONIA	in the water	Calibration, Transponder
2-1	20.02.17 09:10	39,540533	14,704133	580,4	POSIDONIA	information	Calibration. Not submerged, back on deck, new attempt
2-1	20.02.17 09:22	39,540567	14,704467	581	POSIDONIA	in the water	Calibration, Transponder again
2-1	20.02.17 09:44	39,540417	14,704733	580	POSIDONIA	information	Commence calibration
2-1	20.02.17 10:17	39,540317	14,708417	631	POSIDONIA	information	Calibration ceased, no transponder signal
2-1	20.02.17 14:02	39,541717	14,706900	609,4	POSIDONIA	information	Resume calibration
2-1	20.02.17 15:31	39,542283	14,708333	609,4	POSIDONIA	information	Calibration completed
2-1	20.02.17 15:32	39,542517	14,707933	609,4	POSIDONIA	information	Transponder released
2-1	20.02.17 15:38	39,542250	14,705600	609,4	POSIDONIA	information	Transponder at surface
2-1	20.02.17 15:47	39,541200	14,706483	609,4	POSIDONIA	information	Head buoy on deck
2-1	20.02.17 15:51	39,541467	14,706717	609,4	POSIDONIA	information	Transponder on deck
3-1	20.02.17 16:18	39,539933	14,706167	609,4	OBEM	in the water	RX01 (max sl: 590m)
3-1	20.02.17 16:24	39,540050	14,706000	614,2	OBEM	lowering	
3-1	20.02.17 16:44	39,540000	14,705933	625,3	OBEM	max depth/on ground	
3-1	20.02.17 16:47	39,540017	14,706133	610,2	OBEM	deployed	
3-1	20.02.17 16:57	39,539967	14,705917	623,8	OBEM	information	Releaser on deck
4-1	21.02.17 07:15	39,540317	14,707367	636,6	OBEM	in the water	RX02 (max sl: 610m)
4-1	21.02.17 07:17	39,540233	14,707383	635,2	OBEM	lowering	
4-1	21.02.17 07:31	39,540400	14,707450	635,4	OBEM	max depth/on ground	
4-1	21.02.17 07:43	39,540300	14,707400	635,6	OBEM	deployed	
4-1	21.02.17 07:56	39,540267	14,707283	635,5	OBEM	information	Releaser on deck
5-1	21.02.17 08:16	39,541433	14,706600	615,1	OBEM	in the water	RX03 (max sl: 590m)
5-1	21.02.17 08:19	39,541433	14,706417	596,4	OBEM	lowering	
5-1	21.02.17 08:31	39,541533	14,706633	615	OBEM	max depth/on ground	
5-1	21.02.17 08:37	39,541500	14,706617	622	OBEM	deployed	
5-1	21.02.17 08:48	39,541517	14,706600	614,1	OBEM	information	Releaser on deck
6-1	21.02.17 09:09	39,540083	14,708867	630	OBEM	in the water	RX04 (max sl: 600m)
6-1	21.02.17 09:11	39,540033	14,708883	631,4	OBEM	lowering	
6-1	21.02.17 09:23	39,540100	14,709000	632,1	OBEM	max depth/on ground	
6-1	21.02.17 09:29	39,540117	14,708850	630	OBEM	deployed	
6-1	21.02.17 09:37	39,539983	14,708850	630	OBEM	information	Releaser on deck
7-1	21.02.17 09:56	39,541683	14,709033	592,5	OBEM	in the water	RX05 (max sl: 560m)
7-1	21.02.17 09:56	39,541683	14,709033	587,6	OBEM	lowering	
7-1	21.02.17 10:10	39,541700	14,709167	586,9	OBEM	max depth/on ground	

Event	Time [UTC]	Latitude	Longitude	Depth [mbsl]	Gear	Title	Notes
7-1	21.02.17 10:23	39,541600	14,709033	588,9	OBEM	deployed	
7-1	21.02.17 10:35	39,541433	14,708917	594,3	OBEM	information	Releaser on deck
8-1	21.02.17 10:50	39,537783	14,707533	590,3	OBEM	in the water	RX06 (max sl: 570m)
8-1	21.02.17 10:52	39,537833	14,707483	589,4	OBEM	lowering	
8-1	21.02.17 11:12	39,537883	14,707200	592,8	OBEM	max depth/on ground	
8-1	21.02.17 11:14	39,537750	14,707317	590,6	OBEM	deployed	
8-1	21.02.17 11:24	39,538200	14,707017	597,2	OBEM	information	Releaser on deck
9-1	21.02.17 11:53	39,538600	14,707067	616,5	OBEM	in the water	RX07 (max sl: 600m)
9-1	21.02.17 11:55	39,538650	14,707033	637,9	OBEM	lowering	
9-1	21.02.17 12:15	39,538633	14,707033	625,8	OBEM	max depth/on ground	
9-1	21.02.17 12:18	39,538583	14,707117	613,2	OBEM	deployed	
9-1	21.02.17 12:26	39,538667	14,707400	630,9	OBEM	information	Releaser on deck
10-1	21.02.17 12:42	39,539167	14,707933	634	OBEM	in the water	RX08 (max sl: 610m)
10-1	21.02.17 12:43	39,539100	14,707950	633,5	OBEM	lowering	
10-1	21.02.17 13:02	39,539450	14,707900	633,9	OBEM	max depth/on ground	
10-1	21.02.17 13:07	39,539250	14,708217	636,1	OBEM	deployed	
10-1	21.02.17 13:15	39,539367	14,708200	634	OBEM	information	Releaser on deck
11-1	21.02.17 13:37	39,543317	14,710967	585,6	OBEM	in the water	RX02 (max sl: 570m)
11-1	21.02.17 13:40	39,543400	14,711033	587,9	OBEM	lowering	
11-1	21.02.17 13:58	39,543433	14,711033	588,5	OBEM	max depth/on ground	
11-1	21.02.17 14:01	39,543233	14,710867	585,9	OBEM	deployed	
11-1	21.02.17 14:06	39,543450	14,710633	588,1	OBEM	information	Releaser on deck
12-1	21.02.17 14:39	39,540050	14,706917	627,7	Heat Flow	in the water	
12-1	21.02.17 14:41	39,540033	14,707017	633,9	Heat Flow	lowering	
12-1	21.02.17 15:00	39,540183	14,706933	633,7	Heat Flow	max depth/on ground	BoKo = 659 m , SLmax = 665 m
12-1	21.02.17 15:17	39,540033	14,706967	632,4	Heat Flow	hoisting	
12-2	21.02.17 15:31	39,539633	14,706717	626	Heat Flow	lowering	
12-2	21.02.17 15:37	39,539700	14,706783	624,1	Heat Flow	max depth/on ground	BoKo= 657m, SLmax= 662m
12-2	21.02.17 15:51	39,539683	14,706750	624,5	Heat Flow	hoisting	
12-2	21.02.17 15:59	39,539783	14,706850	625,6	Heat Flow	on deck	
12-3	22.02.17 07:05	39,539683	14,707283	632,4	Heat Flow	in the water	
12-3	22.02.17 07:22	39,539617	14,707217	638	Heat Flow	lowering	
12-3	22.02.17 07:37	39,539650	14,707017	626,6	Heat Flow	max depth/on ground	660 m max
12-3	22.02.17 07:54	39,539650	14,707033	637,5	Heat Flow	hoisting	
12-4	22.02.17 08:03	39,539633	14,707617	633,5	Heat Flow	lowering	
12-4	22.02.17 08:06	39,539683	14,707667	638,3	Heat Flow	max depth/on ground	661 m max
12-4	22.02.17 08:23	39,539683	14,707583	632,3	Heat Flow	hoisting	
12-5	22.02.17 08:35	39,539283	14,707033	633,5	Heat Flow	lowering	
12-5	22.02.17 08:40	39,539250	14,706983	634,1	Heat Flow	max depth/on ground	657 m max
12-5	22.02.17 08:58	39,539317	14,706950	629,6	Heat Flow	hoisting	
12-6	22.02.17 09:04	39,539300	14,707550	634,3	Heat Flow	lowering	
12-6	22.02.17 09:13	39,539300	14,707617	634	Heat Flow	max depth/on ground	660 m max

Event	Time [UTC]	Latitude	Longitude	Depth [mbsl]	Gear	Title	Notes
12-6	22.02.17 09:30	39,539183	14,707533	634,2	Heat Flow	hoisting	
12-7	22.02.17 09:44	39,540067	14,707567	633,6	Heat Flow	lowering	
12-7	22.02.17 09:50	39,540033	14,707567	633,5	Heat Flow	max depth/on ground	661 m max
12-7	22.02.17 10:07	39,540067	14,707567	633,9	Heat Flow	hoisting	
12-8	22.02.17 10:16	39,540500	14,707550	637,6	Heat Flow	lowering	
12-8	22.02.17 10:23	39,540483	14,707583	634,8	Heat Flow	max depth/on ground	663 m max
12-8	22.02.17 10:39	39,540417	14,707550	635,7	Heat Flow	hoisting	
12-9	22.02.17 10:53	39,541083	14,707600	621,4	Heat Flow	lowering	
12-9	22.02.17 10:59	39,541050	14,707550	615,6	Heat Flow	max depth/on ground	SLmax = 645 m
12-9	22.02.17 11:16	39,541017	14,707550	613,7	Heat Flow	hoisting	
12-10	22.02.17 11:33	39,540517	14,706867	625,1	Heat Flow	lowering	
12-10	22.02.17 11:39	39,540517	14,706933	628	Heat Flow	max depth/on ground	SL max = 658m
12-10	22.02.17 11:56	39,540517	14,706917	624,4	Heat Flow	hoisting	
12-10	22.02.17 12:17	39,540650	14,705500	583,8	Heat Flow	on deck	
13-1	22.02.17 13:04	39,540317	14,707283	633,7	Gravity Corer | GC	in the water	
13-1	22.02.17 13:30	39,540317	14,707200	633,6	Gravity Corer | GC	max depth/on ground	SL max: 667 m
13-1	22.02.17 13:32	39,540283	14,707183	632,9	Gravity Corer | GC	hoisting	
13-1	22.02.17 13:46	39,540450	14,706200	623,8	Gravity Corer | GC	on deck	
14-1	22.02.17 14:10	39,539700	14,706983	627,3	Gravity Corer | GC	in the water	
14-1	22.02.17 14:28	39,539617	14,706817	625,6	Gravity Corer | GC	max depth/on ground	SL max = 664 m
14-1	22.02.17 14:30	39,539700	14,706950	630,8	Gravity Corer | GC	hoisting	
14-1	22.02.17 14:45	39,539250	14,705917	594,9	Gravity Corer | GC	on deck	
15-1	23.02.17 07:53	39,539017	14,707433	617,3	CSEM (MARTEMIS)	in the water	
15-1	23.02.17 08:50	39,539050	14,707300	637,7	CSEM	max depth/on ground	250 m max
15-1	23.02.17 08:53	39,539050	14,707250	636,4	CSEM	profile start	test circles
15-1	23.02.17 11:04	39,539467	14,712200	633,7	CSEM	profile end	
15-1	23.02.17 11:08	39,539450	14,712167	645,6	CSEM	information	lowering to SL max 600m
15-1	23.02.17 11:25	39,539283	14,711717	656,3	CSEM	max depth/on ground	SL max = 640m
15-1	23.02.17 11:27	39,539317	14,711717	648,3	CSEM	information	hoisting
15-1	23.02.17 11:55	39,539300	14,711967	661,5	CSEM	on deck	
16-1	23.02.17 17:10	39,543300	14,710333	581,6	CSEM	in the water	
16-1	23.02.17 19:24	39,543050	14,709617	594,1	CSEM	max depth/on ground	max 570m
16-1	23.02.17 19:27	39,543033	14,709617	594,4	CSEM	profile start	
16-1	24.02.17 10:06	39,534150	14,704250	662,7	CSEM	profile end	
16-1	24.02.17 11:11	39,533833	14,705167	712,5	CSEM	on deck	
17-1	24.02.17 12:01	39,540083	14,707500	633,3	Gravity Corer | GC	in the water	

Event	Time [UTC]	Latitude	Longitude	Depth [mbsl]	Gear	Title	Notes
17-1	24.02.17 12:22	39,539833	14,707417	634	Gravity Corer | GC	max depth/on ground	SL max = 664 m
17-1	24.02.17 12:23	39,539850	14,707400	632,8	Gravity Corer | GC	hoisting	
17-1	24.02.17 12:37	39,539833	14,707767	634,6	Gravity Corer | GC	on deck	
18-1	24.02.17 13:00	39,539200	14,706400	604,8	Heat Flow	in the water	
18-1	24.02.17 13:02	39,539117	14,706417	627,8	Heat Flow	lowering	
18-1	24.02.17 13:15	39,539050	14,706500	599,5	Heat Flow	max depth/on ground	SL max = 651 m
18-1	24.02.17 13:32	39,539083	14,706433	605,5	Heat Flow	hoisting	
18-2	24.02.17 13:57	39,539533	14,706017	623,8	Heat Flow	lowering	
18-2	24.02.17 14:01	39,539667	14,706050	625,2	Heat Flow	max depth/on ground	SL max = 653 m
18-2	24.02.17 14:18	39,539733	14,706150	623,9	Heat Flow	hoisting	
18-3	24.02.17 14:23	39,539850	14,706383	625	Heat Flow	lowering	
18-3	24.02.17 14:27	39,539950	14,706333	623,5	Heat Flow	max depth/on ground	SL max = 658 m
18-3	24.02.17 14:44	39,539833	14,706483	625,4	Heat Flow	hoisting	
18-4	24.02.17 15:17	39,540217	14,705983	622,4	Heat Flow	lowering	
18-4	24.02.17 15:21	39,540200	14,705950	624,9	Heat Flow	max depth/on ground	boko= 650m, SLmax= 654m
18-4	24.02.17 15:37	39,540233	14,705883	623,9	Heat Flow	hoisting	
18-5	24.02.17 16:01	39,540583	14,706117	623,7	Heat Flow	lowering	
18-5	24.02.17 16:10	39,540400	14,705917	624,1	Heat Flow	hoisting	interrupted due to weather conditions
18-5	24.02.17 16:25	39,540167	14,706817	633	Heat Flow	on deck	
18-6	25.02.17 07:02	39,540750	14,706133	614	Heat Flow	in the water	
18-6	25.02.17 07:16	39,540617	14,706117	602,2	Heat Flow	max depth/on ground	649 m max
18-6	25.02.17 07:32	39,540667	14,706150	604,9	Heat Flow	hoisting	
18-7	25.02.17 07:42	39,541150	14,706350	601,7	Heat Flow	lowering	
18-7	25.02.17 07:46	39,541200	14,706333	600,8	Heat Flow	max depth/on ground	644 m max
18-7	25.02.17 08:02	39,541217	14,706350	596,8	Heat Flow	hoisting	
18-8	25.02.17 08:17	39,540867	14,706550	613,3	Heat Flow	lowering	
18-8	25.02.17 08:21	39,540817	14,706550	611,2	Heat Flow	max depth/on ground	652 m max
18-8	25.02.17 08:37	39,540800	14,706500	616,9	Heat Flow	hoisting	
18-9	25.02.17 08:49	39,540450	14,706533	623,7	Heat Flow	lowering	
18-9	25.02.17 08:53	39,540533	14,706517	618	Heat Flow	max depth/on ground	658 m max
18-9	25.02.17 09:09	39,540483	14,706533	613,7	Heat Flow	hoisting	
18-10	25.02.17 09:22	39,540233	14,706400	625,5	Heat Flow	lowering	
18-10	25.02.17 09:25	39,540300	14,706450	625,4	Heat Flow	max depth/on ground	Boko=655m, SLmax= 660m
18-10	25.02.17 09:41	39,540283	14,706367	623,2	Heat Flow	hoisting	
18-11	25.02.17 09:54	39,540000	14,706483	623,1	Heat Flow	lowering	
18-11	25.02.17 09:56	39,540017	14,706450	627,1	Heat Flow	max depth/on ground	663 m max
18-11	25.02.17 10:12	39,540067	14,706567	625,5	Heat Flow	hoisting	
18-12	25.02.17 10:59	39,539550	14,708083	633,7	Heat Flow	lowering	
18-12	25.02.17 11:03	39,539667	14,708333	634,7	Heat Flow	max depth/on	SL max = 662 m

Event	Time [UTC]	Latitude	Longitude	Depth [mbsl]	Gear	Title	Notes
						ground	
18-12	25.02.17 11:19	39,539400	14,708383	634,2	Heat Flow	hoisting	
18-13	25.02.17 11:31	39,540450	14,708333	635,9	Heat Flow	lowering	
18-13	25.02.17 11:34	39,540333	14,708100	637,4	Heat Flow	max depth/on ground	SLmax = 662 m
18-13	25.02.17 11:50	39,540533	14,708150	635,3	Heat Flow	hoisting	
18-14	25.02.17 11:58	39,540950	14,708317	620,6	Heat Flow	lowering	
18-14	25.02.17 12:01	39,540867	14,708250	635,2	Heat Flow	max depth/on ground	SL max = 662 m
18-14	25.02.17 12:17	39,540733	14,708200	637,2	Heat Flow	hoisting	
18-14	25.02.17 12:32	39,540700	14,708033	636,5	Heat Flow	on deck	
19-1	25.02.17 12:47	39,540333	14,708667	630,5	Gravity Corer | GC	in the water	
19-1	25.02.17 13:02	39,540367	14,708733	630,7	Gravity Corer | GC	max depth/on ground	SL max = 656 m
19-1	25.02.17 13:15	39,540117	14,708533	634,8	Gravity Corer | GC	on deck	
20-1	25.02.17 13:49	39,539483	14,707900	634	Gravity Corer | GC	in the water	
20-1	25.02.17 14:04	39,539567	14,707900	633,8	Gravity Corer | GC	max depth/on ground	SL max = 665 m
20-1	25.02.17 14:17	39,539267	14,707033	634,5	Gravity Corer | GC	on deck	
21-1	26.02.17 08:02	39,543533	14,714450	634,5	CSEM (MARTEMIS)	in the water	
21-1	26.02.17 09:13	39,542700	14,712883	609,4	CSEM	max depth/on ground	614 m max
21-1	26.02.17 09:25	39,542533	14,711667	583,3	CSEM	profile start	
21-1	27.02.17 04:30	39,536967	14,706483	597,2	CSEM	profile end	
21-1	27.02.17 05:17	39,536283	14,706533	599,7	CSEM	on deck	
22-1	27.02.17 06:59	39,542350	14,706317	620,5	Gravity Corer | GC	in the water	
22-1	27.02.17 07:14	39,542500	14,706250	617,6	Gravity Corer | GC	max depth/on ground	647 m max
22-1	27.02.17 07:26	39,542583	14,706050	618,7	Gravity Corer | GC	on deck	
23-1	27.02.17 07:53	39,540067	14,706233	621,8	Gravity Corer | GC	in the water	
23-1	27.02.17 08:07	39,540067	14,706333	618,4	Gravity Corer | GC	max depth/on ground	663 m max
23-1	27.02.17 08:18	39,540067	14,706167	623,5	Gravity Corer | GC	on deck	
24-1	27.02.17 08:43	39,539300	14,708667	635,2	Heat Flow	in the water	
24-1	27.02.17 08:59	39,539333	14,708617	634,4	Heat Flow	max depth/on ground	669 m max
24-1	27.02.17 09:16	39,539250	14,708683	638,7	Heat Flow	hoisting	
24-2	27.02.17 09:30	39,539817	14,708800	636,7	Heat Flow	lowering	
24-2	27.02.17 09:32	39,539800	14,708717	631,4	Heat Flow	max depth/on ground	663 m max
24-2	27.02.17 09:48	39,539717	14,708683	633,3	Heat Flow	hoisting	
24-3	27.02.17 10:01	39,540333	14,709367	634,7	Heat Flow	lowering	
24-3	27.02.17 10:04	39,540267	14,709400	632	Heat Flow	max depth/on ground	643 m max

Event	Time [UTC]	Latitude	Longitude	Depth [mbsl]	Gear	Title	Notes
24-3	27.02.17 10:20	39,540283	14,709383	633,2	Heat Flow	hoisting	
24-4	27.02.17 11:10	39,540317	14,708750	628,6	Heat Flow	lowering	
24-4	27.02.17 11:16	39,540333	14,709050	631,2	Heat Flow	max depth/on ground	SL max = 654 m
24-4	27.02.17 11:31	39,540417	14,708967	631,2	Heat Flow	hoisting	
24-5	27.02.17 11:50	39,540800	14,708833	615,9	Heat Flow	lowering	
24-5	27.02.17 12:16	39,540117	14,708250	638,9	Heat Flow	max depth/on ground	SL max = 660 m
24-5	27.02.17 12:33	39,540150	14,708000	634,5	Heat Flow	hoisting	
24-6	27.02.17 12:53	39,540267	14,706750	625,4	Heat Flow	lowering	
24-6	27.02.17 12:56	39,540350	14,706633	624,6	Heat Flow	max depth/on ground	SL max = 664 m
24-6	27.02.17 13:15	39,540417	14,706583	622,7	Heat Flow	hoisting	
24-7	27.02.17 13:24	39,540050	14,706383	623,1	Heat Flow	lowering	
24-7	27.02.17 13:30	39,539733	14,706100	621,7	Heat Flow	max depth/on ground	SL max = 656 m
24-7	27.02.17 13:46	39,539883	14,705967	619,5	Heat Flow	hoisting	
24-8	27.02.17 14:02	39,541083	14,706317	601,4	Heat Flow	lowering	
24-8	27.02.17 14:06	39,540967	14,706133	598,2	Heat Flow	max depth/on ground	SL max = 649 m
24-8	27.02.17 14:22	39,541217	14,706450	617,9	Heat Flow	hoisting	
24-9	27.02.17 14:36	39,541483	14,707567	616,1	Heat Flow	lowering	
24-9	27.02.17 14:39	39,541417	14,707633	623,1	Heat Flow	max depth/on ground	SL max = 625 m
24-9	27.02.17 14:55	39,541467	14,707767	595,9	Heat Flow	hoisting	
24-10	27.02.17 15:04	39,541500	14,708517	590,8	Heat Flow	lowering	
24-10	27.02.17 15:10	39,541433	14,708350	600,3	Heat Flow	max depth/on ground	SL max= 630m
24-10	27.02.17 15:26	39,541333	14,708317	599,4	Heat Flow	hoisting	
24-10	27.02.17 15:43	39,541283	14,708350	597,5	Heat Flow	on deck	
25-1	28.02.17 05:41	39,544917	14,712167	625,9	OBEM	information	RX05 released
25-1	28.02.17 05:52	39,543867	14,711117	625,9	OBEM	at surface	RX05
25-1	28.02.17 06:02	39,541683	14,709517	625,9	OBEM	on deck	RX05
26-1	28.02.17 06:17	39,543167	14,709883	625,9	OBEM	information	RX04 released
26-1	28.02.17 06:22	39,542683	14,709583	625,9	OBEM	at surface	RX04
26-1	28.02.17 06:30	39,540667	14,710100	625,9	OBEM	on deck	RX04
27-1	28.02.17 06:59	39,543067	14,707667	625,9	OBEM	information	RX03 released
27-1	28.02.17 07:07	39,543233	14,707950	625,9	OBEM	at surface	RX03
27-1	28.02.17 07:16	39,541217	14,707283	625,9	OBEM	on deck	RX03
28-1	28.02.17 07:25	39,541567	14,707850	625,9	OBEM	information	RX02 released
28-1	28.02.17 07:32	39,542200	14,708350	625,9	OBEM	at surface	RX02
28-1	28.02.17 07:42	39,540700	14,708450	625,9	OBEM	on deck	RX02
29-1	28.02.17 07:50	39,541233	14,709067	625,9	OBEM	information	RX01 released
29-1	28.02.17 08:00	39,541400	14,708067	625,9	OBEM	at surface	RX01
29-1	28.02.17 08:08	39,539983	14,707950	625,9	OBEM	on deck	RX01
30-1	28.02.17 08:20	39,541033	14,708883	625,9	OBEM	information	RX08 released
30-1	28.02.17 08:25	39,541283	14,708867	625,9	OBEM	at surface	RX08
30-1	28.02.17 08:33	39,539900	14,709017	625,9	OBEM	on deck	RX08
31-1	28.02.17 08:39	39,540283	14,709433	625,9	OBEM	information	RX07 released
31-1	28.02.17 08:48	39,540650	14,709017	625,9	OBEM	at surface	RX07
31-1	28.02.17 08:56	39,539833	14,708117	625,9	OBEM	on deck	RX07
32-1	28.02.17 09:02	39,540500	14,707950	625,9	OBEM	information	RX06 released

Event	Time [UTC]	Latitude	Longitude	Depth [mbsl]	Gear	Title	Notes
32-1	28.02.17 09:12	39,540700	14,708583	625,9	OBEM	at surface	RX06
32-1	28.02.17 09:20	39,539450	14,709000	625,9	OBEM	on deck	RX06
33-1	28.02.17 14:32	39,544683	14,712850	620,1	CSEM (MARTEMIS)	in the water	
33-1	28.02.17 15:31	39,546100	14,710900	640	CSEM	max depth/on ground	SL max= 645m
33-1	28.02.17 15:57	39,545367	14,710917	625,9	CSEM	profile start	
33-1	28.02.17 16:45	39,543283	14,713833	619,2	CSEM	information	interrupted due to technical problem
33-1	28.02.17 18:50	39,542983	14,713633	626,1	CSEM	on deck	
34-1	01.03.17 07:15	39,544467	14,715083	648	CSEM	information	RX09 released
34-1	01.03.17 07:25	39,544883	14,714400	648	CSEM	at surface	RX09
34-1	01.03.17 07:34	39,542917	14,715283	648	CSEM	on deck	RX09
35-1	02.03.17 07:11	37,677117	15,296517	624,9	OBT	information	released
35-1	02.03.17 07:14	37,676900	15,296367	624,9	OBT	information	at surface
35-1	02.03.17 07:21	37,674817	15,296217	624,9	OBT	information	on deck
37-1	02.03.17 07:28	37,674650	15,296183	624,9	OBT	information	at surface
36-1	02.03.17 07:28	37,674633	15,296167	624,9	OBT	information	released
36-1	02.03.17 07:34	37,674367	15,295933	624,9	OBT	information	on deck
37-1	02.03.17 07:36	37,674150	15,295817	624,9	OBT	information	released
36-1	02.03.17 07:42	37,673300	15,295217	624,9	OBT	information	at surface
37-1	02.03.17 07:53	37,671583	15,292883	624,9	OBT	information	on deck
38-1	02.03.17 08:55	37,560983	15,259900	624,9	OBS	released	
38-1	02.03.17 09:15	37,560533	15,257433	624,9	OBS	information	at surface
38-1	02.03.17 09:23	37,557900	15,258567	624,9	OBS	information	on deck
39-1	02.03.17 09:41	37,549183	15,254183	624,9	OBS	released	
39-1	02.03.17 09:54	37,548467	15,253283	624,9	OBS	information	at surface
39-1	02.03.17 10:03	37,546150	15,254083	624,9	OBS	information	on deck
40-1	02.03.17 10:24	37,548533	15,275267	624,9	OBS	released	
40-1	02.03.17 10:39	37,548033	15,274650	624,9	OBS	information	at surface
40-1	02.03.17 10:49	37,545200	15,277000	624,9	OBS	information	on deck
41-1	02.03.17 11:32	37,534100	15,272617	624,9	OBS	released	
41-1	02.03.17 11:54	37,533017	15,271583	624,9	OBS	information	at surface
41-1	02.03.17 12:04	37,531400	15,273800	624,9	OBS	information	on deck
42-1	02.03.17 12:22	37,536250	15,259500	624,9	OBS	released	
42-1	02.03.17 12:40	37,535683	15,259067	624,9	OBS	information	at surface
42-1	02.03.17 12:48	37,534267	15,256967	624,9	OBS	information	on deck
43-1	02.03.17 13:09	37,545950	15,230567	624,9	OBS	released	
43-1	02.03.17 13:20	37,545617	15,230133	624,9	OBS	information	at surface
43-1	02.03.17 13:30	37,542300	15,231033	624,9	OBS	information	on deck

9.2. Station Protocol Heatflow

HF	Date	Time	Position (39° 32.xxx'N / 14°42.yyy' E)	Depth (Rope Length) [m]	Penetration [cm]	Heat Pulse	Max. tension [kN]	Tmax [°C]	dT/dz [K / m]
01	17.02	15:00 – 15:17	.401 / .430	629 (665)	75	yes	16	15.9	2.47
02		15:36 – 15:51	.382 / .407	627 (662)	210	yes	23	17.0	1.40
03	22.02	07:37 – 07:54	.378 / .435	633 (660)	180	yes	20	16.5	1.36
04		08:06 – 08:23	.380 / .470	634 (661)	140	no	10	14,3	0.18
05		08:40 – 08:58	.356 / .433	630 (657)	170	yes	23	15.5	0.85
06		09:13 – 09:30	.357 / .468	633 (660)	60	no	10	14.3	0.42
07		09:50 – 10:07	.403 / .468	634 (661)	130	yes	13	17.1	2.35
08		10:22 – 10:40	.428 / .466	636 (663)	70	no	10	14.5	0.64
09		10:59 – 11:18	.465 / .467	619 (645)	100	no	11	15.1	1.05
10		11:39 – 11:56	.429 / .424	631 (658)	x	no	10	14.7	x
11	24.02	13:16 – 13:30	.356 / .388	624 (651)	210	yes	22	15.3	0.60
12		14:01 – 14:18	.391 / .364	626 (653)	110	no	11	14.4	0.32
13		14:27 – 14:44	.408 / .380	630 (658)	170	yes	23	26.4	7.12
14		15:21 – 15:38	.420 / .360	626 (654)	210	yes	19	18.3	1.90
15	25.02	07:16 – 07:32	.447 / .376	622 (649)	210	yes	18	32.4	8.74
16		07:46 – 08:02	.480 / .391	617 (644)	210	yes	25	21.3	3.45
17		08:21 – 08:37	.456 / .403	625 (652)	10	yes	12	18.1	40.50
18		08:53 – 09:09	.437 / .403	631 (658)	210	yes	25	34.1	9.55
19		09:25 – 09:42	.424 / .397	633 (660)	210	yes	18	49.4	16.83
20		09:55 – 10:12	.409 / .399	636 (663)	160	yes	18	35.6	13.47
21		11:03 – 11:19	.380 / .512	634 (662)	130	yes	25	15.5	1.12
22		11:34 – 11:15	.424 / .499	635 (662)	130	yes	28	17.2	2.42
23		12:01 – 12:17	.453 / .506	636 (663)	200	yes	23	18.9	2.43
24	27.02	08:59 – 09:16	.359 / .529	642 (669)	70	no	11	14.3	0.36
25		09:32 – 09:48	.388 / .536	636 (663)	130	no	11	14.5	0.35

HF	Date	Time	Position (39° 32.xxx'N / 14°42.yyy' E)	Depth (Rope Length) [m]	Penetration [cm]	Heat Pulse	Max. tension [kN]	Tmax [°C]	dT/dz [K / m]
26		10:04 – 10:20	.417 / .578	617 (643)	100	no	13	14.5	0.45
27		11:16 – 11:32	.420 / .552	627 (654)	100	yes	15	16.2	2.15
28		11:56 – 11:56	.454 / .537	618 (644)	x	no	x		x
29		12:16 – 12:33	.409 / .508	632 (660)	190	yes	25	17.0	1.55
30		12:56 – 13:13	.424 / .415	636 (664)	160	yes	22	30.9	10.53
31		13:30 – 13:47	.393 / .382	628 (656)	210	yes	24	15.9	0.88
32		14:06 – 14:22	.466 / .385	621 (649)	210	yes	23	23.9	4.69
33		14:39 – 14:56	.491 / .474	599 (625)	80	no	11	15.2	1.44
34		15:10 – 15:26	.485 / .513	604 (630)	130	no	12	16.0	1.50

- After ground contact ("BoKo") an extra 5m of winch cable were given as slack.
- There was no change in tension during the bottom time for any measurement with penetration.
- USBL transponder 30m above the probe.

9.3. Core Descriptions

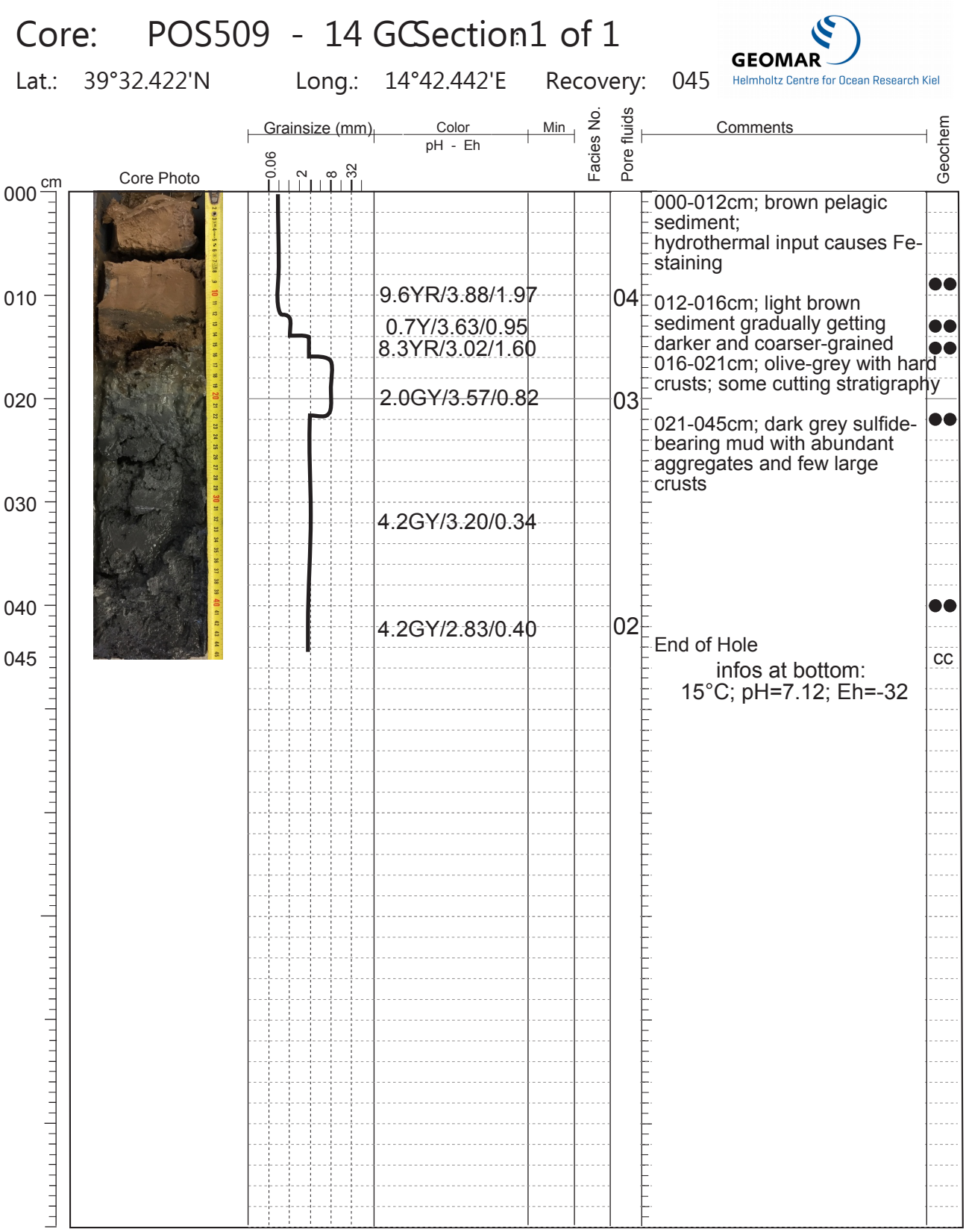

Core: POS509 - 15 GC Section: 1 of 3

Lat.: 39°32.381'N Long.: 14°42.419'E Recovery: 272

GEOMAR Helmholtz Centre for Ocean Research Kiel

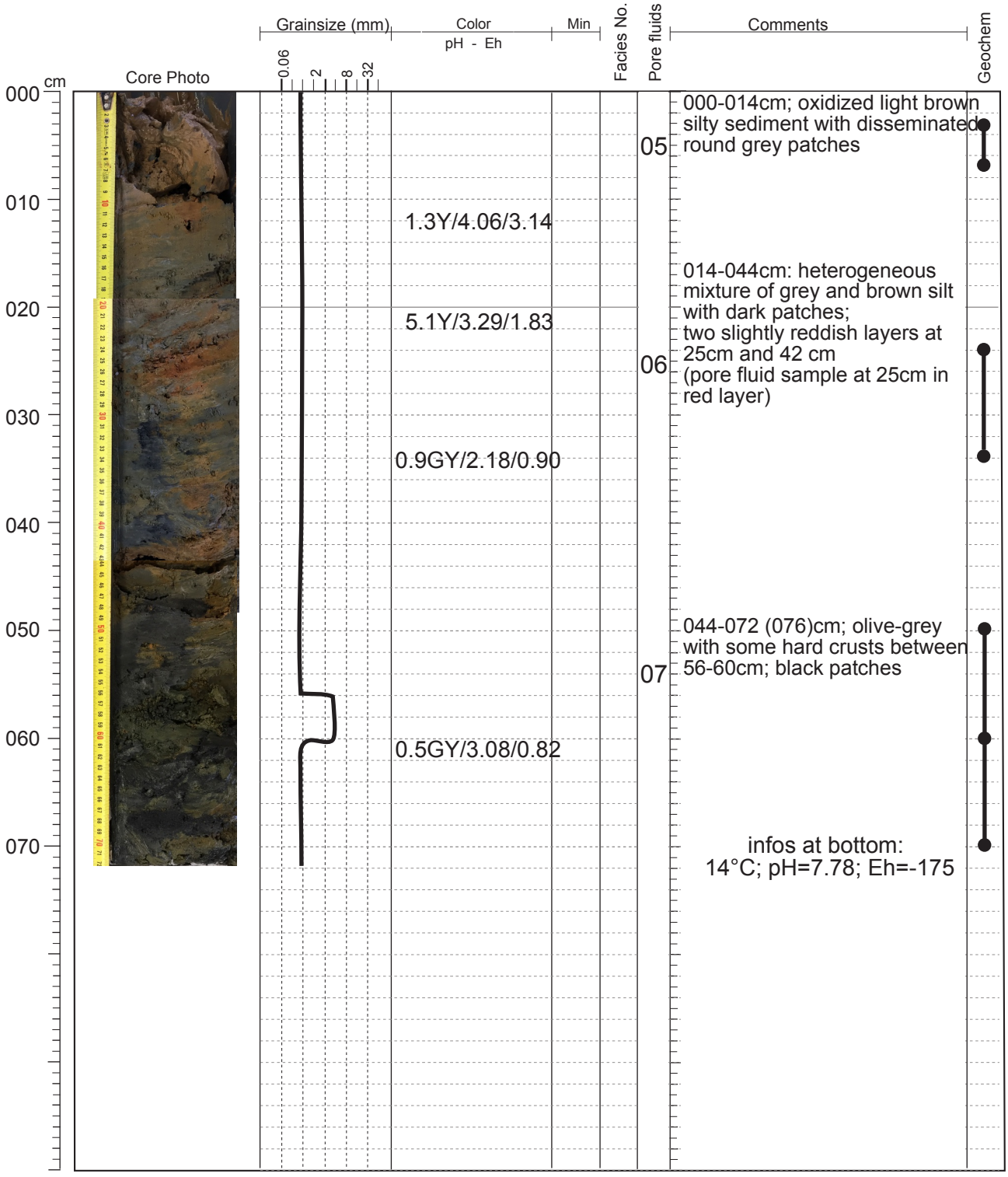

Core: POS509 - 15 GC Section: 2 of 3

Lat.: 39°32.381'N Long.: 14°42.419'E Recovery: 272

GEOMAR Helmholtz Centre for Ocean Research Kiel

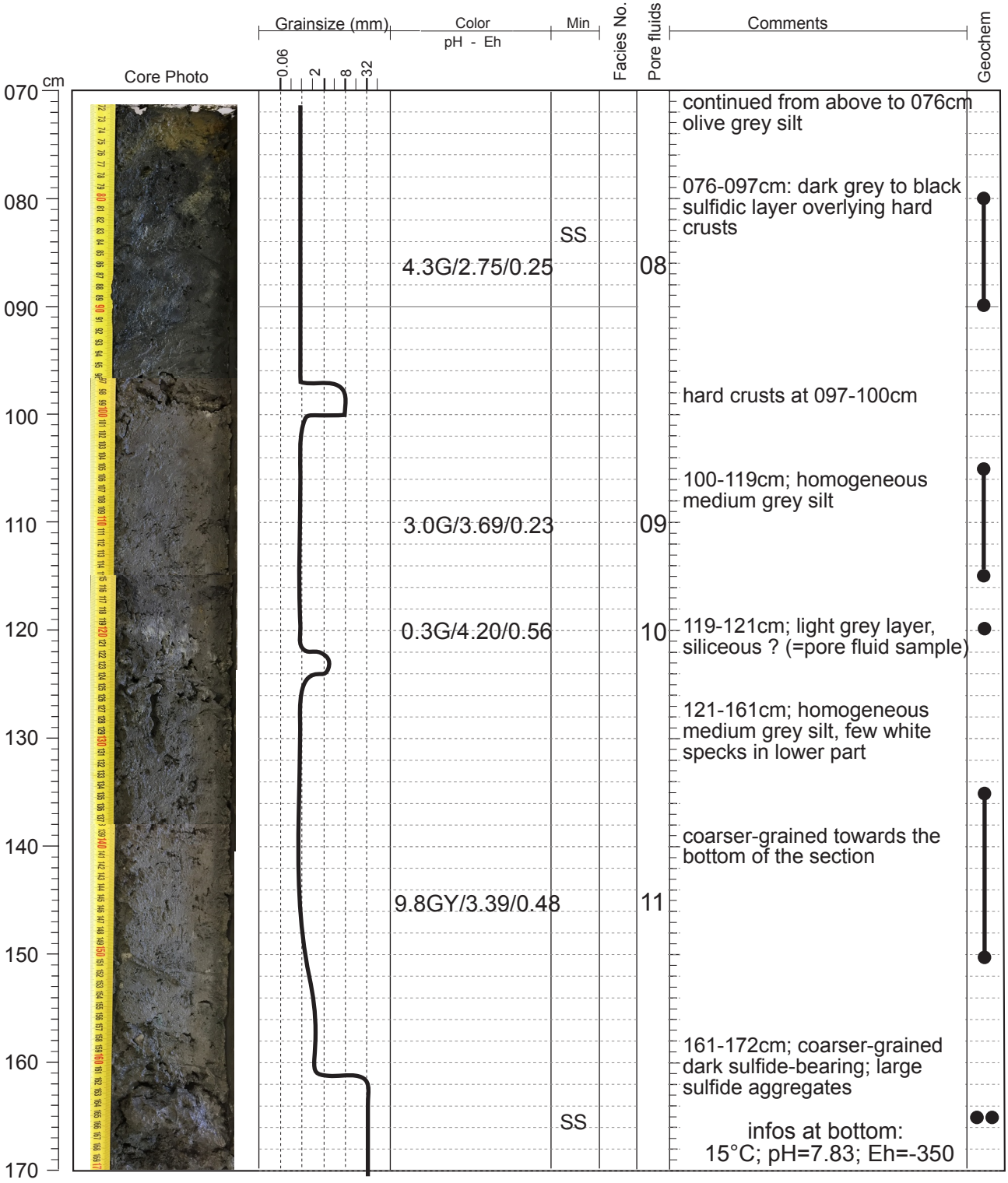

Core: POS509 - 15 GC Section 3 of 3

Lat.: 39°32.381'N Long.: 14°42.419'E Recovery: 272

GEOMAR Helmholtz Centre for Ocean Research Kiel

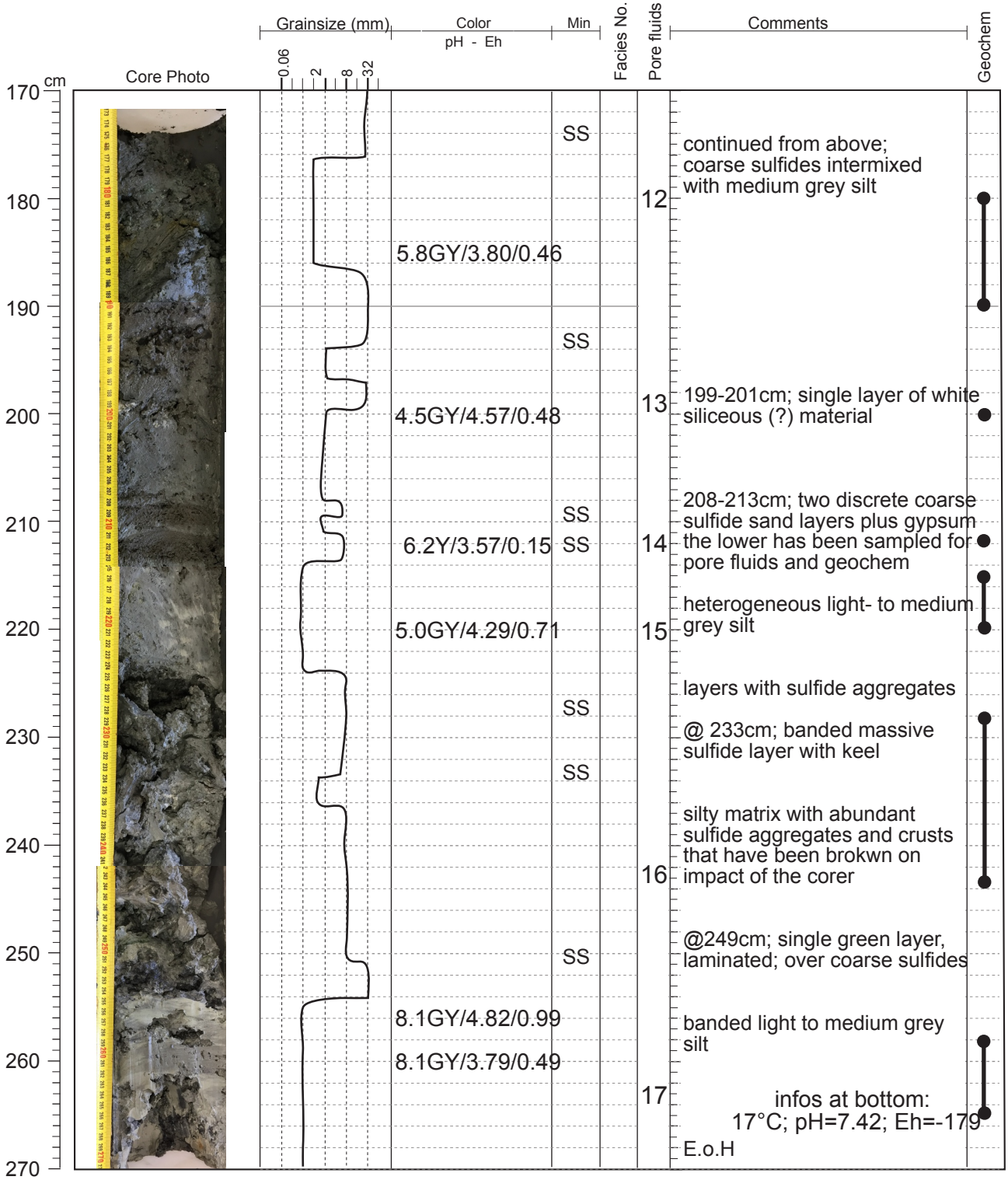

Core: POS509 - 17 GC Section: 1 of 1

Lat.: 39°32.401'N Long.: 14°42.443'E Recovery: 057

GEOMAR Helmholtz Centre for Ocean Research Kiel

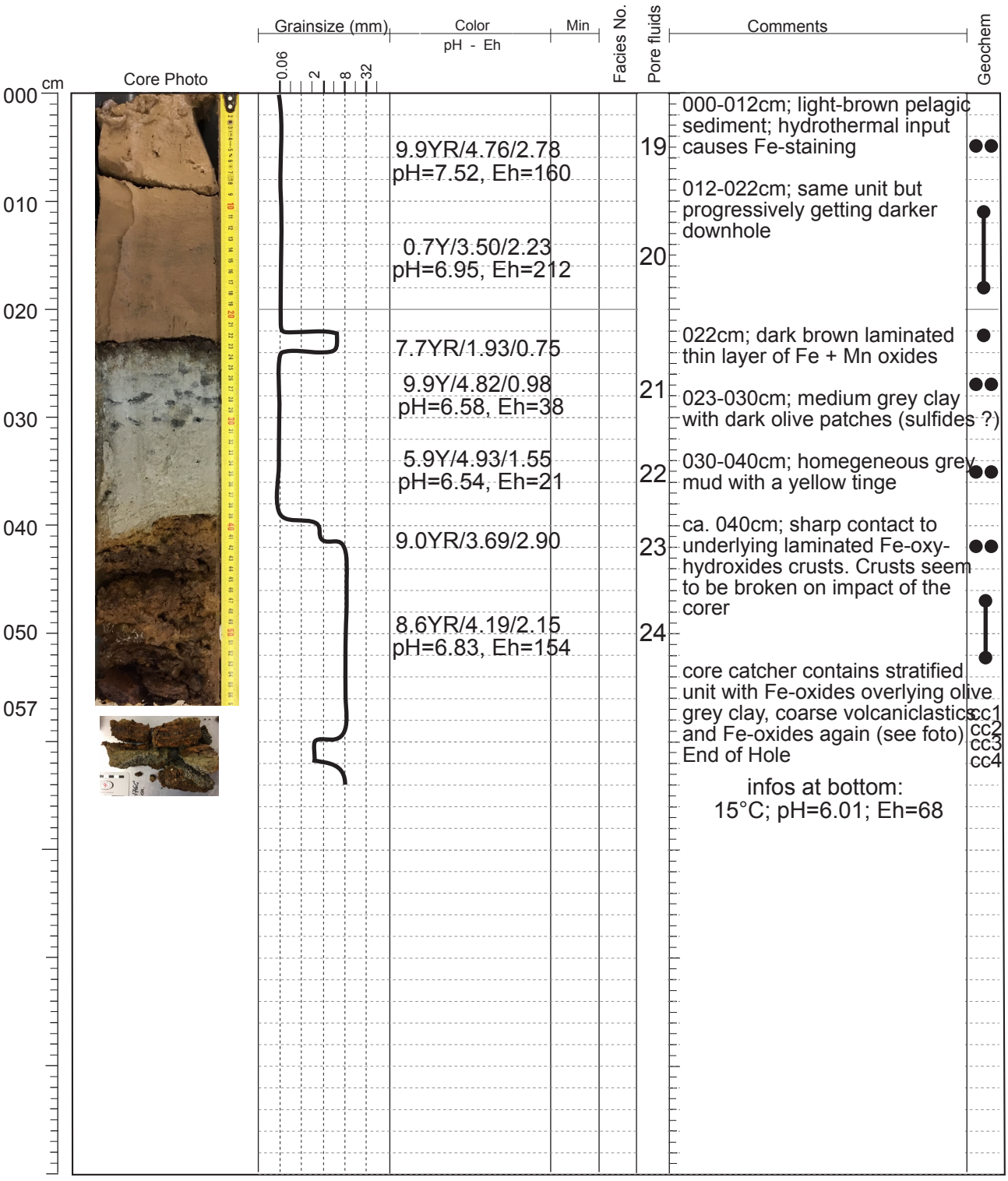

Core: POS509 - 20 GC Section: 1 of 3

Lat.: 39°32.425'N Long.: 14°42.538'E Recovery: 290

GEOMAR Helmholtz Centre for Ocean Research Kiel

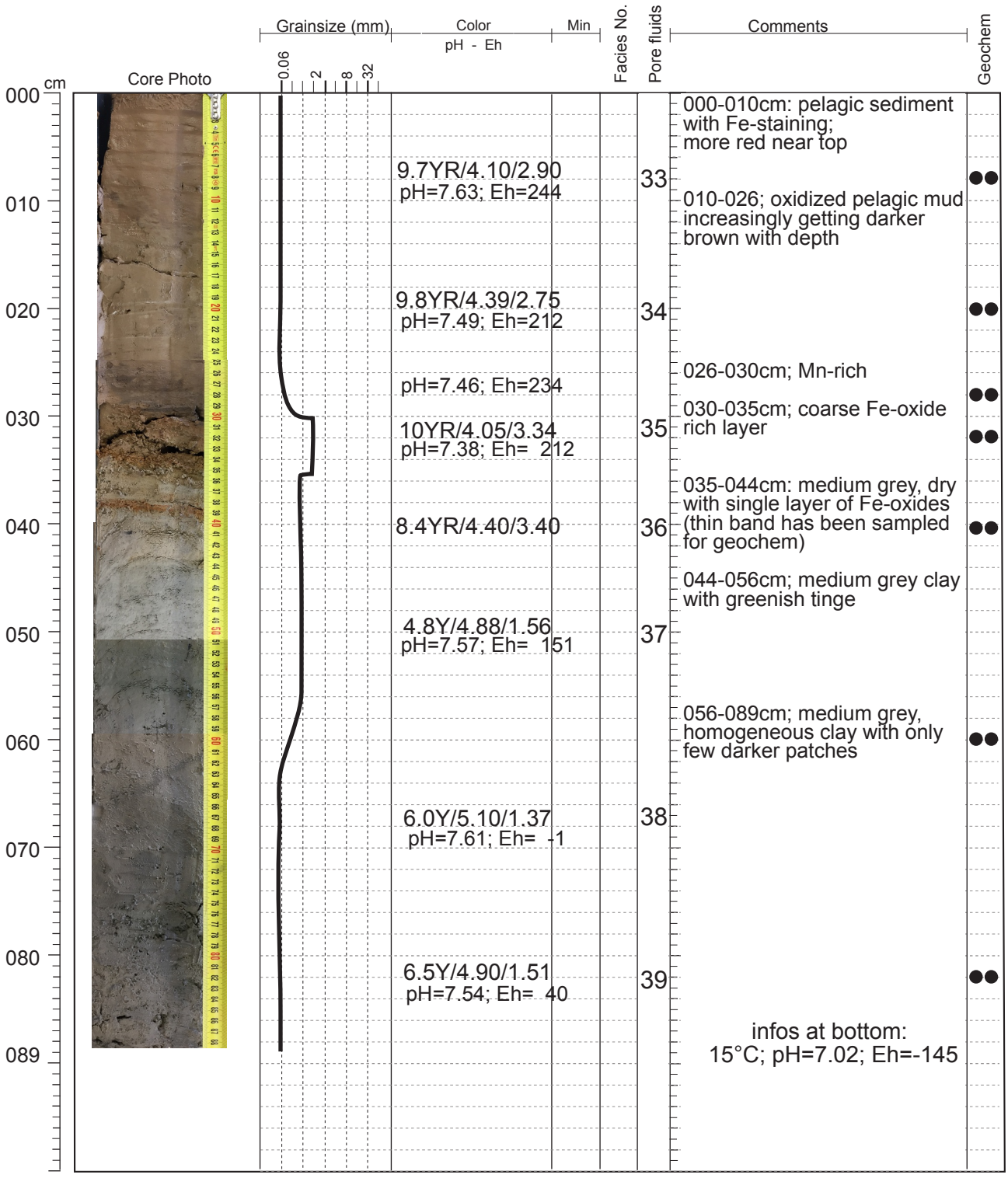

Core: POS509 - 20 GC Section 2 of 3

Lat.: 39°32.425'N Long.: 14°42.538'E Recovery: 290

GEOMAR Helmholtz Centre for Ocean Research Kiel

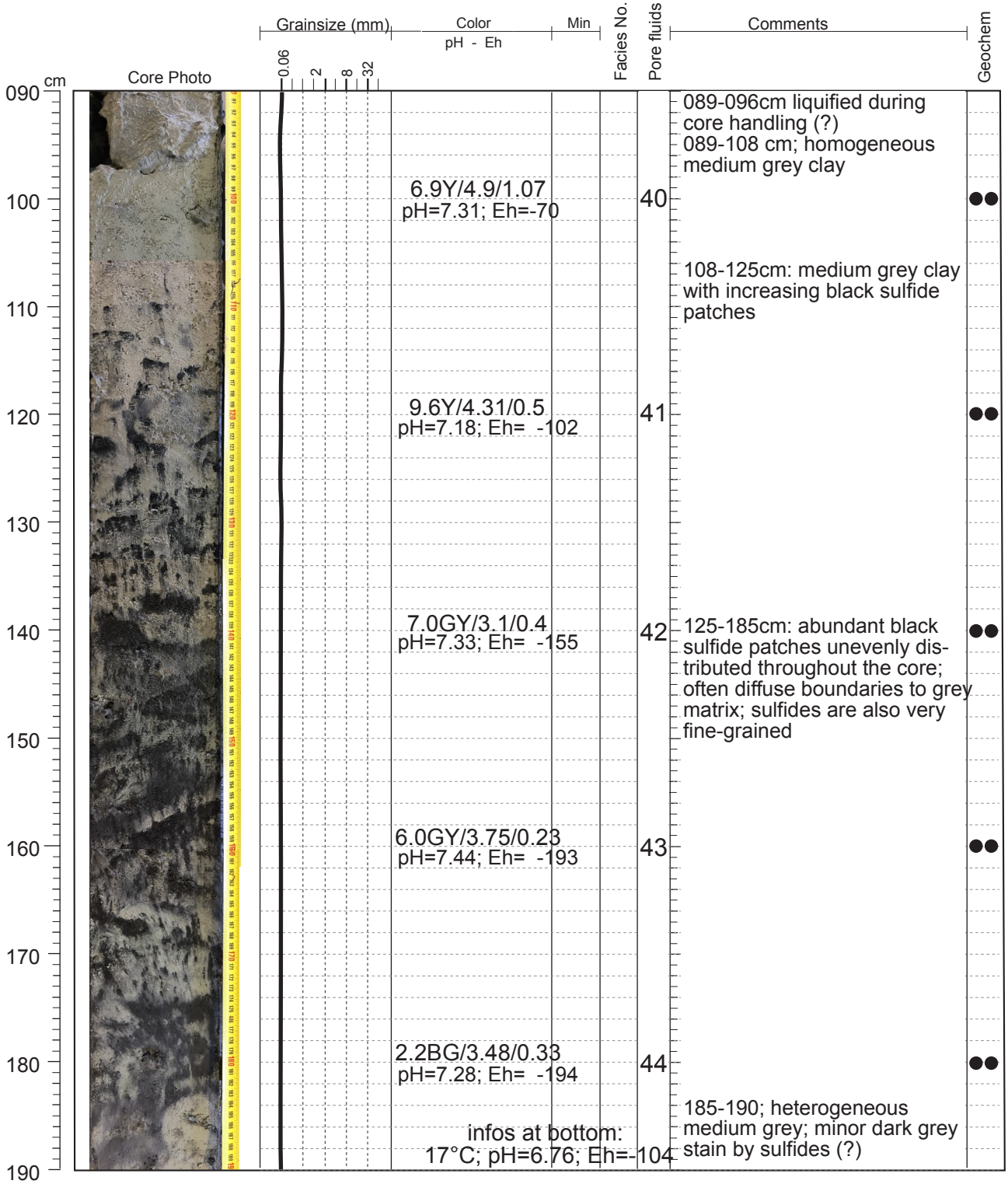

Core: POS509 - 20 GC Section: 3 of 3

Lat.: 39°32.425'N Long.: 14°42.538'E Recovery: 290

GEOMAR Helmholtz Centre for Ocean Research Kiel

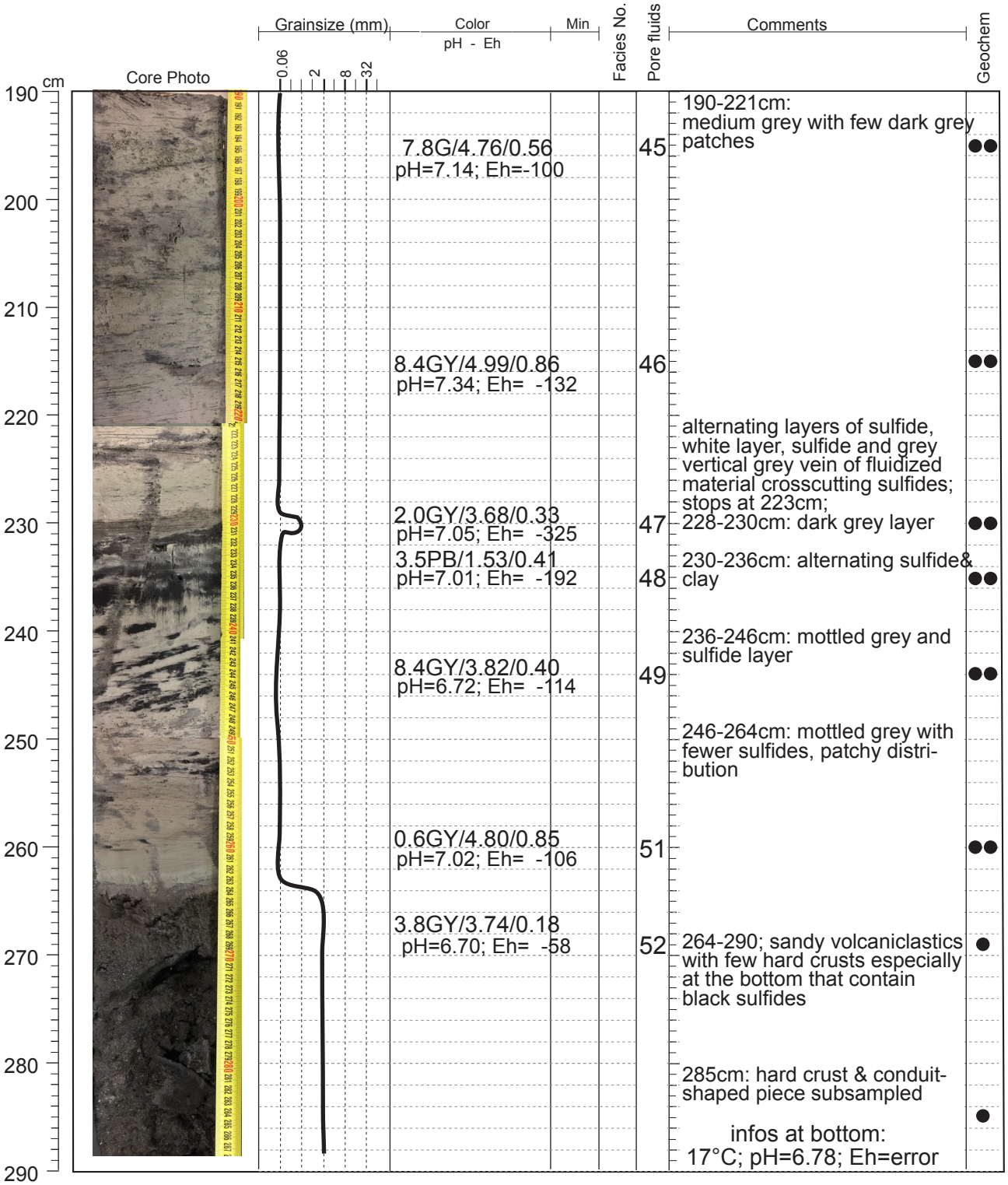

Core: POS509 - 21 GC Section: 1 of 1

Lat.: 39°32.375'N Long.: 14°42.488'E Recovery: 078

GEOMAR Helmholtz Centre for Ocean Research Kiel

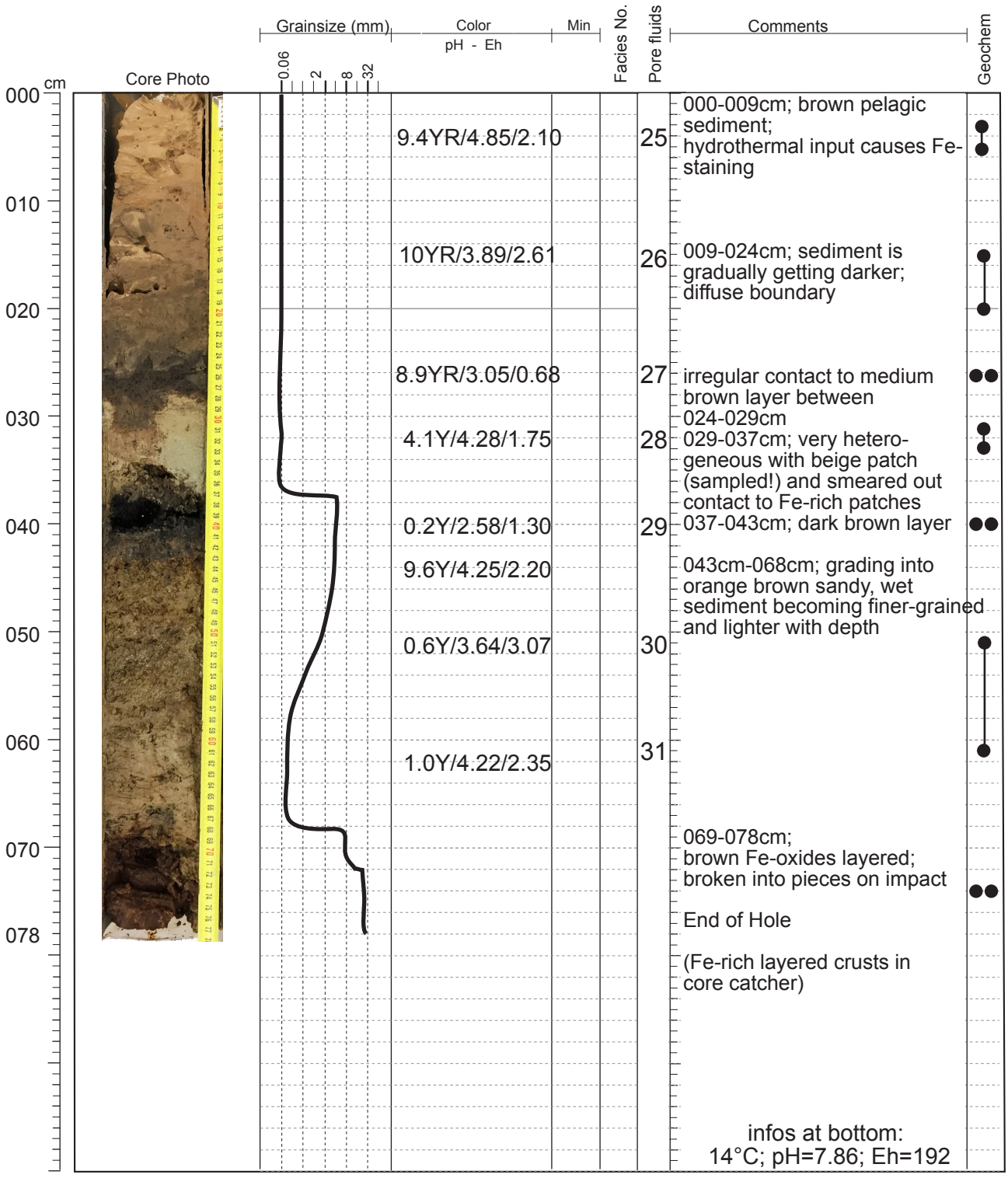

Core: POS509 - 23 GC Section: 1 of 3

Lat.: 39°32.549'N Long.: 14°42.388'E Recovery: 290

GEOMAR Helmholtz Centre for Ocean Research Kiel

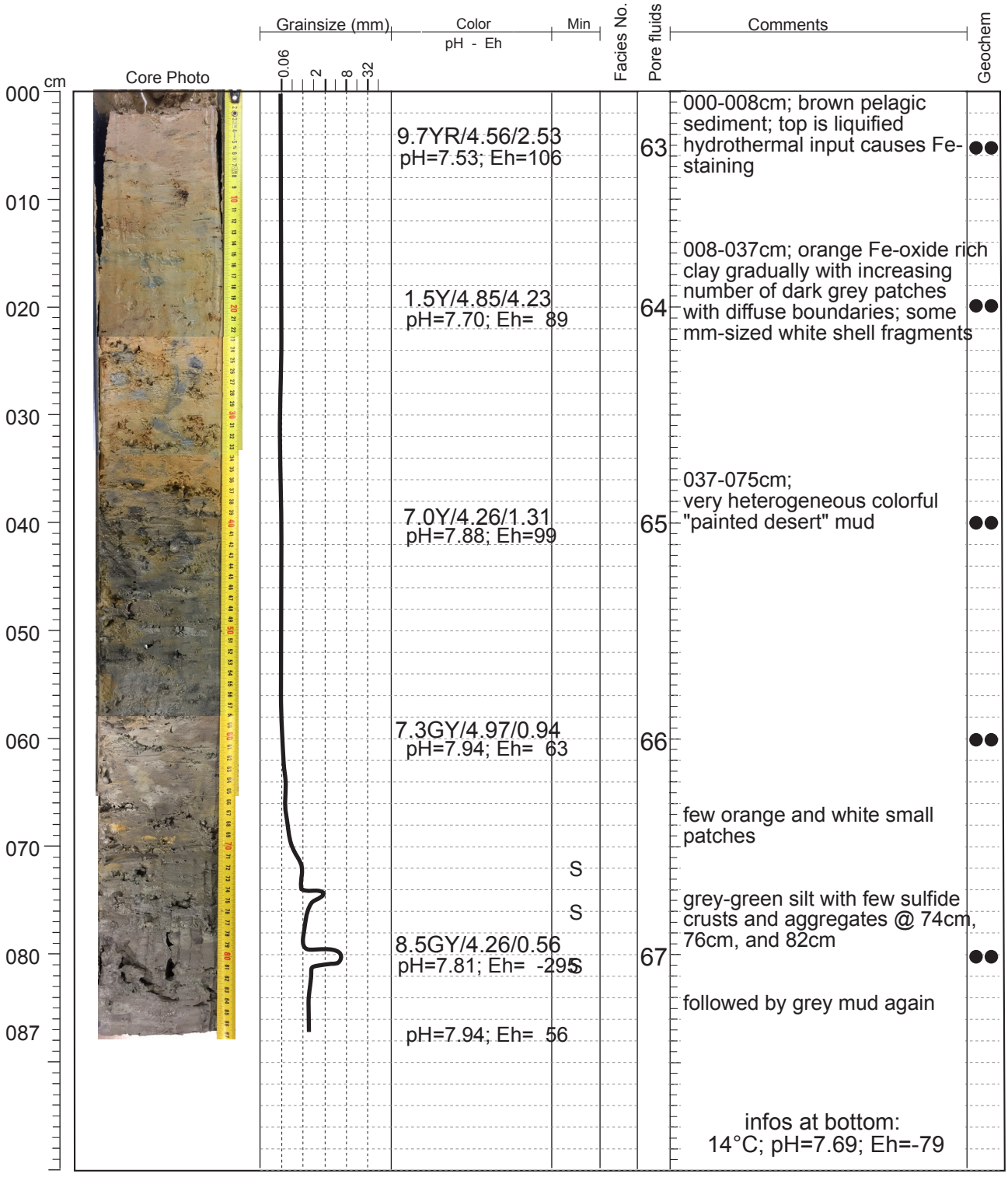

Core: POS509 - 23 GC Section: 2 of 3

Lat.: 39°32.549'N Long.: 14°42.388'E Recovery: 290

GEOMAR Helmholtz Centre for Ocean Research Kiel

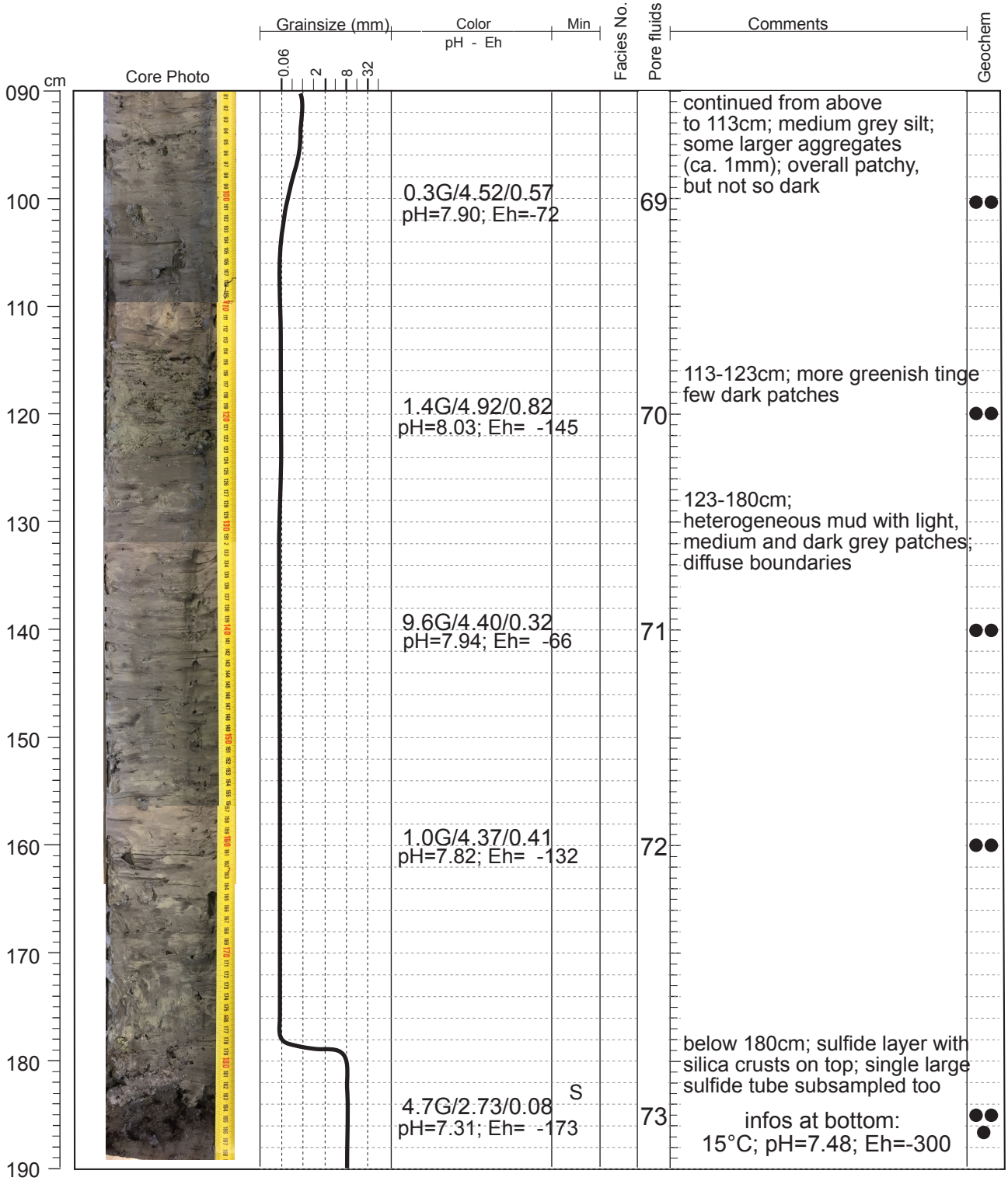

Core: POS509 - 23 GC Section: 3 of 3

Lat.: 39°32.549'N Long.: 14°42.388'E Recovery: 290

GEOMAR Helmholtz Centre for Ocean Research Kiel

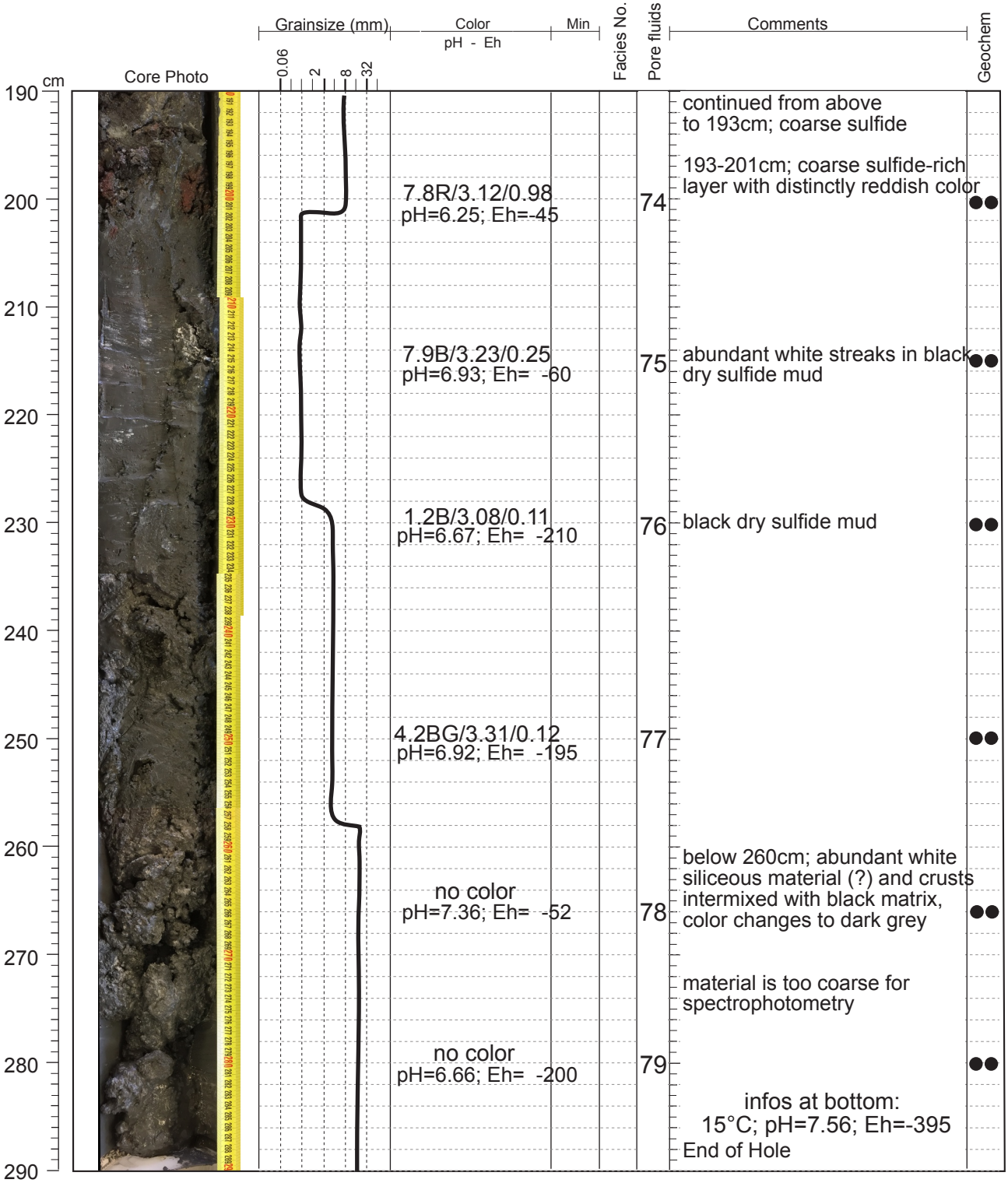

Core: POS509 - 24 GC Section: 1 of 2

Lat.: 39°32.405'N Long.: 14°42.394'E Recovery: 130

GEOMAR Helmholtz Centre for Ocean Research Kiel

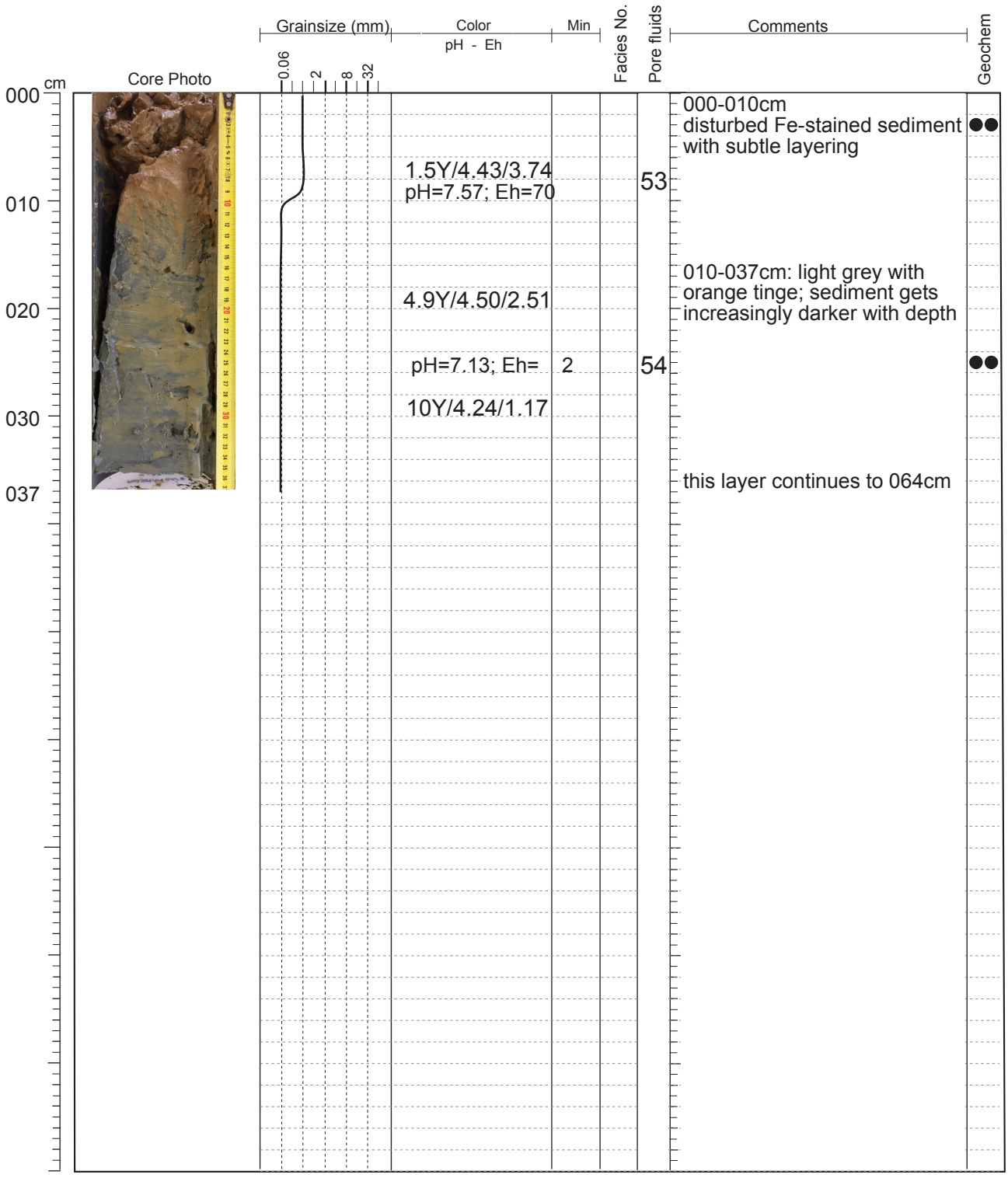

Core: POS509 - 24 GC Section: 2 of 2

Lat.: 39°32.405'N Long.: 14°42.394'E Recovery: 130

GEOMAR Helmholtz Centre for Ocean Research Kiel

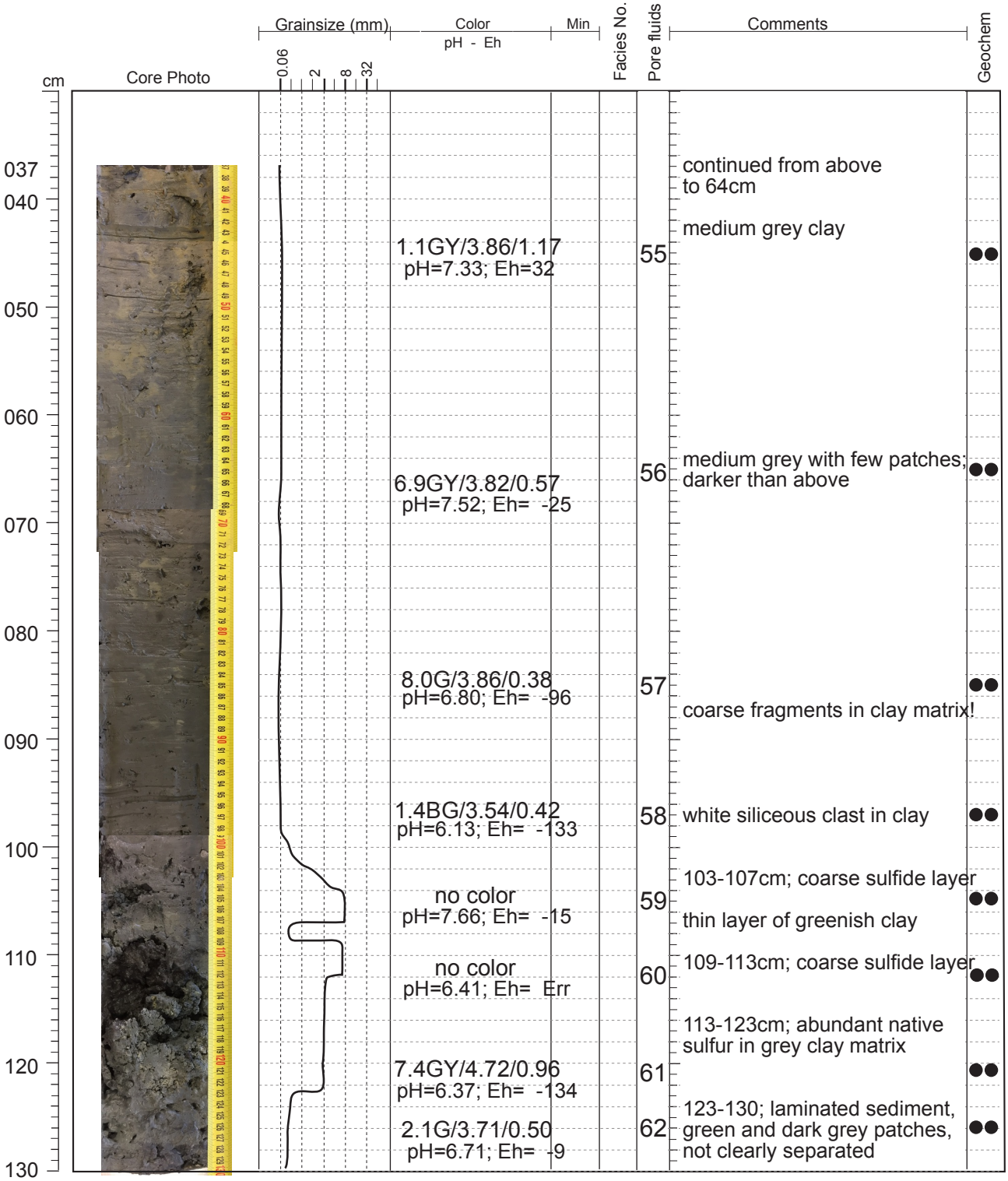

9.4. Pore Fluid Samples

vial Nr	Core	Depth	vial Nr	Core	Depth
POS509-001	blank	blank	POS509-051	20GC (A)	257cm
POS509-002	14GC	040cm	POS509-052	20GC (A)	268cm
POS509-003	14GC	022cm	POS509-053	24GC (B)	008cm
POS509-004	14GC	009cm	POS509-054	24GC (B)	025cm
POS509-005	15GC (C)	005cm	POS509-055	24GC (A)	045cm
POS509-006	15GC (C)	025cm	POS509-056	24GC (A)	065cm
POS509-007	15GC (C)	054cm	POS509-057	24GC (A)	085cm
POS509-008	15GC (B)	086cm	POS509-058	24GC (A)	097cm
POS509-009	15GC (B)	110cm	POS509-059	24GC (A)	105cm
POS509-010	15GC (B)	120cm	POS509-060	24GC (A)	112cm
POS509-011	15GC (B)	145cm	POS509-061	24GC (A)	121cm
POS509-012	15GC (A)	180cm	POS509-062	24GC (A)	126cm
POS509-013	15GC (A)	199cm	POS509-063	23GC (C)	005cm
POS509-014	15GC (A)	212cm	POS509-064	23GC (C)	020cm
POS509-015	15GC (A)	220cm	POS509-065	23GC (C)	040cm
POS509-016	15GC (A)	243cm	POS509-066	23GC (C)	060cm
POS509-017	15GC (A)	263cm	POS509-067	23GC (C)	080cm
POS509-018	blank	blank	POS509-068	blank	blank
POS509-019	17GC	005cm	POS509-069	23GC(B)	100cm
POS509-020	17GC	015cm	POS509-070	23GC(B)	120cm
POS509-021	17GC	027cm	POS509-071	23GC(B)	140cm
POS509-022	17GC	035cm	POS509-072	23GC(B)	160cm
POS509-023	17GC	041cm	POS509-073	23GC(B)	186cm
POS509-024	17GC	050cm	POS509-074	23GC(A)	200cm
POS509-025	21GC	004cm	POS509-075	23GC(A)	215cm
POS509-026	21GC	015cm	POS509-076	23GC(A)	230cm
POS509-027	21GC	026cm	POS509-077	23GC(A)	250cm
POS509-028	21GC	032cm	POS509-078	23GC(A)	266cm
POS509-029	21GC	040cm	POS509-079	23GC(A)	280cm
POS509-030	21GC	051cm	POS509-080	blank	blank
POS509-031	21GC	062cm			
POS509-032	blank	blank			
POS509-033	20GC (C)	008cm			
POS509-034	20GC (C)	020cm			
POS509-035	20GC (C)	031cm			
POS509-036	20GC (C)	040cm			
POS509-037	20GC (C)	050cm			
POS509-038	20GC (C)	067cm			
POS509-039	20GC (C)	082cm			
POS509-040	20GC (B)	100cm			
POS509-041	20GC (B)	120cm			
POS509-042	20GC (B)	140cm			
POS509-043	20GC (B)	160cm			
POS509-044	20GC (B)	180cm			
POS509-045	20GC (A)	195cm			
POS509-046	20GC (A)	215cm			
POS509-047	20GC (A)	230cm			
POS509-048	20GC (A)	235cm			
POS509-049	20GC (A)	244cm			
POS509-050	blank	blank			

GEOMAR
Helmholtz-Zentrum für Ozeanforschung Kiel

GEOMAR Reports

No.	Title
1	FS POSEIDON Fahrtbericht / Cruise Report POS421, 08. – 18.11.2011, Kiel - Las Palmas, Ed.: T.J. Müller, 26 pp, DOI: 10.3289/GEOMAR_REP_NS_1_2012
2	Nitrous Oxide Time Series Measurements off Peru – A Collaboration between SFB 754 and IMARPE –, Annual Report 2011, Eds.: Baustian, T., M. Graco, H.W. Bange, G. Flores, J. Ledesma, M. Sarmiento, V. Leon, C. Robles, O. Moron, 20 pp, DOI: 10.3289/GEOMAR_REP_NS_2_2012
3	FS POSEIDON Fahrtbericht / Cruise Report POS427 – Fluid emissions from mud volcanoes, cold seeps and fluid circulation at the Don-_Kuban deep sea fan (Kerch peninsula, Crimea, Black Sea) – 23.02. – 19.03.2012, Burgas, Bulgaria - Heraklion, Greece, Ed.: J. Bialas, 32 pp, DOI: 10.3289/GEOMAR_REP_NS_3_2012
4	RV CELTIC EXPLORER EUROFLEETS Cruise Report, CE12010 – ECO2@NorthSea, 20.07. – 06.08.2012, Bremerhaven – Hamburg, Eds.: P. Linke et al., 65 pp, DOI: 10.3289/GEOMAR_REP_NS_4_2012
5	RV PELAGIA Fahrtbericht / Cruise Report 64PE350/64PE351 – JEDDAH-TRANSECT -, 08.03. – 05.04.2012, Jeddah – Jeddah, 06.04 - 22.04.2012, Jeddah – Duba, Eds.: M. Schmidt, R. Al-Farawati, A. Al-Aidaroos, B. Kürten and the shipboard scientific party, 154 pp, DOI: 10.3289/GEOMAR_REP_NS_5_2013
6	RV SONNE Fahrtbericht / Cruise Report SO225 - MANIHIKI II Leg 2 The Manihiki Plateau - Origin, Structure and Effects of Oceanic Plateaus and Pleistocene Dynamic of the West Pacific Warm Water Pool, 19.11.2012 - 06.01.2013 Suva / Fiji – Auckland / New Zealand, Eds.: R. Werner, D. Nürnberg, and F. Hauff and the shipboard scientific party, 176 pp, DOI: 10.3289/GEOMAR_REP_NS_6_2013
7	RV SONNE Fahrtbericht / Cruise Report SO226 – CHRIMP CHatham RIse Methane Pockmarks, 07.01. - 06.02.2013 / Auckland – Lyttleton & 07.02. – 01.03.2013 / Lyttleton – Wellington, Eds.: Jörg Bialas / Ingo Klaucke / Jasmin Mögeltönder, 126 pp, DOI: 10.3289/GEOMAR_REP_NS_7_2013
8	The SUGAR Toolbox - A library of numerical algorithms and data for modelling of gas hydrate systems and marine environments, Eds.: Elke Kossel, Nikolaus Bigalke, Elena Piñero, Matthias Haeckel, 168 pp, DOI: 10.3289/GEOMAR_REP_NS_8_2013
9	RV ALKOR Fahrtbericht / Cruise Report AL412, 22.03.-08.04.2013, Kiel – Kiel. Eds: Peter Linke and the shipboard scientific party, 38 pp, DOI: 10.3289/GEOMAR_REP_NS_9_2013
10	Literaturrecherche, Aus- und Bewertung der Datenbasis zur Meerforelle (Salmo trutta trutta L.) Grundlage für ein Projekt zur Optimierung des Meerforellenmanagements in Schleswig-Holstein. Eds.: Christoph Petereit, Thorsten Reusch, Jan Dierking, Albrecht Hahn, 158 pp, DOI: 10.3289/GEOMAR_REP_NS_10_2013
11	RV SONNE Fahrtbericht / Cruise Report SO227 TAIFLUX, 02.04. – 02.05.2013, Kaohsiung – Kaohsiung (Taiwan), Christian Berndt, 105 pp, DOI: 10.3289/GEOMAR_REP_NS_11_2013
12	RV SONNE Fahrtbericht / Cruise Report SO218 SHIVA (Stratospheric Ozone: Halogens in a Varying Atmosphere), 15.-29.11.2011, Singapore - Manila, Philippines, Part 1: SO218- SHIVA Summary Report (in German), Part 2: SO218- SHIVA English reports of participating groups, Eds.: Birgit Quack & Kirstin Krüger, 119 pp, DOI: 10.3289/GEOMAR_REP_NS_12_2013
13	KIEL276 Time Series Data from Moored Current Meters. Madeira Abyssal Plain, 33°N, 22°W, 5285 m water depth, March 1980 – April 2011. Background Information and Data Compilation. Eds.: Thomas J. Müller and Joanna J. Waniek, 239 pp, DOI: 10.3289/GEOMAR_REP_NS_13_2013

GEOMAR
Helmholtz-Zentrum für Ozeanforschung Kiel

GEOMAR Reports

No.	Title
14	RV POSEIDON Fahrtbericht / Cruise Report POS457: ICELAND HAZARDS Volcanic Risks from Iceland and Climate Change:The Late Quaternary to Anthropogene Development Reykjavík / Iceland – Galway / Ireland, 7.-22. August 2013. Eds.: Reinhard Werner, Dirk Nürnberg and the shipboard scientific party, 88 pp, DOI: 10.3289/GEOMAR_REP_NS_14_2014
15	RV MARIA S. MERIAN Fahrtbericht / Cruise Report MSM-34 / 1 & 2, SUGAR Site, Varna – Varna, 06.12.13 – 16.01.14. Eds: Jörg Bialas, Ingo Klaucke, Matthias Haeckel, 111 pp, DOI: 10.3289/GEOMAR_REP_NS_15_2014
16	RV POSEIDON Fahrtbericht / Cruise Report POS 442, "AUVinTYS" High-resolution geological investigations of hydrothermal sites in the Tyrrhenian Sea using the AUV "Abyss", 31.10. – 09.11.12, Messina – Messina, Ed.: Sven Petersen, 32 pp, DOI: 10.3289/GEOMAR_REP_NS_16_2014
17	RV SONNE, Fahrtbericht / Cruise Report, SO 234/1, "SPACES": Science or the Assessment of Complex Earth System Processes, 22.06. – 06.07.2014, Walvis Bay / Namibia - Durban / South Africa, Eds.: Reinhard Werner and Hans-Joachim Wagner and the shipbord scientific party, 44 pp, DOI: 10.3289/GEOMAR_REP_NS_17_2014
18	RV POSEIDON Fahrtbericht / Cruise Report POS 453 & 458, "COMM3D", Crustal Structure and Ocean Mixing observed with 3D Seismic Measurements, 20.05. – 12.06.2013 (POS453), Galway, Ireland – Vigo, Portugal, 24.09. – 17.10.2013 (POS458), Vigo, Portugal – Vigo, Portugal, Eds.: Cord Papenberg and Dirk Klaeschen, 66 pp, DOI: 10.3289/GEOMAR_REP_NS_18_2014
19	RV POSEIDON, Fahrtbericht / Cruise Report, POS469, "PANAREA", 02. – 22.05.2014, (Bari, Italy – Malaga, Spain) & Panarea shallow-water diving campaign, 10. – 19.05.2014, Ed.: Peter Linke, 55 pp, DOI: 10.3289/GEOMAR_REP_NS_19_2014
20	RV SONNE Fahrtbericht / Cruise Report SO234-2, 08.-20.07.2014, Durban, -South Africa - Port Louis, Mauritius, Eds.: Kirstin Krüger, Birgit Quack and Christa Marandino, 95 pp, DOI: 10.3289/GEOMAR_REP_NS_20_2014
21	RV SONNE Fahrtbericht / Cruise Report SO235, 23.07.-07.08.2014, Port Louis, Mauritius to Malé, Maldives, Eds.: Kirstin Krüger, Birgit Quack and Christa Marandino, 76 pp, DOI: 10.3289/GEOMAR_REP_NS_21_2014
22	RV SONNE Fahrtbericht / Cruise Report SO233 WALVIS II, 14.05-21.06.2014, Cape Town, South Africa - Walvis Bay, Namibia, Eds.: Kaj Hoernle, Reinhard Werner, and Carsten Lüter, 153 pp, DOI: 10.3289/GEOMAR_REP_NS_22_2014
23	RV SONNE Fahrtbericht / Cruise Report SO237 Vema-TRANSIT Bathymetry of the Vema-Fracture Zone and Puerto Rico TRench and Abyssal AtlaNtic BiodiverSITy Study, Las Palmas (Spain) - Santo Domingo (Dom. Rep.) 14.12.14 - 26.01.15, Ed.: Colin W. Devey, 130 pp, DOI: 10.3289/GEOMAR_REP_NS_23_2015
24	RV POSEIDON Fahrtbericht / Cruise Report POS430, POS440, POS460 & POS467 Seismic Hazards to the Southwest of Portugal; POS430 - La-Seyne-sur-Mer - Portimao (7.4. - 14.4.2012), POS440 - Lisbon - Faro (12.10. - 19.10.2012), POS460 - Funchal - Portimao (5.10. - 14.10.2013), POS467 - Funchal - Portimao (21.3. - 27.3.2014), Ed.: Ingo Grevemeyer, 43 pp, DOI: 10.3289/GEOMAR_REP_NS_24_2015
25	RV SONNE Fahrtbericht / Cruise Report SO239, EcoResponse Assessing the Ecology, Connectivity and Resilience of Polymetallic Nodule Field Systems, Balboa (Panama) – Manzanillo (Mexico), 11.03. -30.04.2015, Eds.: Pedro Martínez Arbizu and Matthias Haeckel, 204 pp, DOI: 10.3289/GEOMAR_REP_NS_25_2015

GEOMAR
Helmholtz-Zentrum für Ozeanforschung Kiel

GEOMAR Reports

No.	Title
26	RV SONNE Fahrtbericht / Cruise Report SO242-1, JPI OCEANS Ecological Aspects of Deep-Sea Mining, DISCOL Revisited, Guayaquil - Guayaquil (Equador), 29.07.-25.08.2015, Ed.: Jens Greinert, 290 pp, DOI: 10.3289/GEOMAR_REP_NS_26_2015
27	RV SONNE Fahrtbericht / Cruise Report SO242-2, JPI OCEANS Ecological Aspects of Deep-Sea Mining DISCOL Revisited, Guayaquil - Guayaquil (Equador), 28.08.-01.10.2015, Ed.: Antje Boetius, 552 pp, DOI: 10.3289/GEOMAR_REP_NS_27_2015
28	RV POSEIDON Fahrtbericht / Cruise Report POS493, AUV DEDAVE Test Cruise, Las Palmas - Las Palmas (Spain), 26.01.-01.02.2016, Ed.: Klas Lackschewitz, 17 pp, DOI: 10.3289/GEOMAR_REP_NS_28_2016
29	Integrated German Indian Ocean Study (IGIOS) - From the seafloor to the atmosphere - A possible German contribution to the International Indian Ocean Expedition 2 (IIOE-2) programme – A Science Prospectus, Eds.: Bange, H.W. , E.P. Achterberg, W. Bach, C. Beier, C. Berndt, A. Biastoch, G. Bohrmann, R. Czeschel, M. Dengler, B. Gaye, K. Haase, H. Herrmann, J. Lelieveld, M. Mohtadi, T. Rixen, R. Schneider, U. Schwarz-Schampera, J. Segschneider, M. Visbeck, M. Voß, and J. Williams, 77pp, DOI: 10.3289/GEOMAR_REP_NS_29_2016
30	RV SONNE Fahrtbericht / Cruise Report SO249, BERING – Origin and Evolution of the Bering Sea: An Integrated Geochronological, Volcanological, Petrological and Geochemical Approach, Leg 1: Dutch Harbor (U.S.A.) - Petropavlovsk-Kamchatsky (Russia), 05.06.2016-15.07.2016, Leg 2: Petropavlovsk-Kamchatsky (Russia) - Tomakomai (Japan), 16.07.2016-14.08.2016, Eds.: Reinhard Werner, et al., DOI: 10.3289/GEOMAR_REP_NS_30_2016
31	RV POSEIDON Fahrtbericht/ Cruise Report POS494/2, HIERROSEIS Leg 2: Assessment of the Ongoing Magmatic-Hydrothermal Discharge of the El Hierro Submarine Volcano, Canary Islands by the Submersible JAGO, Valverde – Las Palmas (Spain), 07.02.-15.02.2016, Eds.: Hannington, M.D. and Shipboard Scientific Party, DOI: 10.3289/GEOMAR_REP_NS_31_2016
32	RV METEOR Fahrtbericht/ Cruise Report M127, Extended Version, Metal fluxes and Resource Potential at the Slow-spreading TAG Midocean Ridge Segment (26°N, MAR) – Blue Mining@Sea, Bridgetown (Barbados) – Ponta Delgada (Portugal) 25.05.-28.06.2016, Eds.: Petersen, S. and Shipboard Scientific Party, DOI: 10.3289/GEOMAR_REP_NS_32_2016
33	RV SONNE Fahrtbericht/Cruise Report SO244/1, GeoSEA: Geodetic Earthquake Observatory on the Seafloor, Antofagasta (Chile) – Antofagasta (Chile), 31.10.-24.11.2015, Eds.: Jan Behrmann, Ingo Klaucke, Michal Stipp, Jacob Geersen and Scientific Crew SO244/1, DOI: 10.3289/GEOMAR_REP_NS_33_2016
34	RV SONNE Fahrtbericht/Cruise Report SO244/2, GeoSEA: Geodetic Earthquake Observatory on the Seafloor, Antofagasta (Chile) – Antofagasta (Chile), 27.11.-13.12.2015, Eds.: Heidrun Kopp, Dietrich Lange, Katrin Hannemann, Anne Krabbenhoeft, Florian Petersen, Anina Timmermann and Scientific Crew SO244/2, DOI: 10.3289/GEOMAR_REP_NS_34_2016
35	RV SONNE Fahrtbericht/Cruise Report SO255, VITIAZ – The Life Cycle of the Vitiaz-Kermadec Arc / Backarc System: from Arc Initiation to Splitting and Backarc Basin Formation, Auckland (New Zealand) - Auckland (New Zealand), 02.03.-14.04.2017, Eds.: Kaj Hoernle, Folkmar Hauff, and Reinhard Werner with contributions from cruise participants, DOI: 10.3289/GEOMAR_REP_NS_35_2017

GEOMAR
Helmholtz-Zentrum für Ozeanforschung Kiel

GEOMAR Reports

No.	Title
36	RV POSEIDON Fahrtbericht/Cruise Report POS515, CALVADOS - CALabrian arc mud VolcAnoes: Deep Origin and internal Structure, Dubrovnik (Croatia) – Catania (Italy), 18.06.-13.07.2017, Eds.: M. Riedel, J. Bialas, A. Krabbenhoeft, V. Bähre, F. Beeck, O. Candoni, M. Kühn, S. Muff, J. Rindfleisch, N. Stange, DOI: 10.3289/GEOMAR_REP_NS_36_2017
37	RV MARIA S. MERIAN Fahrtbericht/Cruise Report MSM63, PERMO, Southampton – Southampton (U.K.), 29.04.-25.05.2017, Eds.: Christian Berndt and Judith Elger with contributions from cruise participants C. Böttner, R.Gehrmann, J. Karstens, S. Muff, B. Pitcairn, B. Schramm, A. Lichtschlag, A.-M. Völsch, DOI: 10.3289/GEOMAR_REP_NS_37_2017
38	RV SONNE Fahrtbericht/Cruise Report SO258/1, INGON: The Indian - Antarctic Break-up Engima, Fremantle (Australia) - Colombo (Sri Lanka), 07.06.-09.07.2017, 29.04.-25.05.2017, Eds.: Reinhard Werner, Hans-Joachim Wagner, and Folkmar Hauff with contributions from cruise participants, DOI: 10.3289/GEOMAR_REP_NS_38_2017
39	RV POSEIDON Fahrtbericht/Cruise Report POS509, ElectroPal 2: Geophysical investigations of sediment hosted massive sulfide deposits on the Palinuro Volcanic Complex in the Tyrrhenian Sea, Malaga (Spain) – Catania (Italy), 15.02.-03.03.2017, Ed.: Sebastian Hölz, DOI: 10.3289/GEOMAR_REP_NS_39_2017

For GEOMAR Reports, please visit:
https://oceanrep.geomar.de/view/series/GEOMAR_Report.html

Reports of the former IFM-GEOMAR series can be found under:
https://oceanrep.geomar.de/view/series/IFM-GEOMAR_Report.html

GEOMAR
Helmholtz-Zentrum für Ozeanforschung Kiel

Das GEOMAR Helmholtz-Zentrum für Ozeanforschung Kiel ist Mitglied der Helmholtz-Gemeinschaft Deutscher Forschungszentren e.V.

The GEOMAR Helmholtz Centre for Ocean Research Kiel is a member of the Helmholtz Association of German Research Centres

Helmholtz-Zentrum für Ozeanforschung Kiel / Helmholtz Centre for Ocean Research Kiel
GEOMAR
Dienstgebäude Westufer / West Shore Building
Düsternbrooker Weg 20
D-24105 Kiel
Germany

Helmholtz-Zentrum für Ozeanforschung Kiel / Helmholtz Centre for Ocean Research Kiel
GEOMAR
Dienstgebäude Ostufer / East Shore Building
Wischhofstr. 1-3
D-24148 Kiel
Germany

Tel.: +49 431 600-0
Fax: +49 431 600-2805
www.geomar.de